Alma Mater Studiorum – Università di Bologna

DOTTORATO DI RICERCA IN

Scienze Biomediche

Ciclo XXIX

Settore Concorsuale di afferenza: 06/F4

Settore Scientifico disciplinare: MED/33

To evaluate the synergistic effect of different crosslinking strategies on collagen derivatives to develop functional biomimetic scaffolds

Presentata da: Gopal Shankar Krishnakumar

Coordinatore Dottorato

Prof. Lucio Cocco

Relatore

Prof. Lucio Cocco

Correlatore

Prof. Marcacci Maurilio

Esame finale anno 2017

Dedicated to my future kid and my family

Acknowledgments

I am thankful to **The Lord Almighty** for his copious blessing and guidance during the whole period of my research.

I would like to express my utmost gratitude to **Prof. Marcacci Maurilio** and **Dott.ssa Elizaveta Kon** for providing me opportunity to work as Marie Curie Researcher and pursue my Ph. D degree at Rizzoli Orthopaedic centre – University of Bologna.

I thank **Dott.ssa Anna Tampieri,** Director, ISTEC-CNR, for her permission to carry out my research work at her institute. I express my profound gratitude to **Dott. Simone Sprio** and **Dott.ssa Monica Sandri** for their constant encouragement, kind support, suggestions and advice.

I wish to record my thanks to **Dott.ssa Silvia Panseri and Dott.ssa Monica Montesi** at ISTEC-CNR for their scientific contribution, support, generosity and affection.

I owe a special note of gratitude to **Dott.ssa Alice Roffi, Dott. Giuseppe Filardo** and **Dott. Berardo Di Matteo** at Rizzoli Orthopaedic Institute for their support and invaluable suggestions.

It is my pleasure to thank my dear friends **Dott.ssa Natalia Gostynska, Dott.ssa Gloria Belen Ramirez Rodriguez, Dott.ssa Tatiana Patricio, Dott. Massimiliano Dapporto, Dott. Alberto Ballardini, Dott.ssa Elisabetta Campodoni** and **Dott. Samuele Dozio** for their constant help and encouragement throughout my research period.

Finally, I am obliged to my Ph. D coordinator **Prof. Lucio Cocco,** at the Department of Biomedical and Neuromotor Science, University of Bologna for his cordial guidance and help in time of need.

I am extremely grateful to **Marie Curie Actions – European Commission** for providing me financial assistance in the form of Early Stage Researcher (BIO-INSPIRE: PITN-GA- 2013-607051).

I attribute all my success to my beloved **Family** for their understanding, unflinching patience and conviction which have helped me to reach this destination.

TABLE OF CONTENTS

PART II – ANALYTICAL TECHNIQUES

PART III – EXPERIMENTAL PART

Chapter I: To evaluate the different crosslinking strategies on functional modification of gelatin for tissue engineering applications

Chapter II: Reinforcement of mineralized collagen through ribose glycation

Research Significance

Tissue and organ repair still endures to be a clinical challenge. To this concern, the global prevalence of bone diseases and disorders has expanded voluminously and is foreseen to double in 2020. Bone disorders are commonly seen in all ages of population due to obesity, lack of physical activities, trauma and sporting injuries. Therefore, there is a continuous demand in the field of bone tissue engineering to outpace the classical treatment methods and to introduce new therapeutic approaches to treat bone defects. Engineered, synthetic bone scaffolds with biomimetic features are considered to be elective substitutes of conventional biological grafts, thanks to the possibility to overcome the drawbacks commonly associated to autologous or heterologous bone tissues. Furthermore, there are increasing evidence that scaffolds with high compositional and structural affinity with native tissues can provide enhanced instructions to cells towards tissue regeneration. Therefore, evolving bone tissue engineering approaches aim at providing new functional therapies or mastering innovative therapies through synergistic combinations of biomaterials, cells and growth factor therapy. This project was financially supported by Marie Curie Actions – European Commission (BIO-INSPIRE: PITN-GA- 2013-607051). The project consists of five work packages dedicated to material synthesis, in vitro and in vivo assessment with the mission to generate new mineralized bio-devices obtained by bio-inspired synthesis methods providing enhanced mimesis of bone tissue, through coordination and integration of several research groups with global expertise in materials development and testing.

In this project, we aimed at validating the osteogenic potential of bone-like scaffolds obtained by bio-inspired synthesis under *in-vitro* and *in-vivo* conditions. In particular, pre-clinical trials target to evaluate the efficacy and functionality of the biomineralized scaffolds developed in this project. Generally, despite of remarkable performance in pre-clinical studies, the new functional bone tissue engineering therapies do not progress to human application due to several limitations and challenges. Therefore, the BIO-INSPIRE project aims to develop new class of bone-like scaffolds, primarily targeting for the clinical translation of these scaffolds for bone diseases with tuneable properties based upon individual patient needs. In detail, my study firstly evaluated the potential need for different crosslinkers in functional modification of biological macromolecules. Though bioinspired scaffolds are potentially bioactive their mechanical and resorption properties are extremely poor, thus making them unsuitable for any biological application. Crosslinking macromolecules using potential agents are highly useful in developing mechanically stable structures. As different crosslinking strategies are employed extensively to develop biologically active materials, there is sufficient dearth in comparative studies, that analyzes the overall effectiveness of different crosslinkers for tissue engineering applications. Despite the encouraging

benefits of crosslinkers, the correlation between how different crosslinkers can modify the overall features of a macromolecule differently in terms of physical-chemical, structural and biological properties is of greater importance in order to standardize the scaffold design procedure to an anatomic specific application. Therefore, with greater paucity in the literature for comparative studies on various crosslinkers for tissue engineering applications, we aimed to study the effect of three common crosslinkers (DHT, BDDGE, genipin) in functionalization of gelatin. The significant results of this study revealed that the DHT crosslinking process was more appropriate to obtain a three-dimensional (3D) scaffold with physical-chemical, mechanical and biological features suitable for tissue engineering. Moreover, the absence of any chemical residues within the protein network would absolutely avoid the antigenicity in physiological conditions. Similarly, the BDDGE crosslinked scaffold showed good mechanical behaviour with favourable chemical composition, topography, hydrophilicity and satisfying biological properties. Whereas, the genipin crosslinked scaffold also showed good morphological features however lower cytocompatibility was observed when compared to other two scaffolds but there was slow recovery in the compatibility in the later days of culture due to the cell and dose dependent effect of genipin. Finally, the results suggest that, out of the three-crosslinking mechanism, the dehydrothermal treatment (DHT) is most effective in obtaining promising scaffolds for tissue engineering.

As a next step, though DHT, BDDGE and genipin crosslinking has imparted beneficial properties, the search for novel, low-cost, alternative crosslinking strategies were never-ending. In this scenario, an interesting, sugar-based, non-enzymatic, ribose crosslinking strategy gained significant importance in the past few years due to its simple biological crosslinking reaction. In spite of its favourable and beneficial crosslinking reactions, the ribose crosslinking methodologies in 3D scaffolds was reported scarcely with limited information. Therefore, in order to better assimilate the usage of this novel, low-cost ribose crosslinking reaction on functional modification of biomineralized scaffolds was investigated. In this work, we explored for the first time the application of ribose as a highly biocompatible agent for the crosslinking of hybrid mineralized constructs, obtained by bio-inspired mineralization of self-assembling Type I collagen matrix with magnesium-doped-hydroxyapatite nanophase, so to obtain biomimetic mineralized 3D scaffolds (MgHA/Coll) with excellent compositional and structural mimicry of bone tissue. To this aim, two different crosslinking mechanisms in terms of pre-ribose glycation (before freeze drying) and post-ribose glycation (after freeze drying) were investigated. The study results, demonstrated the feasibility in developing a highly anisotropic, and mechanically stable scaffold with the ability to mimic the physical-chemical features of the natural bone. The biocompatibility test also supported the potential use of ribose as an alternative crosslinker to collectively improve the

mechanical performance of MgHA/Coll scaffolds thereby offering new opportunities in tailoring scaffolds for tissue engineering applications. Therefore, the ribose glycation of collagen can serve as a value tool to study, (i) altered tissue mechanical properties due to glycation, (ii) cell behaviour in response to glycation, (iii) as *in-vitro* model to study extra cellular matrix changes in age-related bone pathologies. As a proof of concept, the study demonstrated that ribose crosslinking is cost-effective, safe and functionally effective.

As a final step, again a comparative study on functional modification of biomineralized composites as effect of DHT, BDDGE and ribose crosslinking was studied. The results demonstrated that different crosslinking reactions can greatly modify the physical-chemical and mechanical features of MgHA/Coll composite. Taken together, the results obtained demonstrates that the analyzed crosslinking mechanisms and their respective composites are promising candidates in hard tissue engineering to develop to tissue specific biomimetic biomaterials. In case of bone tissue engineering all the above studied composites (DHT, BDDGE and ribose) would be beneficial, because these composites possess enhanced enzymatic resistivity, sufficient swelling ability, good mechanical resistivity, adequate structural and dimensional (porosity and pore size) properties and satisfactory biological performance.

Finally, the final choice of crosslinkers largely depends upon the applicability of the developed material, because the different crosslinkers can tune/tailor the final properties of the material differently towards a tissue specific application. Moreover, the overall results of this work provide crucial findings on the bioactivity of the biological macromolecule due to various crosslinking strategies. Though gelatin and collagen are being ubiquitously used in all aspects of science, these fundamental details on how individual crosslinker can help in achieving the desired features of a scaffold can influence numerous research areas with greater impact in multidisciplinary fields of material science. To conclude, this study offers new insights and opportunities to develop promising scaffolds and the possibility to tailor composites differently through various crosslinking reactions for hard tissue engineering application with suitable biomimetic properties that may be used for diverse applications in tissue engineering.

PART I – GENERAL INTRODUCTION

Chapter 1: Brief background on bone and cartilage formation

1.1. Bone biology

Among the various organs which functions productively and periodically within the human system, bone has outstanding ability to regenerate and repair itself. In contrast to other tissues, which always manifest a poor quality of connective scar tissue formation, the bone is able to regenerate completely and restore the original functionality. This unique quality of the bone can be accredited to the healing cascade of bone fracture or the cyclic remodelling of the human skeleton [1,2]. The complex bone healing pathway has been well inferred, which illustrates that the coordination of molecular, patho-physiological and biomechanical aspects is highly imperative for bone repair [3,4]. At birth, there are about 300 soft bones in the human skeleton, as the age increases and on approaching adolescence, there is a replacement of some bones by cartilaginous layer and few bones fuse together, so an adult skeleton has 206 bones [5].

1.2. Structure of bone

The bone is composed of two principal components, the cortical (compact) bone and trabecular (cancellous) bone (Fig.1 (A)). The cortical bone is further separated into 2 layers, the inner endosteal and the outer periosteal surface. The periosteal is a highly connective fibrous layer which contains blood vessels, nerve fibres, osteoblasts and osteoclasts. It mainly functions in protecting and nourishing the bone [6]. In addition, it also plays a crucial role in appositional growth and fracture repair. The periosteal contains the (volkmann's canals) which are tiny channels within the cancellous bone which functions predominantly in exchange of nutrients to the harvesian canals, thereby nourishing the osteons [7]. The cancellous bone or the inner spongy trabecular bone is highly characterized by the presence of light or less dense trabecular layer (Fig.1 (B)). Moreover, the cancellous bone is highly vascularised with enormous red bone marrow, where the synthesis of red blood cells (haematopoiesis) occurs [8]. This apart, the subchondral bone region includes the subchondral plate, underlying trabecular and the sub articular layer. This region contains the calcified cartilage and the cortical bone layer. The subchondral bone acts as a protective layer

helping in shock absorption and exchange of metabolite products for the nourishment of the tissues. Moreover, the subchondral layer also helps in load bearing activities, approximately up to 30% of the joint load is dissipated through the subchondral bone, thereby ensuring good joint stability [9,10].

Furthermore, based upon the collagen formation and deposition pattern of the osteoids, two types of bones are identified, the woven bone and the lamellar bone (Fig.2 (B)). The woven bone is characterized by the presence of haphazard organisation of collagen fibres with weaker mechanical properties. Usually, during the foetal bone formation, the osteoblast produce osteoid rapidly, thereby producing more woven bone in a disordered manner. However, the woven bone is replaced through the remodelling process to produce more resilient lamellar bone. Eventually, all the mature healthy bones in adults are lamellar bone. The lamellar bone is characterized by the presence of homogenous parallel alignment of collagen fibres into sheets (lamellae) with significantly stronger mechanical properties [11,12].

1.3. Articular bone region

The cartilage layer along with the bone supports and protects the human skeleton. Cartilage is a highly flexible and elastic layer present in between the bones, joints, intervertebral disc, ear and nose (Fig.2 (B)). The cartilage contains a sparse population of single typed cells known as chondrocytes and lacks vascularisation. This protective layer contributes to the compressive strength and provides frictionless motion during load bearing situations [13]. The chondrocytes reside within the extracellular matrix (ECM) which includes the collagen (50-60%), proteoglycans (25-35%) and glycoproteins (10-15%). The cartilage layer is also differentiated into three different types which are widely distributed in the human exoskeleton as (i) elastic cartilage, (ii) hyaline cartilage and (iii) fibro cartilage. Among this, the hyaline cartilage is the most widespread layer and offers high resistance to compressive force owing to its highly-organised type II collagen fibres orientation [14,15].

(A) **(B)**

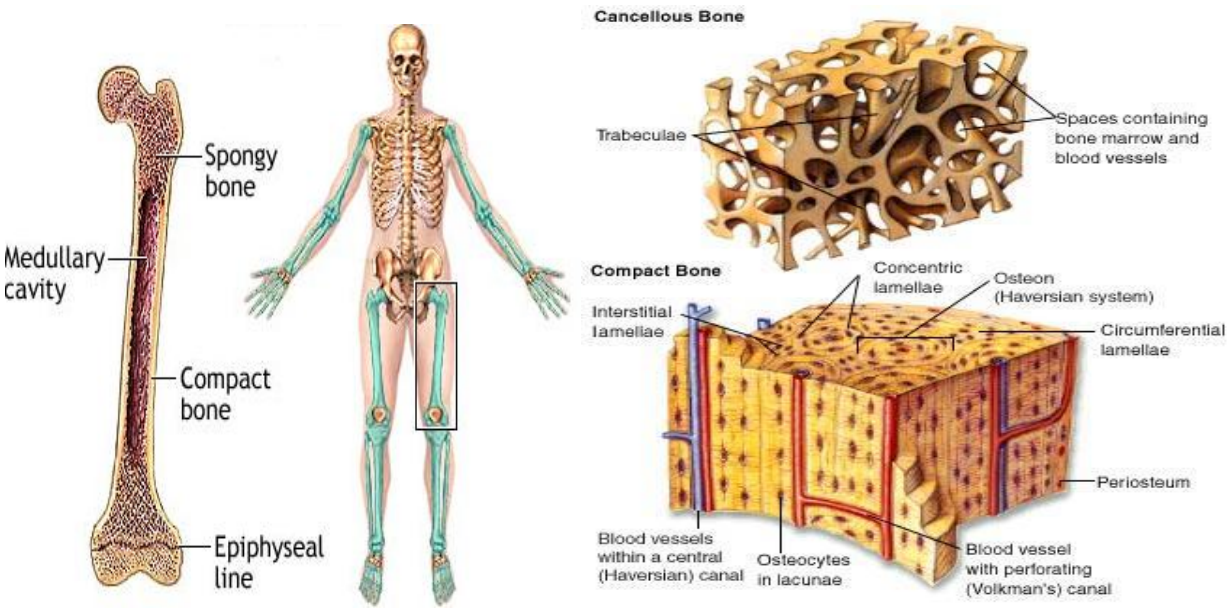

Figure 1: *(A); Two major components of human bone, (B); Detailed schematic representation of bone components*

(A) **(B)**

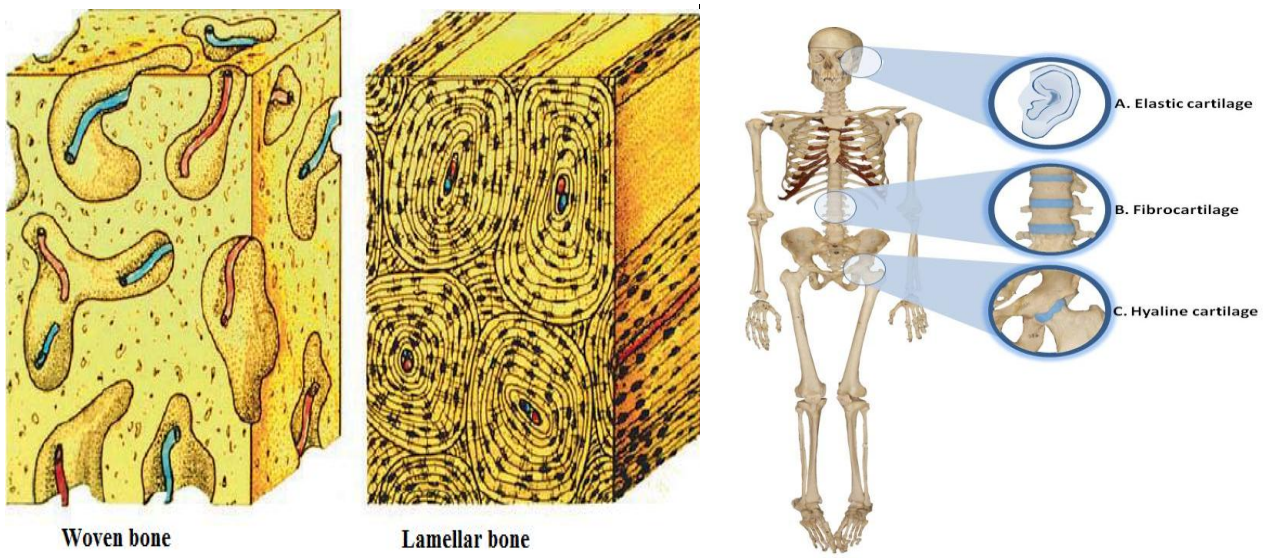

Figure 2: *(A); Microscopic representation of woven and lamellar bone, (B); Cartilage distribution in the human skeleton*

1.4. Bone cells

There are three different types of cells that regularly modulate and control the bone homeostasis and remodelling (Fig.3 (A)),

i) ***Osteoblasts***: The origin of these cells are from mesenchymal stem cells (MSCs), whose principal responsibility is to synthesis bone matrix. Osteoblasts are mononucleated and their shape is dependent upon the cellular activity which varies from flat to plump shape. As the process of differentiation proceeds, these cells produce bone matrix and controls osteoclast regulation [16].

ii) ***Osteocytes***: These are osteoblast cells, derived from the newly formed osteoid. Osteocytes are considered to be the most abundant bone cells, which communicates in the surrounding medium through their plasma membrane projections also known as canaliculi process. Osteocytes tend to serve as mechanosensors and guides osteoclasts in bone resorption [17].

iii) ***Osteoclasts***: These are multinucleated, macrophage like cells, derived from the hematopoietic cell lineage. These cells are actively involved in resorption of mineralized tissue (Fig.3 (B)). These cells possess a unique ruffled edge surface, where the resorption occurs through secretion of bone-resorbing enzymes to digest the bone matrix [18].

1.5. Physiology of bone formation

The bone formation occurs through two major modes (Fig.4),

(i) ***Intra-membranous Ossification:*** The direct transformation of MSCs tissue into bone, usually occurs in flat bones such as skull, maxillae and clavicles. The MSCs within the medullary cavity initiates the intra-membranous ossification through the following steps, (i) formation of ossification centres, (ii) calcification, (iii) formation of trabeculae and (iv) development of periosteum [19].

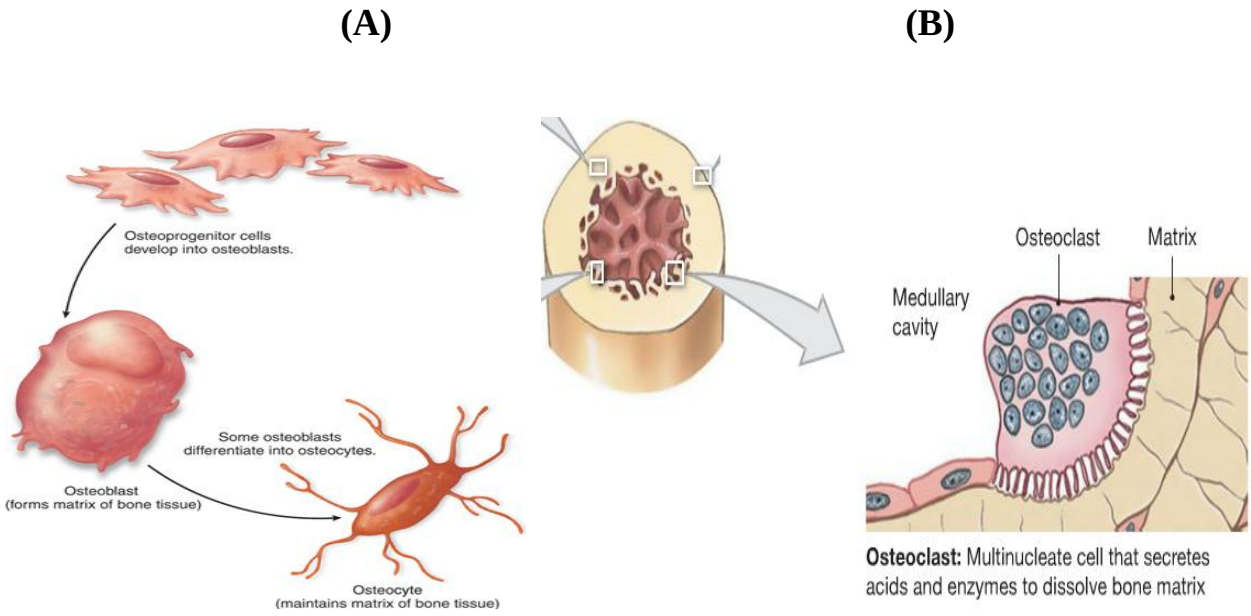

Figure 3: *(A); Multi-lineage of bone cells, (B); Bone resorption by osteoclasts*

(ii) ***Endochondral Ossification:*** The differentiation of MSCs into cartilage and later replacement of cartilage into bone is known as endochondral ossification. It commonly involves the formation of hyaline cartilage, which is primarily responsible for the growth of long bones and for the natural fracture healing process. The process is usually initiated by the development and growth of cartilage model and later the development of primary and secondary ossification occurs, resulting in the formation of articular cartilage and epiphyseal plate. This process occurs during the foetal development and mainly responsible for the formation of diaphysis of long and short bones [20].

1.6. Bone matrix

The bone matrix is essentially constituted into two phases: a) the inorganic (69%) phase, containing (99%) hydroxyapatite and b) organic (22%) phase, containing (90%) collagen and other non-collagenous proteins (NCPs) such as proteoglycans, sialprotein, gla-containing proteins and 2HS-glycoprotein. The rigid mechanical property of the bone is attributed to the mineral phase in the osteoid matrix, which is especially the crystalline mixture of calcium and phosphate

(hydroxyapatite). The calcified bone consists of 25% organic phase, 5% water and 70% inorganic phase. Predominantly, type I collagen constitutes 90-95% of the organic matrix of bone [21,22].

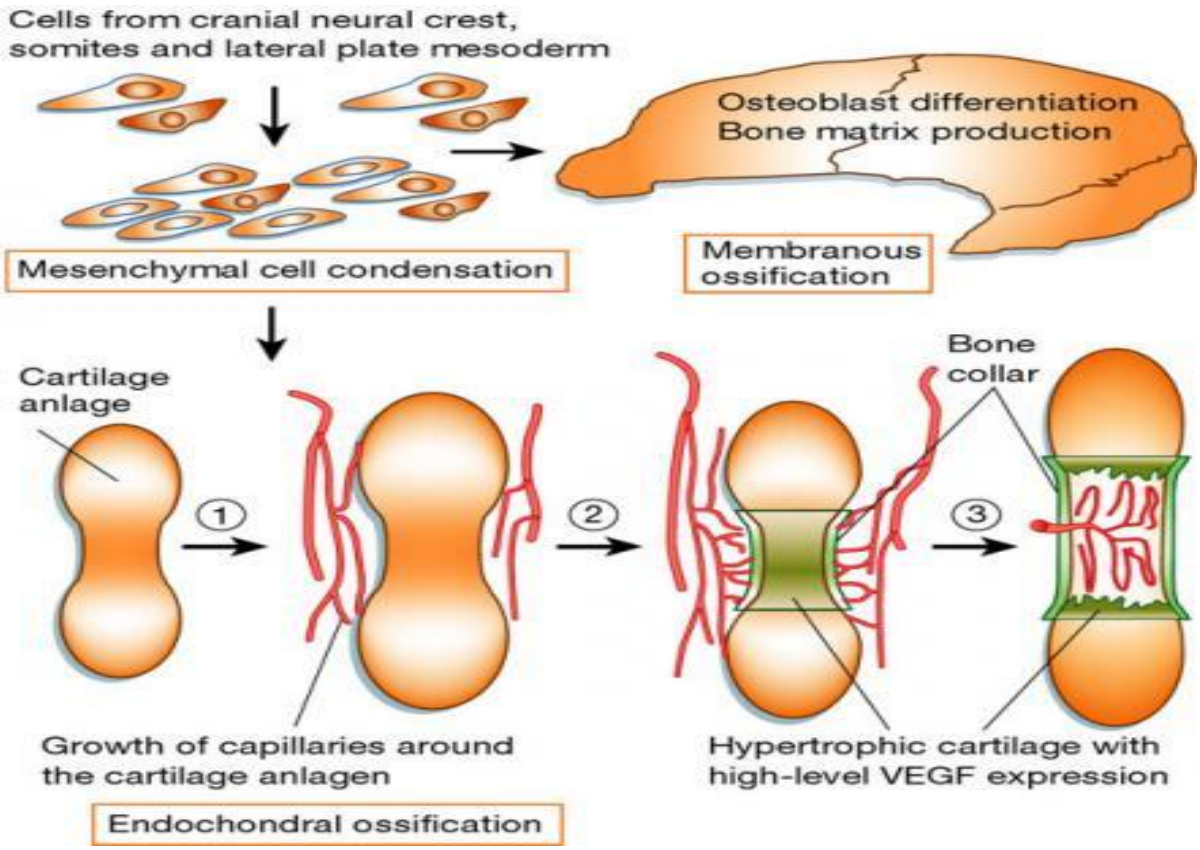

Figure 4: *Physiology of bone formation*

1.7. Bone mineralization

There are several models demonstrated in the literature, to describe the complex process of bone mineralization, which includes the classical theories and the recent insights on mineralization. The classical theories strongly believe that NCPs are actively involved in matrix mineralization process. In contrary, the recent finding suggests two different mechanisms (i) formation of stable mineral droplet (pre-nucleation clusters) which transforms into an amorphous phase and then binds and diffuses into the collagen fibrils, (ii) matrix vesicle assisted mineralization by the osteoblast cells [23] (Fig.5).

However, the matrix assisted nucleation theory is most commonly acknowledged. The bone mineralization is a process where the mineral crystal deposition occurs in orchestrated manner on the organic collagen template. Usually, the mineralization is initiated by the osteoblast cells which

secrete the vesicles containing the alkaline phosphates which cleaves the phosphate group and also serves as local foci for the calcium and phosphate precipitation. Initially, the collagen micro-fibrils of mean diameter of 1.5 nm, begins to self-assemble as fibres [24]. The self-assembling process of collagen fibres results in formation of a quarter-staggered arrangement of parallel of precursor tropocollagen (a triple helical-shaped) molecule with a regular array of 40 nm gaps within each periodic unit [25]. These units are considered to be the preferential site for mineral nucleation and also known as hole zones with length of 40 nm and width of 5 nm. The chemical binding of calcium ions induces the precipitation and nucleation of the mineral phase as nano-sized, plate or needle shaped particles, which are initially confined to the hole zones, and gradually extends along the *c*-axes of collagen fibrils to form organised crystalline array [26]. The interaction of organic and inorganic phase at the molecular or nano-scale level can highly influence the bone at macro-scale level as well. The chemical interaction of hydroxyapatite (HA, $Ca_5(PO_4)_3OH$) with collagen results in apatite-like lattice which is amorphous in nature. During this process, the size and shape of the nuclei is often limited due to the presence of NCPs which are actively modulating and controlling the nucleation process [27]. The growth of the nuclei is limited to very thin lamellae resulting in a mineral-collagen composite with several levels of hierarchy to the macroscopic bone (Fig.6).

The mineral phase of the bone is composed of hydroxyapatite with a Ca/P ratio of less than 1.67 which strongly attributes to the bone stiffness. However, in the natural hydroxyapatite, there are impurities such as carbonates (4-6%), sodium (0.9%) and magnesium (0.5%) which acts as a replacement ions at the phosphate and hydroxyl sites thereby causing poor crystalline structure [28]. The mineral phase of the bone greatly determines the stiffness and the breaking strain of the bone. Therefore, during in vivo mineralization, the mineral content is subjected to variability, increasing from low to intermediate and later achieving complete mineralization.

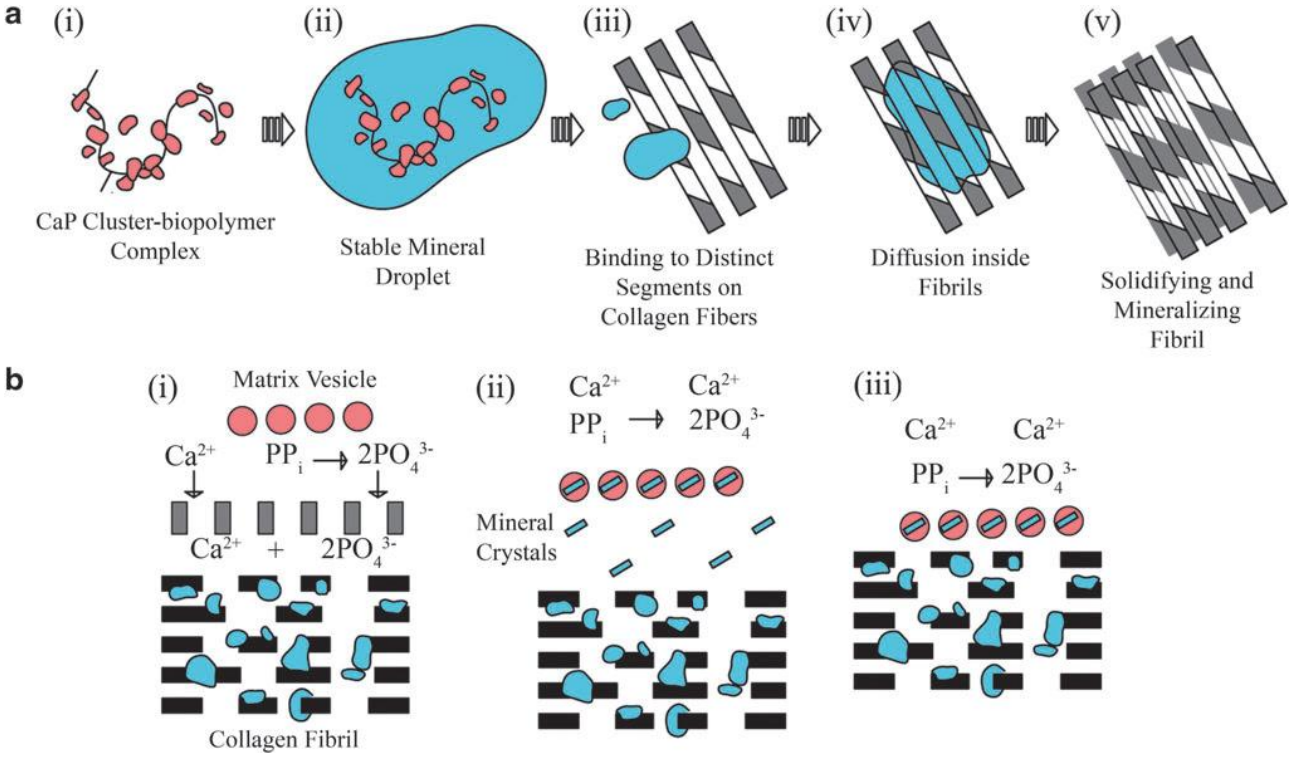

Figure 5: *Diagrammatic representation of new findings in matrix nucleation, (A): Direction of calcium phosphate mineralization, (B): Matrix vesicle aided mineralization*

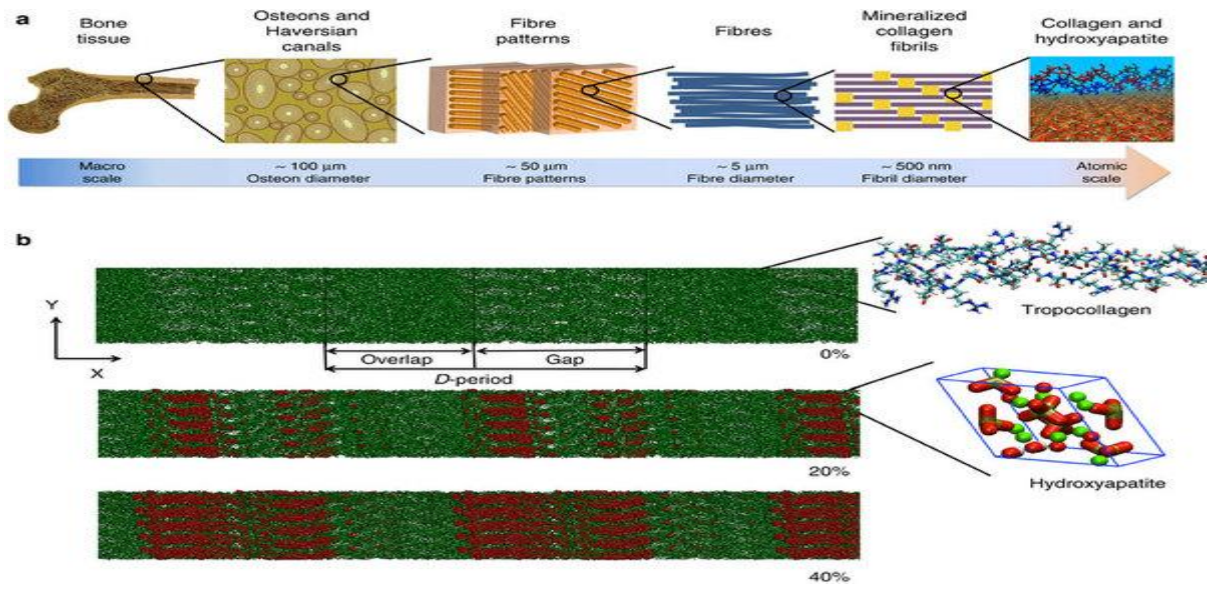

Figure 6*: Mechanism of bone mineralization, (A): Bone mineralization from macro to nano scale level, (B): Collagen micro fibril model with increase in percentage of mineralization*

In regard to the HA crystal shape, many studies have demonstrated, the needle or plate like shape of HA crystals with thickness of 2-10 nm, length of 20-50 nm and width of 15-30 nm [29]. The presence of NCPs contributes up to 10% of the organic matrix, these molecules are highly responsible for the mineral nucleation and growth in bone mineralization. This apart, water (10%) present in between both mineralized and non-mineralized bone as small channels, provides structural and mechanical properties to the bone. Moreover, the presence of water molecules is responsible for the decreased spacing of the molecule after dehydration [30].

1.8. Reference

1) Giannoudis PV, Einhorn TA, Marsh D. Injury. 2007;38 Suppl 4:S3-6. Review.

2) Lyritis GP. J Musculoskelet Neuronal Interact. 2000;1(1):1-3.

3) Aaron RK, Ciombor DM, Wang S, Simon B. Ann N Y Acad Sci. 2006;1068:513-31.

4) Giannoudis PV, Einhorn TA, Schmidmaier G, Marsh D. Injury. 2008;39 Suppl 2:S5-8.

5) Dermience M, Lognay G, Mathieu F, Goyens P. J Trace Elem Med Biol. 2015;32:86-106.

6) Usha Kini, B. N. Nandeesh. Radionuclide and Hybrid Bone Imaging.2012, pp 29-57.

7) Eriksen EF. Endocr Rev 1986,7:379–40.

8) Netter FH. Ciba-Geigy Corporation, 1987, Summit, pp 129–130. ISBN 0914168886.

9) Li B, Marshall D, Roe M, Aspden RM. J Anat. 1999;195 (Pt 1):101-10.

10) B. Li, R. Aspden. Ann Rheum Dis. 1997; 56(4): 247–254.

11) Hernandez CJ, Majeska RJ, Schaffler MB. Bone. 2004 ;35(5):1095-9.

12) Weiner S, Traub W, Wagner HD. J Struct Biol. 1999, 30;126(3):241-55.

13) Sophia Fox AJ, Bedi A, Rodeo SA. Sports Health. 2009;1(6):461-8.

14) Yue Gao, Shuyun Liu, Jingxiang Huang. BioMed Research International, 2014, Article ID 648459, 8 doi:10.1155/2014/648459.

15) Buckwalter JA, Mankin HJ. J Bone Joint Surg Am. 1997;79:600-611.

16) Lawrence G. Raisz. Clinical Chemistry 1999 vol. 45 no. 8, 1353-1358.

17) Palumbo C. Cell Tissue Res. 1986;246(1):125-31.

18) Raggatt LJ, Partridge NC. J Biol Chem. 2010, 13;285(33):25103-8.

19) Cheung WH, Miclau T, Chow SK, Yang FF, Alt V.Injury. 2016;47 Suppl 2:S21-6.

20) Berendsen AD, Olsen BR. Bone. 2015;80:14-8.

21) Kuttappan S, Mathew D, Nair MB. Int J Biol Macromol. 2016. pii: S0141-8130(16)30581-5. doi: 10.1016/j.ijbiomac.2016.06.043.

22) Liu Y, Luo D, Wang T. Small. doi: 10.1002/smll.201600626.

23) Farbod K, Nejadnik MR, Jansen JA, Leeuwenburgh SC. Tissue Eng Part B Rev. 2014;20(2):173-88.

24) Rony Sapir-Koren, Gregory Livshits. IBMS Bone Key (2011) 8, 286–300.

25) Lowenstam HA, Weiner S (1989). Oxford University Press, Oxford.

26) Falini G, Fermani S. Cryst Res Technol 48:864–876.

27) Palmer LC, Newcomb CJ, Kaltz SR, Spoerke ED, Stupp SI. Chem Rev. 2008;108(11):4754-83.

28) M. J. Olszta, X. Cheng, S. S. Jee, R. Kumar, Y.-Y. Kim, M. J. Kaufman, E. P. Douglas, L. B. Gower. Mater. Sci. Eng. R. 2007, 58, 77.

29) T. Hassenkam, G. E. Fantner, J. A. Cutroni, J. C. Weaver, D. E. Morse, P. K. Hansma. Bone 2004, 35, 4.

30) P. Fantazzini , V. Bortolotti , R. J. Brown , M. Camaiti , C. Garavaglia ,R. Viola , G. Giavaresi J. Appl. Phys. 2004, 95, 339.

Chapter II: Concept of tissue engineering

1.1. Background of tissue engineering

In the mid 1980's the term tissue engineering was first defined at the National Science Foundation workshop, which aims at developing functional tissue substitutes to restore, replace or regenerate defective tissues [1]. However, the concept of tissue engineering is relatively new and it is still evolving up to date, the idea of this innovative strategy dates back to the 16^{th} century. This approach was first adopted by Professor Gasparo Tagliacozzi (1546-99), University of Bologna, who demonstrated nose replacement using the forearm flap in his studies – "De Custorum Chirurigia per Insitionem' (The Surgery of defects by implantation) in 1597 [2]. The field of tissue engineering is a highly multidisciplinary, which actively involves the synergism of material and clinical science in developing an appropriate tissue-specific biological substitutes. The key components of tissue engineering are the, (i) scaffolds, (ii) cells and (iii) growth factors, which are often known as tissue engineering traids (Fig.1) [3].

1.2. Clinical need of bone tissue engineering

Bone is a highly dynamic and vascularised tissue which has an ability to self heal and remodel through a well-orchestrated process. However, the high regenerative capacity is lost when there is a large segmental defect, severe non-unions or bone tumour resection due to the lack of template. Such critical sized defect often requires invasive surgical procedures to reconstitute the structural integrity of the collapsed bone and eventually causes a significant socio-economic burden. The healing pattern of bone disorder is greatly dependent on several factors such as age, infection, inflammation, pre-existing diseases and medication. Moreover, the location and severity of the defect is highly important, especially the distance between the fractured bones, biomechanical forces, soft tissue damage and the type and stability of fixation, determines the healing prognosis of bone repair [3,4]. Despite of all new innovations in bone repair, the autologous bone grafting (ABG) is still considered to be the "gold standard" treatment in augmenting bone defects.

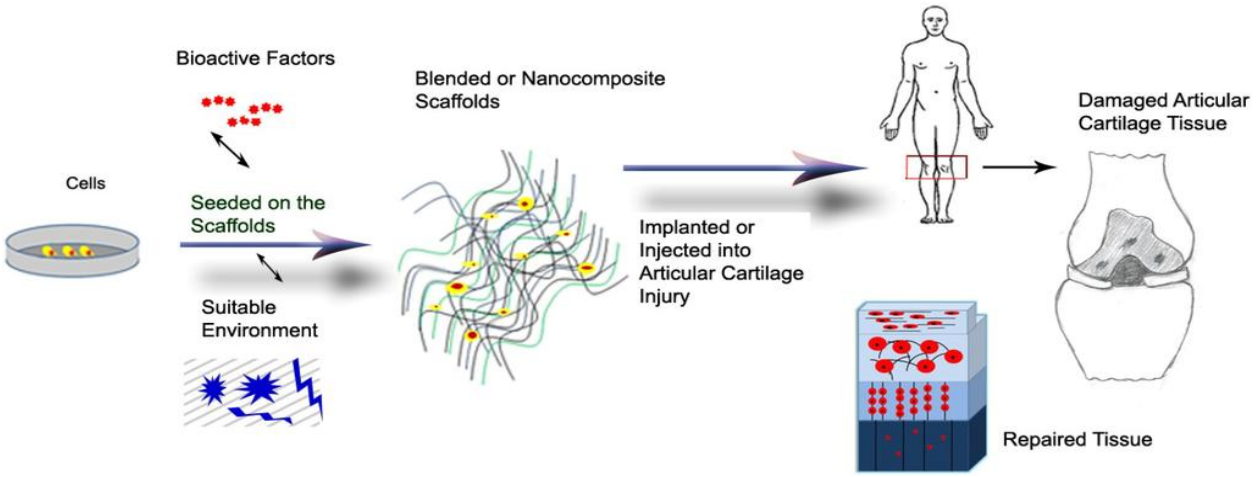

Figure 1: *Tissue engineering paradigms with scaffolds, cells and bioactive factors*

However, the ABG treatment has been subjected to intensive research due to its related drawbacks such as longer operating time, little availability of material and significant morbidity [5-8]. Another option could be the treatment with allografts or xenografts but several disadvantages are reported, such as immune rejection and graft sequestration [9]. Therefore, the quest for developing alternative strategies to treat bone disease was of greater importance in the medicinal field. Therefore, the expedition of biological substitutes fuelled the researchers in developing targeted tissue-specific scaffolds from natural and synthetic materials.

1.3. Birth of biomaterials for bone regeneration

In 1976, at the European society for Biomaterials (ESB) conference, the term biomaterials were defined as ‘a nonviable material used in a medical device, intended to interact with biological systems’; however, the ESB’s current definition is a ‘material intended to interface with biological systems to evaluate, treat, augment or replace any tissue, organ or function of the body [2].

The concept of bone tissue engineering (BTE) has been developed to produce tailor-made scaffolds with ability to fine-tune the tissue regeneration process. The typical paradigm of BTE, is the four biological factors which are, (i) osteogenic cells, (ii) osteoinductive stimulus, (iii) osteoconductive matrix scaffolds and (iv) mechanical environment which is collectively known as the diamond concept [10]. In order to adopt this diamond concept in BTE strategy, what is highly crucial is the appropriate scaffold with opportune macro porous structure, good degradability and better

osteoconductive properties [11-13]. Thus, 3D scaffolds are developed with hierarchically organized structures similar to the anatomical bone with the ability to activate mechano-transduction processes, yielding regeneration of well-organized bone [14,15].

The contemporary concept of 3D scaffolding in BTE is also to obtain biomimictic scaffolds with structural and biological features similar to the natural native ECM components. Accordingly, any biomimictic scaffold should possess the following quality (i) adequate architecture, (ii) biocompatible, (iii) bioactivity and (iv) good mechanical properties. The above-mentioned characteristics are highly essential in tailoring a tissue-specific scaffolds [16]. The currently available biomaterials are classified into the following categories,

(i) Natural polymers: Biological derivatives such as collagen, gelatin, chitosan and hyaluronic acid are considered to potential candidates in BTE. These biological polymers are inherently biocompatible where they play beneficial role in favouring cellular activities and promotes chemo-tactic response. However, there are few disadvantages in terms of disease transmission due to their allogenic or xenogenic origin, weak mechanical properties and poor handling characteristics [17].

(ii) Synthetic polymers: Synthetic materials such as polylactic acid (PLA), polyglycolic acid (PGA), copolymers of PLA and PGA (PLGA), polyfumarates and polycaprolactone are considered to potent alternatives to natural polymers. These synthetic materials offer advantage in terms of, easy availability, feasibility in developing wide range of scaffolds with modifications in porosity and surface properties. Additionally, the synthetic polymers can be processed by using a broad range of techniques such as (porogen leaching, gas foaming, phase separation, fiber meshing, supercritical fluid processing, microsphere sintering, and three-dimensional printing) which allows to control and modulate the shape and size of the scaffolds for tissue-specific application. However, there are few concerns over the synthetic materials in regard with poor biocompatibility and release of acidic by-products [18].

(iii) Bioactive inorganic materials: Tri-calcium phosphate (TCP), Hydroxyapatite (HA) and bioactive glass are the common bioactive inorganic materials that possess chemical composition similar to the mineral phase of bone. These materials upon contact with the biological fluid, they produce a hydroxycarbonate apatite layer to bind the biological tissue. These materials are often used as delivery vehicle's in release of certain ions such as silicon (Si) to enhance cell differentiation and osteogenesis. However, the issues in regard with biocompatibility and brittle nature of these materials often limits its potential application [19].

***(iv) Bio composites*:** The combination of organic/inorganic phases to produce a bio composite material led to innovative concept of biomimicry strategy. This strategy is gaining much importance nowadays in order to develop tailor-made bone scaffolds with nano-sized inorganic components because of their increased bioactivity. Accordingly, collagen-HA bio composite is a promising and extensively investigated material in BTE application [20].

However, the bio composites are scrutinized under the following categories,

a) Porous scaffolds: 3D scaffolds with porous, form-like morphology are commonly used in BTE application because of their ability to induce bone re-growth and tissue vascularisation. The porous sponge like structure can be developed with isotropic or anisotropic properties with varying level of porosity and interconnectivity based upon the tissue-specific application. These porous materials, are the most commonly investigated bio composites in BTE because of the following beneficial advantages such as, (i) acts as a template for tissue re-growth, (ii) serves as a medium to transport nutrients and metabolic products and (iii) helps in faster tissue regeneration [21]. Few examples of porous bio composites are MaioRegen® [22,23] and RegenOss® [24].

b) Hydrogels: Biodegradable hydrogels have controlled structural and morphological features similar to the macromolecular based components of the human body. These materials offer advantages in terms of high biocompatibility, cell-controlled degradation, intrinsic cell interaction and enhanced visco-elastic properties. Additionally, these materials have certain interesting characteristics such as ability to retain high water content, increase nutrient diffusion, promote cell

migration and angiogenesis [25]. Few examples of hydrogels are self-assembling RAD16-I (PuraMatrix™) [26] and gelatin methacrylate (GelMA) [27].

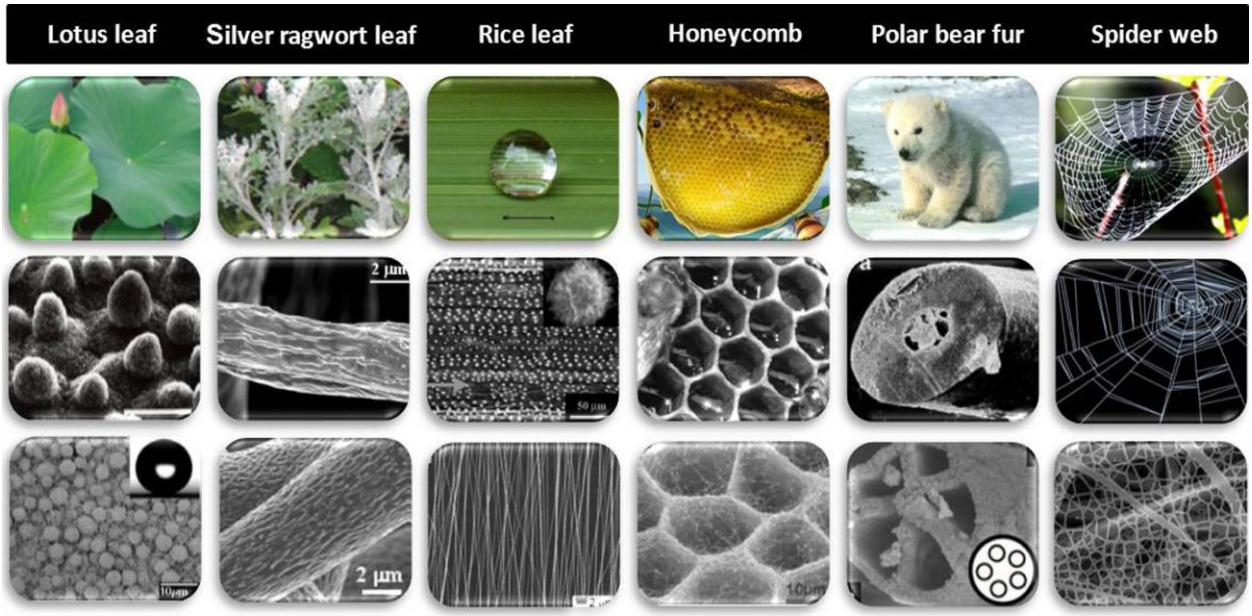

Figure 2: *Bioinspired electrospun nanofibrous morphogical features from nature*

c) Fibrous scaffolds: The rapid evolution of BTE has led to the development of scaffolds analogous to the human tissue even at the nanometer level. Currently, there are three techniques used to develop fibrous scaffolds such as electro spinning, phase separation and self-assembly. The fibrous scaffolds have increased surface-area-to-volume ratio which eventually increases the cell adhesion, migration, proliferation and differentiation (Fig.2). In addition, the fibrous scaffolds act as carrier to delivery growth factors, drugs and genes at the target site with controlled release properties [28]. For example, there are currently six FDA-approved synthetic polymers which includes poly(α-hydroxy esters), poly(glycolic acid) (PGA), poly(L-lactic acid) (PLLA), poly(D,L-lactic acid) (PDLLA), poly(D,L-lactic-*co*-glycolic acid 50:50) (PLGA5050), poly(D,L-lactic-*co*-glycolic acid 85:15) (PLGA8515), and poly(ε-caprolactone) (PCL) to produce fibrous scaffolds [29].

(d) Microspheres: Microspheres are commonly used as drug delivery system with sustained release of growth factors over a prolonged period of time. The use of microspheres has several benefits such as (i) ease in fabrication, (ii) control over morphology, (iii) physico-chemical characteristics and (iv) control over release kinetics. The molecular weight of polymers used to

develop microspheres has a greater role in sustained release of growth factors, because the high molecular weight polymers offers slow release prolife and low molecular weight polymers has rapid release prolife. The use of microspheres has several potential advantages such as allowing 3D porous space for new bone in growth and improves the integrative bone and cartilage interface [30]. Few examples of microspheres are, macroporous gelatin beads (CultiSpher-G) [31] and GELIBEAD® [32].

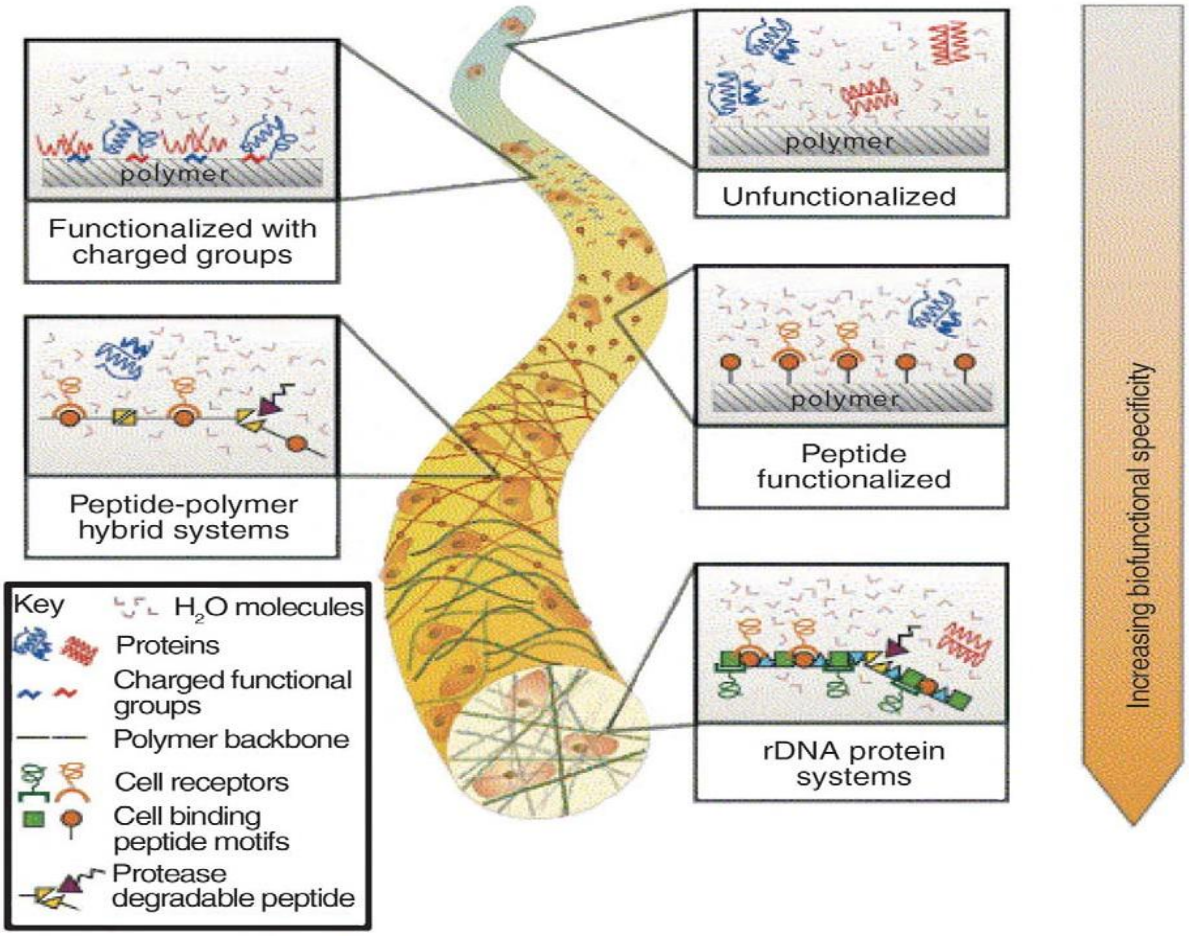

Figure 3: *Ways to enhance material bio-functionality through biomaterial design*

1.4. Ways to enhance the bio-functionality of materials

Incorporation of appropriate biological cues in the biomaterials are highly essential for achieving an enhanced regeneration rate. Hence, the concept of synergetic coordination of cells and materials was of greater interest since the early 1980's. BTE approach has successfully used cells such as MSCs and osteoblasts in handful of orthopaedic applications. Additionally, the use of

exogenous potent angiogenic factors such as vascular endothelial growth factor (VEGF) are used to stimulate vessel growth (Fig.3). Other osteogenic proteins, such as bone morphogenetic proteins (BMP-2 and BMP-7) are used in clinical practice which plays a crucial role in signalling of chemotactic proliferation and differentiation of osteoprogenitor cells thereby inducing bone formation. However, the use of BMPs are often limited due to their exorbitant price and post-operative complications (heterotopic ossification). Additionally, a newly evolving approach gene therapy offers possibility in genetically modifying the cells with sustained gene expression, however yet promising and encouraging results from gene therapy is to be achieved [33,34]

The consecutive points address the necessary physical and biological cues to follow in order to obtain a true biomimictic bone scaffold,

(i) The cell behaviour at the micro and nano scale varies greatly, hence controlling the topographical features of the biomaterials at the hierarchal range is highly important. For examples, the MSCs were able to produce more bone mineral at disordered nano scale than the highly organised nano-topographical feature.

(ii) The length scale of topography (10 nm to 100 μm) has known to greatly influence the bulk-tissue property and cell behaviour. Hence, the nanophase reinforcements such as HA-collagen nano composites and carbon nanotube polymers greatly attributes to the increased flexural and compressive modulus of the material.

(iii) It is more interesting to recreate the topographical context of the native ECM through nano fibrous matrices which could be achieved through electro spinning, phase separation or protein self-assembly.

(iv) Another approach to increase the bio-functionality is to introduce bioactive peptide motifs such as arginine-glycine-aspartic acid (RGD) which can fine-tune tissue remodelling and regeneration.

(v) Incorporation of ECM components such as glycosaminoglycans (GAGs) and heparin can help in producing functionalized scaffolds which can increase cell attachment, proliferation and differentiation abilities.

(vi) The use of bioreactors, can help in achieving hierarchical bone organisation with anisotropy and mechanical properties similar to the native bone under dynamic conditions [19,35]

1.5. Bone disorders

A continuous process of bone remodelling is highly necessary for maintaining a healthy skeleton, usually this process is coordinated and modulated by the bone-absorbing osteoclasts and bone-forming osteoblast. The bone remodelling is a constant process, targeting to replace odd bone through resorption and to produce new bone which usually completes in 4-6 months. This process occurs at specific sites, where the osteoclasts are recruited to the defect site due to the stress-induced fracture through the osteocytes signalling. Therefore, during remodelling numerous pathways such as (RANKL) and (Wnt) signalling molecules are actively involved in restoring the functionality of the bone through synthesising new bone [36].

(i) Osteoporosis: Osteoporosis is defined according to the world health organisation (WHO) as an asymptomatic bone disorder characterized by the presence of low bone mineral density (BMD) which eventually cause weak and porous bone with an increased fracture risk (Fig.4 (A)). Osteoporosis is mainly caused due to the improper coordination of bone cells (osteoblasts and osteoclasts). The lack of synergic coordination between the bone cells cause increased bone resorption and decreased bone formation. However, osteoporosis is classified as, (A): Primary osteoporosis: mainly caused due to post menopausal complications as the result of hormone (estrogen) deficiency or due to vitamin D deficiency as the result of natural ageing process. (B): Secondary osteoporosis: induced by disease or use of long term medications such as glucocorticoids, proton pump inhibitors, selective serotonin receptor inhibitors, androgen deprivation therapy,

thiazolidinedione, heparin, calcineurin inhibitors, and some chemotherapies such as methotrexate which has very detrimental effects on bone health

The etiology of osteoporosis is categorized as, (A): Uncontrollable factors: age, race, sex, heredity problems, gastrointestinal disorders, hormonal imbalance and hematologic disorders. (B): Controlled factors: diet, exercise, bone mineral density, intake of calcium, magnesium and vitamin D, proper body mass index (BMI), social and lifestyle habits. [37,38].

The current therapeutic options to treat osteoporosis includes wide range of anti-resorptive drugs (Bisphosphonates, Denosumab, Calcitonin) and anabolic drugs (Teriparatide, Strontium ranelate and Raloxifene). However, the recently introduced, the next generation therapeutic options includes, anti-sclerostin antibodies, cathepsin k inhibitors and stem cell therapy [39].

(ii) Osteoarthritis: Osteoarthritis or degenerative bone disease also abbreviated as OA is caused due to wear and tear at the joints. Cartilages are highly proteinous tissue in between the joints providing cushioning effects to the joints (Fig.4 (B)). Osteoarthritis is common among older population affecting 20 million people in United States and males are more susceptible to degenerative disease than females. Osteoarthritis affects hands, spine and load bearing joints. When the cause of the degenerative disease is unknown it is referred as primary osteoarthritis, if the cause of the tissue damage is known it is known as secondary osteoarthritis. Mostly the primary osteoarthritis is prior to aging, with aging the protein concentration within the cartilage starts deteriorating due to increased water content. Cushioning effect of the cartilages is lost due to degeneration and fissure formation at the surfaces, this causes knee swelling and joint pain. It is also believed that genetic and hereditary factors can also influence osteoarthritis.

Secondary osteoarthritis is caused due to obesity, congenital disorders, repeated surgery or trauma and gout diabetes. Early onset of OA in younger population is due to obesity, adding more mechanical stress at the cartilages can lead to tissue tear and degeneration. Other risk factors such as crystal deposits (uric acid and calcium pyrophosphate), hormone imbalance and congenital disease also contribute to tissue degeneration [40,41].

The treatment options include medication of Nonsteroidal anti-inflammatory drugs (NSAIDs) such as Aspirin (Ecotrin), Ibuprofen (Motrin), Nabumetone (Relafen), and Naproxen (Naprosyn). Newly designed NSAIDs known as COX-2 inhibitors has been proven to have lesser toxicity and side effects. The necessity of surgery is when the drug treatment is fruitless, arthroscopy and osteotomy is the common surgical techniques used to treat osteoarthritis. Under severe conditions joint replacement (Arthoplasty), Arthodesis (fusion treatment) and knee replacement are done to improve the physiological and biomechanical function [42].

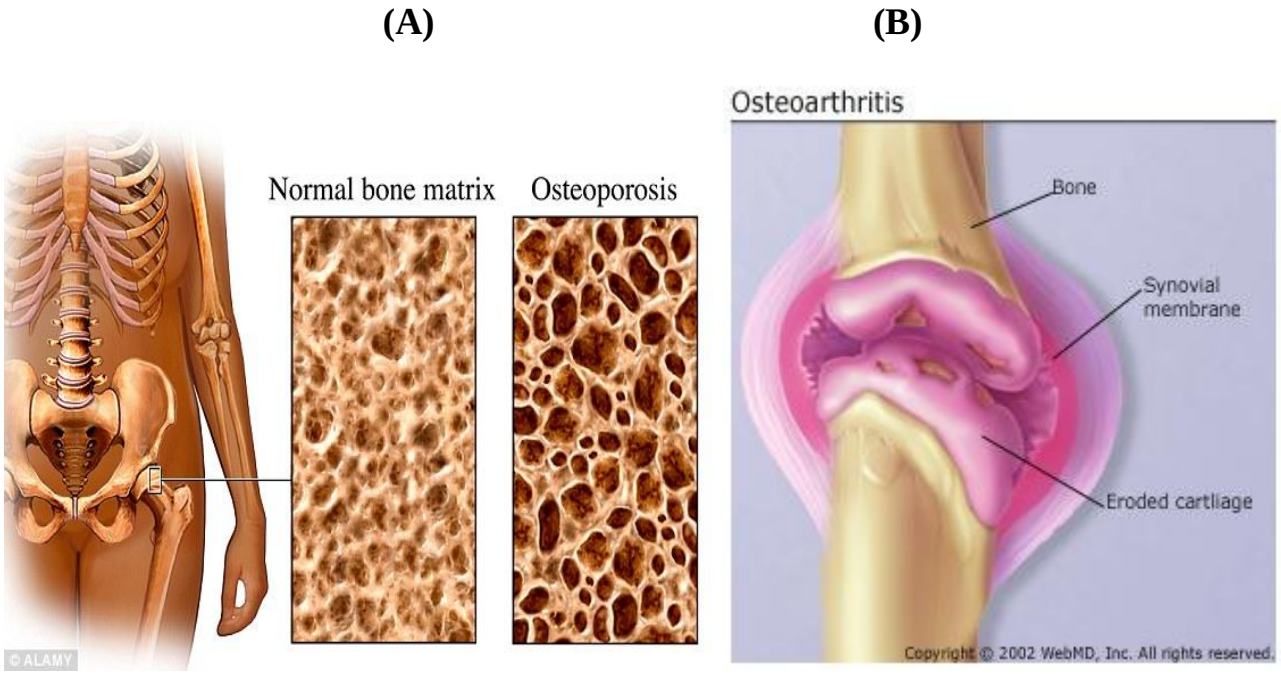

Figure 4: *(A): Difference between normal and osteoporotic bone, (B): Diagrammatic representation of knee osteoarthritis*

1.6. Therapeutic options from BTE strategies

The recent advances in material engineering has influenced the need of biomaterials, cells and growth factors in developing biological substitutes for bone cartilage tissue engineering. In this current scenario, there are plenty of commercial products on the market to treat bone or cartilage disorders (Fig.5)

(i) Natural products: Among the protein based matrices, type I and III collagen is commonly used in BTE application. For example, in matrix associated chondrocyte implantation (MACI® Germany, Maix® Germany, Chondro-Gide®, Switzerland and Atelocollagen®, Japan) are being extensively used in clinical practice. Several studies have demonstrated that MACI is an effective and safe in treating isolated cartilage defects of the knee [43,44]. As part of the MACI procedure (HYAFF-11® Italy) a hyaluronic acid matrix was shown to have proven clinical results, however due to lack of overall safety and efficacy, the HYAFF-11® is retracted from the market as per guidance of the European medicines agency. Additional, (BST-CarGel®, Canada) a chitosan based matrix with β-glycerophosphate is also being used as part of MACI procedure and has demonstrated proven success especially in improving the patient quality of life [45].

Figure 5: *Different categories of biomaterials for bone tissue engineering applications*

(ii) Synthetic products: Bio-Seed®-C, Germany is a biphasic, porous scaffold fabricated from polyglycolic acid (PGA), polylactic acid (PLA) and polydioxanone. This bi-layered scaffold has shown to improve hyaline cartilage formation and also resulted in better clinical success in treating osteochondrol scaffolds [46]. Similarly, another biphasic polymer with PGA and PLA with calcium sulphate (TrueFit™, USA) to treat articular defects is commercially available however several clinical studies have disclosed controversial results with less evidence of osteoconduction. A crystalline coral aragonite-hyaluronic acid bi-layer scaffold (Agili-C™, Israel) has showed promising results with the restoration of the articular surface. A bio-ceramic with gradient layers of cartilage like and bone like components with magnesium enriched hydroxyapatite (MaioRegen®, Italy) has shown to provide encouraging results in treating challenging osteochondrol lesions [47].

(iii) Bone cements: Bone cements are most suitable for osteoporotic fractures, the polymethylmethacrylate (PMMA) cements are more commonly used in vertebral compression fractures due to their high efficacy and safety (Fig.6 (A)). This apart, tailor made calcium phosphate cements are also used to due their high bioresorbability and bioactivity. Strontium containing calcium phosphate cements have shown to inhibit cell-driven bone resorption and simultaneously promote new bone formation in osteoporotic fractures. Nanotechnology offers new opportunities in tailoring bone cements with nano-structured additives such as (MgO, Ag, or BaSO4) nano particles to improve osseointegration. Additionally, the use of carbon nano tubes (CNTs) in calcium phosphate cements has resulted in highly reinforced material with enhanced bioactivity and compressive strength. This apart, there are thermo sensitive hydrogels with long term sustained drug delivery with chitosan nano particles, however, the soft nature of the material with weak mechanical features often limits its potential use. Micron-sized (BaSO4 or ZrO2) particles are being used as radiopacifiers in bone cements to enhance bone-material integration [48]. In the commercial market, there are several bone cement products such as (Palacos R, Belgium), (Palamed G, Germany), and (Simplex P, USA) to treat compressed vertebral fractures [49].

(iv) Cell therapy: Chondrocytes, fibroblasts and stem cells from various sources have been used in treating cartilaginous defects. However, chondrocytes and MSCs remains to be the widely-investigated cells for cartilage repair. Currently, there are two procedures available in the market involving the use of articular chondrocytes which includes the (Carticel®, USA) and (Celect®, Belgium). However, there are few concerns over the instability of their phenotype in monolayer culture which causes the cells to orient towards fibroblastic phenotype with increased expression of type I collagen [50]. Multipotent MSCs is another viable alternative which has a potential to proliferate and differentiate in several lineages. Several studies have shown the potential benefits of using autologous MSCs in treating bone and cartilage defects. However most of the studies have benefited from using MSCs regardless of various sources (Bone marrow derived stem cells (BMSCs), adipose derived stem cells (ADSCs), peripheral blood derived stem cells (PBSCs) and bone marrow concentrates (BMCs)) and administration (injective or surgical) method (Fig.6 (B)). [51].

(A) (B)

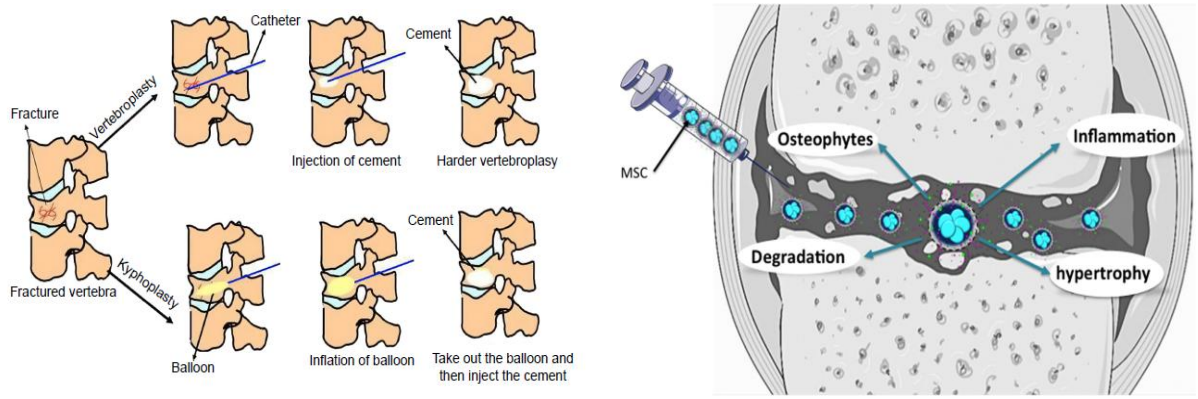

Figure 6: *(A): Application of bone cements in vertebral fractures, (B): Schematic representation of stem therapy at knee lesions*

(v) Growth factors: In the last decades, the therapeutic application of growth factors (GFs) for bone regeneration is gaining increasing attention in the scientific community, since these functional biological enhancers can trigger the reactive cells to facilitate the intracellular signal transduction for endochondral and intramembranous bone formation. Recombinant human bone morphogenetic

protein (rhBMP-2) and rhBMP-7, tested in several preclinical and clinical studies showed the ability to induce bone regeneration in various bone disorders such as non-unions, open fractures and osteonecrosis with promising results. However, a major concern in regard to the available BMPs therapy is the rapid release which cause the rapid accumulation of supraphysiological concentrations of BMPs, which in term causes severe complication such as heterotopic ossification [52]. Another promising therapy is, Plasma rich platelet (PRP) therapy, a facile, economical and non-invasive method that allows a natural concentrate of autologous growth factors to be obtained from blood. The evidence for PRP to be osteogenic is highly proven in several in-vitro studies, primarily showing the ability of PRP to induce proliferation and differentiation of human osteoblasts. The adaptation of PRP therapy in preclinical and clinical studies is also commonly investigated but there exists a discrepancy in the results with lack of conviction in the final outcomes. Despite of the beneficial role of PRP in bone repair, the controversial point lies in the quality and quantity of the PRP used, which is mainly dependent on the preparation methodologies (blood volume and no. of centrifugation steps) and final constituents of PRP (White Blood Cells (WBCs), fibrinogen and neutrophils) [53]. This apart there are other GFs such as transforming growth factors (TGF), fibroblast growth factors (FGF), insulin-like growth factors (IGF) used to treat bone defects but with limited literature evidence.

The field of BTE has plethora of biomaterials to offer, but choosing an appropriate material for clinical use is high dependent upon the bone anatomical region. The recent advances in this field has catered the need to investigate the micron and nanoscale features of the scaffolds, in order to achieve a better interplay between the material and cells for improved tissue regeneration. Moreover, more encouraging preclinical studies are needed in large animal models for the future clinical transition. This exciting, interdisciplinary and multidisciplinary field of BTE will grow exponentially in future years to provide more novel biomaterials with improved functionality.

1.7. References

1) Langer R, Tirrell DA (2004). Nature 428(6982):487–492.

2) Fergal J. O'Brien. Materials today. 2011, 14(3);88-95.

3) B. P. Chan, K. W. Leong. Eur Spine J (2008) 17 (Suppl 4):S467–S479.

4) Cesar S. Molina, MD. Daniel J. Stinner, MD. William T. JBJS Reviews 2014;2(4):e1.

5) Horner EA, Kirkham J, Wood D, Curran S, Smith M, Thomson B, Yang XB. Tissue Eng Part B Rev. 2010;16(2):263-71.

6) Blokhuis TJ, Wippermann BW, den Boer FC, van Lingen A, Patka P, Bakker FC, Haarman HJ. J Biomed Mater Res. 2000 Sep 5;51(3):369-75.

7) Zhi W, Zhang C, Duan K, Li X, Qu S, Wang J, Zhu Z, Huang P, Xia T, Liao G, Weng J. J Biomed Mater Res A. 2014 Aug;102(8):2491-501.

8) Fan H, Zeng X, Wang X, Zhu R, Pei G. Biomaterials. 2014 Aug;35(26):7407-15.

9) Reichert JC, Saifzadeh S, Wullschleger ME, Epari DR, Schütz MA, Duda GN, Schell H, van Griensven M, Redl H, Hutmacher DW. Biomaterials. 2009 Apr;30(12):2149-63.

10) Giannoudis PV, Einhorn TA, Marsh D. Injury. 2007 Sep;38 Suppl 4:S3-6. Review.

11) Smith EL, Kanczler JM, Gothard D, Roberts CA, Wells JA, White LJ, Qutachi O, Sawkins MJ, Peto H, Rashidi H, Rojo L, Stevens MM, El Haj AJ, Rose FR, Shakesheff KM, Oreffo RO. Acta Biomater. 2014 Oct;10(10):4186-96.

12) Amorosa LF, Lee CH, Aydemir AB, Nizami S, Hsu A, Patel NR, Gardner TR, Navalgund A, Kim DG, Park SH, Mao JJ, Lee FY. Int J Nanomedicine. 2013;8:1637-43.

13) Guo Y, Tran RT, Xie D, Wang Y, Nguyen DY, Gerhard E, Guo J, Tang J, Zhang Z, Bai X, Yang J. J Biomed Mater Res A. 2015 Feb;103(2):772-81.

14) Filardo G, Kon E, Tampieri A, Cabezas-Rodríguez R, Di Martino A, Fini M, Giavaresi G, Lelli M, Martínez-Fernández J, Martini L, Ramírez-Rico J, Salamanna F, Sandri M, Sprio S, Marcacci M. Tissue Eng Part A. 2014 Feb;20(3-4):763-73.

15) Griffin M, Iqbal SA, Bayat A. J Bone Joint Surg Br. 2011;93(4):427-34.

16) Berger J, Reist M, Mayer JM, Felt O, Peppas NA, Gurny R. Eur. J Pharm Biopharm.2004,57(1):19–34.

17) B. D. Ratner, A. S. Hoffman, F. J. Schoen, and J. Lemons, Eds., pp. 127–136, Elsevier Academic Press, San Diego, Calif, USA, 2004.

18) Gunatillake PA, Adhikari R.Eur Cell Mater. 2003, 20;5:1-16.

19) Molly M. Stevens. Materials today. 2008,(11):18-25.

20) Tampieri A, Sprio S, Sandri M, Valentini F. Trends Biotechnol. 2011;29(10):526-35.

21) R. Zhang and P. X. Ma. Journal of Biomedical Materials Research.1999.vol. 45, no. 4, pp. 285–293.

22) Elizaveta Kon, Francesco Perdisa, Giuseppe Filardo, Maurilio Marcacci.Techniques in Cartilage Repair Surgery. 2014, Part III, pp 81-95.

23) Delcogliano M, Menghi A, Placella G, Speziali A, Cerulli G, Carimati G, Pasqualotto S, Berruto M. Joints. 2014,1;2(3):102-8.

24) S. J. Bryant and K. S. Anseth. Biomaterials.2001 vol. 22, no. 6, pp. 619–626.

25) Misawa H, Kobayashi N, Soto-Gutierrez A, Chen Y, Yoshida A, Rivas-Carrillo JD. Cell Transplant. 2006;15(10):903–910.

26) Nichol JW, Koshy ST, Bae H, Hwang CM, Yamanlar S, Khademhosseini A. Biomaterials. 2010;31:5536–5544.

27) Brahatheeswaran Dhandayuthapani, Yasuhiko Yoshida, Toru Maekawa, and D. Sakthi Kumar. International Journal of Polymer Science, vol. 2011, Article ID 290602, 19 pages, 2011. doi:10.1155/2011/290602.

28) Wan-Ju Li, Rocky S. Tuan. Curr Protoc Cell Biol. 2009 Mar; Chapter: Unit–25.2.

29) C. Berkland, M. King, A. Cox, K. Kim, and D. W. Pack. Journal of Controlled Release, vol. 82, no. 1, pp. 137–147, 2002.

30) J. S. Rasey, M. M. Cornwell, B. J. Maurer, D. J. Boyles, P. Hofstrand, L. Chin, C. Cerveny. Br J Cancer Suppl. 1996; 27: S78–S81.

31) Bingyan Li, Xin Wang, Yu Wang, Wenlong Gou, Xueling Yuan, Jiang Peng, Quanyi Guo, Shibi Lu. Journal of Orthopaedic Translation. Volume 3, Issue 2,2015, Pages 51–57.

32) Seeherman H, Wozney JM. Cytokine Growth Factor Rev. 2005;16(3):329-45.

33) Verma IM, Somia N. Nature. 1997, 18;389(6648):239-42.

34)J. Huang, S. N. Jayasinghe, S. M. Best, M. J. Edirisinghe, R. A. Brooks, N. Rushton, W. Bonfie ld. Journal of Materials Science: Materials in Medicine.2005, Volume 16, Issue 12, pp 1137–1142.

35) Li WJ, Tuli R, Huang X, Laquerriere P, Tuan RS. Biomaterials. 2005;26(25):5158-66.

36) Clarke B. Clin J Am Soc Nephrol. 2008;3Suppl 3:S131–S139.

37) Rachner T, Khosla S, Hofbauer A. The Lancet 2011;377 (9773):1276-87.

38) Ivanova S, Vasileva L, Ivanova S, Peikova L, Obreshkova D. Folia Med (Plovdiv). 2015;57(3-4):181-90.

39) Das S, Crockett JC. Drug Des Devel Ther. 2013, 31;7:435-48.

40) Brandt KD. In: Kelly W, Harris E, Ruddy S, et al. (eds). Textbook of rheumatology. 2nd ed. Philadelphia: Sauders; 1985:1432.

41) Manal Hasan, Rhonda Shuckett. British Columbia Medical Journal, Vol. 52, No. 8, 2010, page(s) 393-398.

42) Loveless MS, Fry AL. Med Clin North Am. 2016;100(4):869-90.

43) Vinatier C, Guicheux J. Ann Phys Rehabil Med. 2016;59(3):139-44.

44) Ebert JR, Fallon M, Smith A, Janes GC, Wood DJ. Am J Sports Med. 2015;43(6):1362-72.

45) Steinwachs MR, Waibl B, Mumme M. Arthrosc Tech 2014;3:e399–402.

46) Ossendorf C, Kaps C, Kreuz PC, Burmester GR, Sittinger M, Erggelet C. Arthritis Res Ther 2007;9:R41.

47) Kon E, Filardo G, Perdisa F, Venieri G, Marcacci M. J Exp Orthop. 2014;1(1):10.

48) Gao C, Wei D, Yang H, Chen T, Yang L. Int J Nanomedicine. 2015,13;10:5139-57.

49) Hallan G, Aamodt A, Furnes O, Skredderstuen A, Haugan K, Havelin LI. J Bone Joint Surg Br. 2006;88(9):1143-8.

50) Darling EM, Athanasiou KA. J Orthop Res 2005;23:425–32.

51) Filardo G, Perdisa F, Roffi A, Marcacci M, Kon E. J Orthop Surg Res. 2016 Apr 12;11:42.

52) Shankar KG, Gostynska N, Montesi M, Panseri S, Sprio S, Kon E, Marcacci M, Tampieri A, Sandri M. Int J Biol Macromol. 2016 Nov 9. pii: S0141-8130(16)31045-5. doi: 10.1016/j.ijbiomac.2016.11.010.

53) Argintar E, Edwards S, Delahay. Injury, (2011) . 42(8):730-4.

Chapter III: Crosslinking of biological macromolecules

1.1. The need for biomaterial crosslinking

A plethora of biomaterials have been developed in the past decades, with each of them having their own characteristics features. Biomaterials derived from collagen, gelatin, chitosan, starch, cellulose, silk and poly(lactic acid) have been extensively investigated for prospective tissue engineering applications. In contempt of its attractive characteristics and as a template for tissue remodelling, these biomaterials possess few disadvantages such as low mechanical strength and high solubility in aqueous solution. Therefore, in order to improve the physical and mechanical parameters, the macromolecule moieties are often crosslinked by stabilizing agents [1,2].

1.2. Physical crosslinking

The physical crosslinking methods include the dehydrothermal (DHT), ultraviolet (UV) and gamma irradiation. Generally, physical crosslinking is considered to be potentially non-toxic but the dehydration of the scaffold surface makes the material less favourable for cell culture application.

1.2.1 DHT treatment

DHT is a physical treatment method, where the biomaterial is subjected to higher temperature of 160 °C under vacuum. The increased temperature removes the bound water molecules from the material resulting in formation of intermolecular crosslinks through esterification or amide formation. Usually the bonding occurs between the amine and the carboxyl groups of the protein backbone. In addition to forming crosslinks, the high temperature exposure can also simultaneously sterilize the material thereby reducing the immunogenic response and increasing the cellular activity on application [3,4]. It has been also reported that DHT crosslinking can occur only when the amino and carboxyl groups are close to each other [5]. DHT method is widely used in tissue engineering application mainly due to its non-toxic effects. For example, DHT was used to crosslink, (i) collagen-glycosaminoglycan scaffolds for soft tissue application [3], (ii) collagen and gelatin based films for vascular prosthesis [6] and (iii) silk-fibroin based scaffolds for bone tissue engineering [7]. The high temperature (DHT) crosslinking causes the complete removal

of bound water molecules within the macromolecule with less availability of surface energy which eventually results in lower crosslinking degree [8,3].

1.2.2. UV treatment

Exposure of polymeric substances to UV radiation can generate free radicals on the aromatic amino acids (tyrosine and phenylalanine) which results in intermolecular crosslinking. UV crosslinking is easy to obtain as the treatment is facile, robust and time-effective. Moreover, the crosslinking mechanism results in completely non-toxic end-products due to absence of any external chemical additives. However, there are few drawbacks associated with UV treatment which is mainly limited with the penetrability of radiation, which is effective only at micron-scale depth. Therefore, UV treatment of crosslinking is more suitable for thin films or transparent scaffolds where there is sufficient irradiation through the material for effective crosslinking [9]. UV treatment is also common method in biomaterial synthesis. For example, (i) to optimize and tailor collagen scaffolds [10], (ii) to enhance osteogenesis in gelatin scaffolds [11] and (iii) in-situ crosslinking of electrospun gelatin fibres [12].

1.3. Chemical crosslinking

Chemical crosslinking results in higher crosslinking degree due to the presence of several functional side groups within the backbone which readily undergoes chemical modifications. Usually the chemical crosslinkers are bi-functional agents such as glutaraldehyde (GTA), 1-ethyl-3-(3-dimethylamino propyl) carbodiimide hydrochloride (EDC) and 1,4-butanediol diglycidyl ether (BDDGE).

1.3.1 Glutaraldehyde (GTA) crosslinking

The bi-functional crosslinking of GTA with a protein causes covalent bonding between the amine groups of lysine or hydroxylysine residues to increase the protein stabilization as seen in Fig.1. GTA is one of the first reported crosslinker for biomedical applications, however the cytocompatibility of GTA is still a concern, nevertheless several studies have effectively utilized GTA to produce functional scaffolds [13]. For example, (i) gelatin/polyvinyl alcohol scaffolds for

tissue engineering applications [14], (ii) poly-e-caprolactone (PCL)-gelatin/hydroxyapatite scaffolds for bone tissue engineering [15], (iii) chitosan/polyvinyl alcohol scaffolds with chondroitin sulphate for articular regeneration [16].

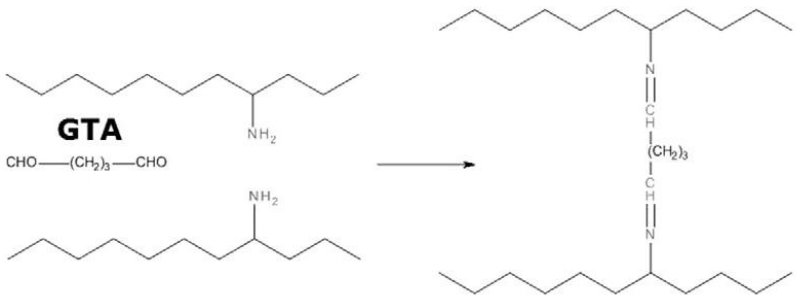

Figure:1: *GTA crosslinking mechanism with gelatin.*

1.3.2. 1-ethyl-3-(3-dimethylamino propyl) carbodiimide hydrochloride (EDC) crosslinking

EDC crosslinking involves the formation of an amide bond through the activation of the side chain carboxylic groups (aspartic and glutamic acid residues). This causes the aminolysis of the O-isoacylurea products by the hydroxylysine groups, thus forming the intra-and-inter helical crosslinks as seen in Fig.2. The use of EDC is very common is tissue engineering applications mainly due to the non-cytotoxicity and EDC behaves as catalysts, therefore the end-products can be removed through dialysis. However, due to extremely low coupling efficiency, EDC is often coupled with N-hydroxysuccinimide (NHS) to act as a stabilizer in order to avoid hydrolysis under aqueous conditions [17,18]. For example, (i) EDC-collagen-hyaluronic acid scaffolds for skin regeneration [19], (ii) to effectively crosslink collagen fibres to increase fibrillar order and alignment [20] and (iii) to improve the mechanical properties of mineralized collagen scaffolds [21].

1.3.3. 1,4-butanediol diglycidyl ether (BDDGE) crosslinking

BDDGE is a bi-functional epoxy based chemical reactant whose crosslinking strategy is pH and temperature dependent. BDDGE is able to form functional covalent bridges with the macromolecular substrate through hydroxyl group bonding [22]. The crosslinking mechanism with the macromolecule occurs through secondary amide bonding via formation of epoxide ring opening by the amine groups under basic pH conditions as seen in Fig.3 [23]. The use of BDDGE in tissue

engineering application is also reported. For example, BDDGE was used to crosslink, (i) magnesium-doped hydroxyapatite collagen scaffold to treat osteochondral defects [24], (ii) hyaluronan scaffolds for soft tissue repair [25], (iii) acellular collagen bladder matrix for wound healing application [26]. Even though the chemical crosslinkers result in stable end products but their degradation derivatives always contain chemical residues which generally causes cytotoxic response [27].

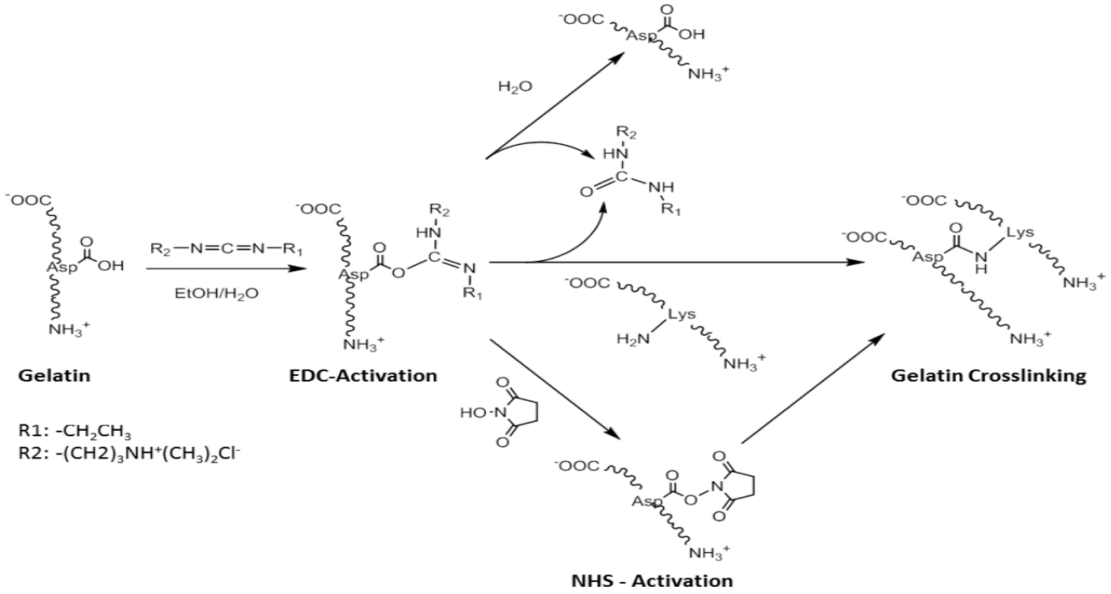

Figure.2: *NHS assisted EDC crosslinking reactions on gelatin*

1.4. Natural crosslinking

Herbal crosslinker such as genipin an iridoid glucoside derived from gardenia fruits can effectively crosslink with protein macromolecules through intra and inter molecular crosslinking without exhibiting any toxicity [28]. The natural genipin crosslinking method involves two-step reaction. In the first step, there is a nucleophilic attack of the genipin C3 carbon atom to form an intermediate aldehyde group. The newly formed aldehyde group reacts with secondary amine to form a heterocyclic compound. Then there is a replacement of ester group occurring on the protein backbone via secondary amide linkage which is termed as nucleophilic substitution as seen in Fig.4. In the final step, the bluish-green colour formation is due to the formation of the heterocyclic compound through oxygen-radical-induced polymerization of genipin [29,30]. In tissue engineering,

genipin has been extensively used as crosslinker due to its less toxicity than GTA. For example, genipin was used to crosslink, (i) chitosan-hyaluronic acid for drug delivery [31], (ii) as sporicidal agent for cortical bone allograft treatment [32], (iii) electrospun hydroxyapatite and chitosan nanofibers for bone tissue engineering [33].

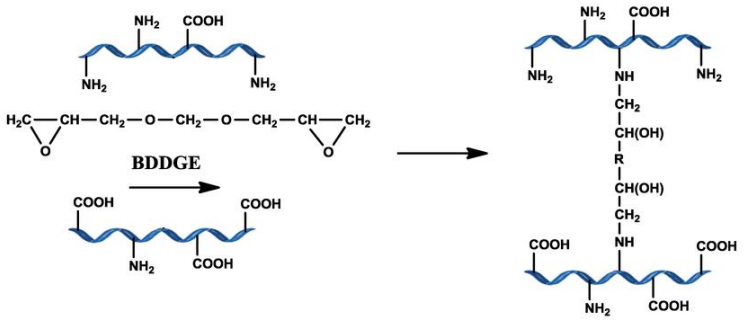

Figure.3: *BDDGE crosslinking reactions on collagen*

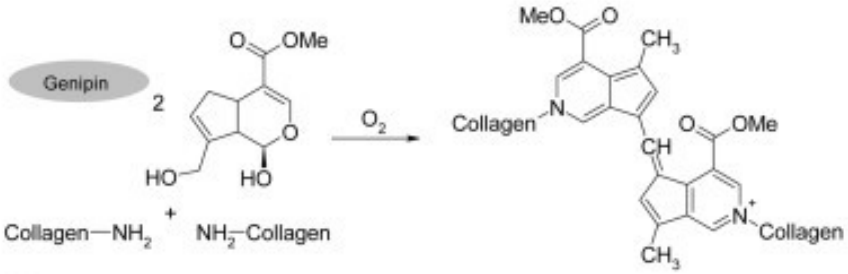

Figure.4: *Genipin crosslinking reactions on collagen*

1.5. Non-enzymatic crosslinking

Non-enzymatic crosslinking is a simple and natural glycation reaction, where the reducing sugar interacts with the amino group of proteins to create chemical alteration in protein structure which is known as Schiff's base alteration. This Schiff's base rearranges to form a Amadori product, which allows the protein-to-protein crosslinking to occur, eventually leading to the formation of advanced glycation products (AGEs) through Maillard reaction as seen in Fig.5 [34,35]. The formation of AGEs attributes to the increased matrix stiffness, decreased solubility and high enzymatic resistivity of the crosslinked tissue [36-38]. This glycation process is a normal biochemical reaction happening in the living system as result of natural ageing. This interesting

glycation technique is widely investigated nowadays to improve tissue functionality in tissue engineering applications. For example, (i) *in-vitro* studies have demonstrated that ribose glycation has a significant role in modifying the mechanical properties of cortical bone [39-41], (ii) studies have shown that minimal concentration of ribose (30 mM) has a significant effect on intermolecular crosslinking of collagen [42]. (iii) glucose modified gelatin/collagen matrix, demonstrated to be a safe and effective biomaterial with excellent biocompatibility [43].

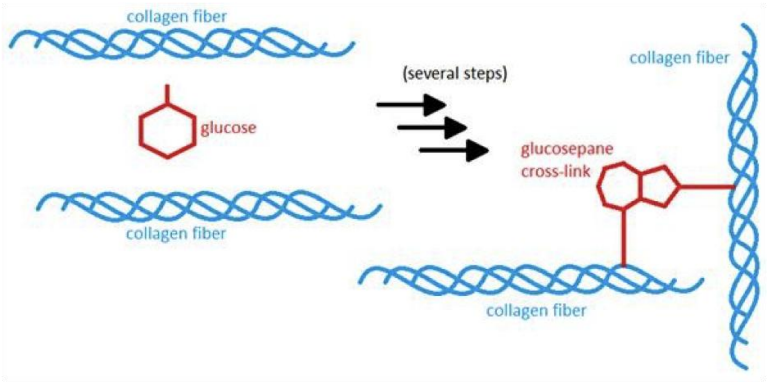

Figure.5: *Glucose glycation to form crosslinks on collagen fibres.*

1.6 Reference

1) Ostrovidov S, Shi X, Zhang L, Liang X, Kim SB, Fujie T, Ramalingam M, Chen M, Nakajima K, Al-Hazmi F, Bae H, Memic A, Khademhosseini A. Biomaterials. 2014;35(24):6268-77.

2) Hodde J. Tissue Eng. 2002;8(2):295-308.

3) Haugh MG, Jaasma MJ, O'Brien FJ. Journal of Biomedical Materials Research A. 2009;89(2):363-9.

4) Gomes SR, Rodrigues G, Martins GG, Henriques CM, Silva JC. Mater Sci Eng C Mater Biol Appl. 2013;33(3):1219-27.

5) Ratanavaraporn J, Rangkupan R, Jeeratawatchai H, Kanokpanont S, Damrongsakkul S. Int J Biol Macromol. 2010;47(4):431-8.

6) Madaghiele M, Piccinno A, Saponaro M, Maffezzoli A, Sannino A. J Mater Sci Mater Med. 2009;20(10):1979-89.

7) Tungtasana H, Shuangshoti S, Shuangshoti S, Kanokpanont S, Kaplan DL, Bunaprasert T, Damrongsakkul S. J Mater Sci Mater Med. 2010;21(12):3151-62.

8) I.Prasertsung, R.Mongkolnavin, S.Damrongsakkul, C.S.Wong. Surface and Coatings Technology. 2010;205(1):133-138.

9) Parenteau-Bareil, R.; Gauvin, R.; Berthod, F. Materials 2010, 3, 1863-1887.

10) Davidenko N, Bax DV, Schuster CF, Farndale RW, Hamaia SW, Best SM, Cameron RE. J Mater Sci Mater Med. 2016;27(1):14.

11) Lin WH, Yu J, Chen G, Tsai WB. Colloids Surf B Biointerfaces. 2016;138:26-31.

12) Lin WH, Tsai WB. Biofabrication. 2013;5(3):035008.

13) Cheung DT, Tong D, Perelman N, Ertl D, Nimni ME. Connect Tissue Res. 1990;25(1):27-34.

14) Ceylan S, Göktürk D, Bölgen N. Biomed Mater Eng. 2016;27(4):327-340.

15) Hamlekhan A, Moztarzadeh F, Mozafari M, Azami M, Nezafati N. Biomatter. 2011 (1):91-101.

16) Shivani Nanda, Nikhil Sood, B. V. K. Reddy, and Tanmay S. Markandeywar. Indian Journal of Materials Science, vol. 2013, Article ID 516021, 8 pages, 2013.

17) Davidenko N, Schuster CF, Bax DV, Raynal N, Farndale RW, Best SM, Cameron RE. Acta Biomater. 2015;25:131-42.

18) Krishnamoorthy G, Sehgal PK, Mandal AB, Sadulla S. J Biomater Sci Polym Ed. 2013;24(3):344-64.

19) Park SN, Lee HJ, Lee KH, Suh H. Biomaterials. 2003;24(9):1631-41.

20) Shepherd DV, Shepherd JH, Ghose S, Kew SJ, Cameron RE, Best SM. APL Mater. 2015;3(1). pii: 014902.

21) Bou-Akl T, Banglmaier R, Miller R, VandeVord P. J Biomed Mater Res A. 2013;101(9):2507-14.

22) Maier V, Lefter CM, Maier SS, Butnaru M, Danu M, Ibanescu C, Popa M, Desbrieres J. Mater Sci Eng C Mater Biol Appl. 2014;42:243-53.

23) Koh, L.B.; Islam, M.M.; Mitra, D.; Noel, C.W.; Merrett, K.; Odorcic, S.; Fagerholm, P.; Jackson, W.B.; Liedberg, B.; Phopase, J.; Griffith, M. J. Funct. Biomater. 2013, *4*, 162-177.

24) Nicoletti A, Fiorini M, Paolillo J, Dolcini L, Sandri M, Pressato D. J Mater Sci Mater Med. 2013;24(1):17-35.

25) La Gatta A, Schiraldi C, Papa A, D'Agostino A, Cammarota M, De Rosa A, De Rosa M. Carbohydr Polym. 2013 25;96(2):536-44.

26) Kumar V, Kumar N, Gangwar AK, Singh H, Singh R. J Surg Res. 2015;197(2):436-46.

27) Chiono V, Pulieri E, Vozzi G, Ciardelli G, Ahluwalia A, Giusti P. J Mater Sci Mater Med. 2008;19(2):889-98.

28) Huang-Chien Liang, Wen-Hisung Chang, Hsiang-Fa Liang, Meng-Horng Lee Hsing-Wen Sung. Journal of Applied Polymer Science. 2004;91(6):4017-4026.

29) Michael F. Butler, Yiu-Fai Ng, Paul D. A. Pudney. Journal of Polymer Science Part A: Polymer Chemistry. 2003;41(24):3941-3953.

30) Tonda-Turo C, Gentile P, Saracino S, Chiono V, Nandagiri VK, Muzio G, Canuto RA, Ciardelli G. Int J Biol Macromol. 2011;49(4):700-6.

31) Nath SD, Abueva C, Kim B, Lee BT. Carbohydr Polym. 2015 22;115:160-9.

32) Reich MS, Kishore V, Iglesias R, Akkus O. J Biomater Appl. 2014;28(9):1336-42.

33) Frohbergh ME, Katsman A, Botta GP, Lazarovici P, Schauer CL, Wegst UG, Lelkes PI. Biomaterials. 2012;33(36):9167-78.

34) Siimon K, Reemann P, Põder A, Pook M, Kangur T, Kingo K, Jaks V, Mäeorg U, Järvekülg M. Mater Sci Eng C Mater Biol Appl. 2014, 42:538-45.

35) Willems NM, Langenbach GE, Stoop R, den Toonder JM, Mulder L, Zentner A, Everts V. Mater Sci Eng C Mater Biol Appl. 2014, 42:15-21.

36) Mason BN, Reinhart-King CA. Organogenesis. 2013, 9(2):70-5.

37) Francis-Sedlak ME, Uriel S, Larson JC, Greisler HP, Venerus DC, Brey EM. Biomaterials. 2009, 30(9):1851-6.

38) Francis-Sedlak ME, Moya ML, Huang JJ, Lucas SA, Chandrasekharan N, Larson JC, Cheng MH, Brey EM. Microvasc Res. 2010, 80(1):3-9.

39) Boonkaew B, Tompkins K, Manokawinchoke J, Pavasant P, Supaphol P. Biomed Mater. 2014, 9(2):025001.

40) Wang J, He C, Cheng N, Yang Q, Chen M, You L, Zhang Q. J Nanosci Nanotechnol. 2015;15(7):4844-50.

41) Vicens-Zygmunt V, Estany S, Colom A, Montes-Worboys A, Machahua C, Sanabria AJ, Llatjos R, Escobar I, Manresa F, Dorca J, Navajas D, Alcaraz J, Molina-Molina M. Respir Res. 2015, 16:82.

42) Chiue H, Yamazoye T, Matsumura S. Biochem Biophys Res Commun. 2015, 461(3):445-9.

43) Lam PL, Kok SH, Bian ZX, Lam KH, Tang JC, Lee KK, Gambari R, Chui CH. Colloids Surf B Biointerfaces. 2014, 117:277-83.

PART II – ANALYTICAL TECHNIQUES

1. X-Ray Diffraction (XRD)

XRD is the most commonly used x-ray based analytical technique to characterize materials which provides accurate information about the crystallographic structure, size and orientation. Almost 95 % of solid substances are considered to be crystalline, on interaction with X-rays, solid substance gives a diffraction pattern. In the early 1900's, this innovative concept of identifying crystalline phases in solid substance was found by A. W. Hull in his paper titled, "A New Method of Chemical Analysis". The x-ray diffraction patterns are considered to be fingerprints of the pure substance. So far, around 50,000 inorganic and 25,000 organic single component crystalline phases, and diffraction patterns have been collected and stored on magnetic or optical media as standards.

1.1 Working principle of XRD

In order to understand the basic working principle, it is highly essential to understand the two different phases of solid substances which is the amorphous phase and crystalline phase.

(i) Amorphous: Random distribution of atoms representing a disordered arrangement

(ii) Crystalline: Homogenous distribution of atoms in a regular pattern, where the smallest volume element in three dimensions describes the crystal and is called as a unit cell. The dimensions of the unit cell are described by three axes: a, b, c and the angles between them as alpha, beta, gamma.

Under the influence of alternating electromagnetic field an electron will oscillate with the same frequency as the field. The electrons start to oscillate when an x-ray source hits a atom with the same frequency as the incoming beam. The resultant destructive interference is observed in all directions, which means the combining waves are out of phase and there is no resultant energy leaving the solid sample. Whereas in crystalline phase the atoms are in a regularly arranged pattern and there is a resultant constructive interference (Fig.1). Which means the resultant waves are in phase and there is a well defined x-ray beam from the sample at various directions. Therefore, the diffracted beam can be defined as a beam constituted by numerous scattered rays mutually reinforcing one another.

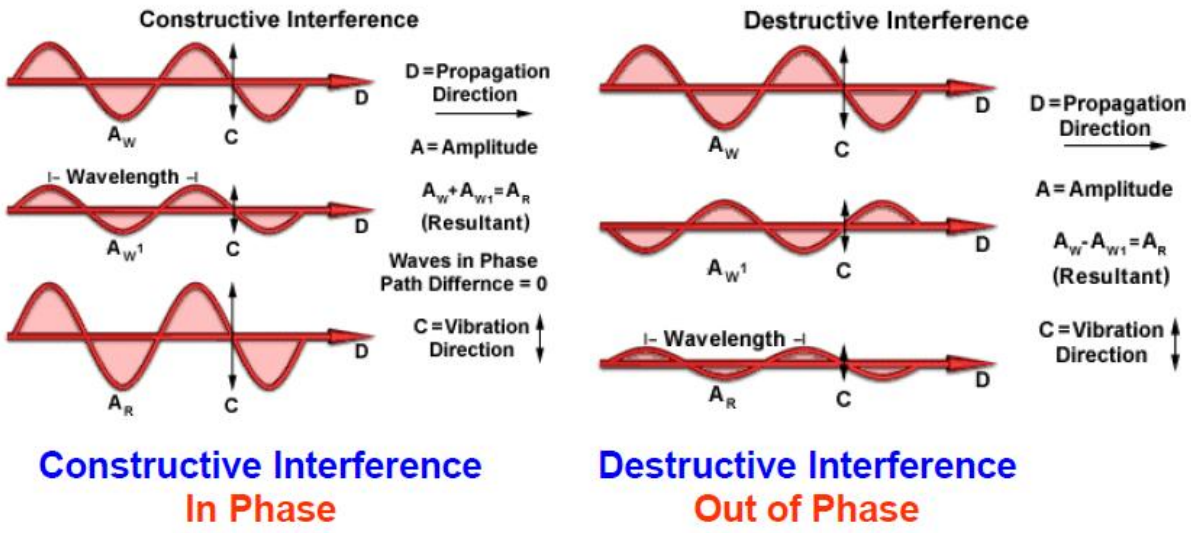

Figure 1: *Schematic representation of constructive and destructive interference*

The x-ray reflections from a series of parallel planes inside the crystal can be described from the orientation and inter-planar spacing's of the planes which are explained by the three integers h, k, l also called as indices. Therefore any given set of planes with indices h, k, l will cut the a-axis of the unit cell in h sections, the b axis in k sections and the c axis in l sections. Where, zero indicates that the planes are parallel to the corresponding axis. For example, if an x-ray beam incident on a pair of parallel planes P1 and P2 and is separated by an inter-planar spacing d. The parallel incident rays 1 and 2 makes an angle (THETA) with these planes. A reflected beam of maximum intensity will result if the waves represented by 1' and 2' are in phase (Fig.2). The difference in path length between 1 to 1' and 2 to 2' must then be an integral number of wavelengths, (LAMBDA). This can be mathematically expressed in Bragg's law as,

2d * sin q = n * l - Equation (1)

Here the reflection occurs from the plane set at angle THETA taken collectively from the incident and reflected beam. The unit cell determines the possible d-spacing within the three indices, thereby rewriting the Bragg's law as,

sin q = l / 2d – Equation (2)

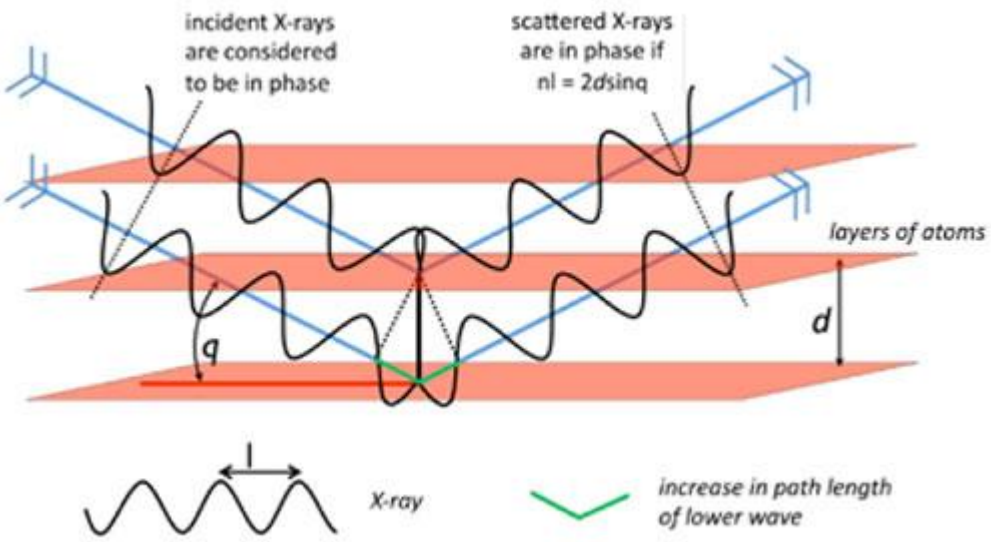

Figure.2: *Scattering of X-rays by crystalline substance*

Therefore, the unit cell dimensions determine the 2-THETA values based upon the reflection patterns and the spread of the reflection patterns are greatly dependent upon the distribution of the electrons in the unit cell where there is a relatively higher electron density around the atom. So, the intensities of the reflections are strongly dependent upon the location of the unit cell and the kind of atoms within the crystal. Therefore, the planes through high electron density will reflect strong intensities and planes with low electron density will reflect weak intensities. The invention of Bragg's law led to the award of Nobel Prize in physics in 1915 for (William Henry Bragg and William Lawrence Bragg) for their work in exploring the crystal structures of NaCl, ZnS and diamond.

1.2 Basics of crystallography

A crystal is defined by the periodic arrangement of several unit cells within the lattice, which contains a single atom or several atoms in a fixed planar arrangement. The crystal lattice defines the atom positions regularly. The distribution of atoms in crystal structure is based upon the any one of 14 Bravais Lattices derived from 6 Crystal System (Fig.3). Accordingly, each crystal system has a different axis length and angles that separate the atoms. The lengths of the axes are described as a, b, and c and the angles between the atom planes are described α, β and γ. The particular plane of an atom can be defined from the miller indices which clearly describes the

orientation with respect to the three axes of the unit cell. Miller indices can be calculated from the intercepts of the three axes by obtaining the reciprocal of the axis length.

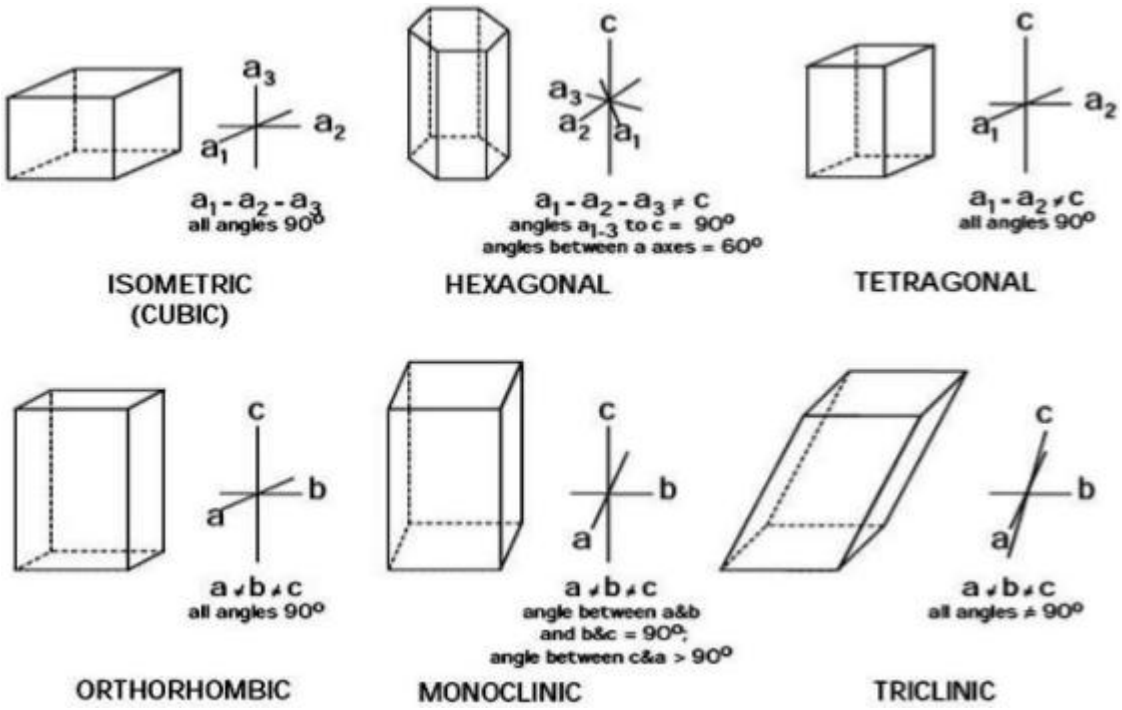

Figure.3: *Three-dimensional representation of Bravais lattice*

1.3 Instrumental set-up

Using an x-ray diffraction instrument two different categories of samples can be analysized which as follows,

(i) *Single crystal sample:* Also, known as perfect crystal, where all unit cells are aligned in an ordered extended pattern with average crystal cross section of 0.3 mm. The single crystal diffractometer can be used to identity molecular structure of novel compounds (natural or synthetic molecules).

(ii) *Powder or polycrystalline sample*: The sample can be ground to fine particles of 0.002 mm to 0.005 mm cross section ensuring to have a homogenous and smooth plane surface. Here, there is a random distribution of all planes (h, k, l) with reflected intensities parallel to the specimen surface.

The XRD instrument typically consists of four principal components, (i) X-ray tube, (ii) Goniometer and optical path, (iv) Sample holder and (iv) Detector (Fig.4)

The high-energy source of electrons causes the bombardment of atoms and eventually leads to the transition of electrons (excited state) from their shell to fill up the vacancy (ground state). The subsequent electron transition generates X-rays of a specific energy (with wave length in the range from 0.1Å to 100Å).

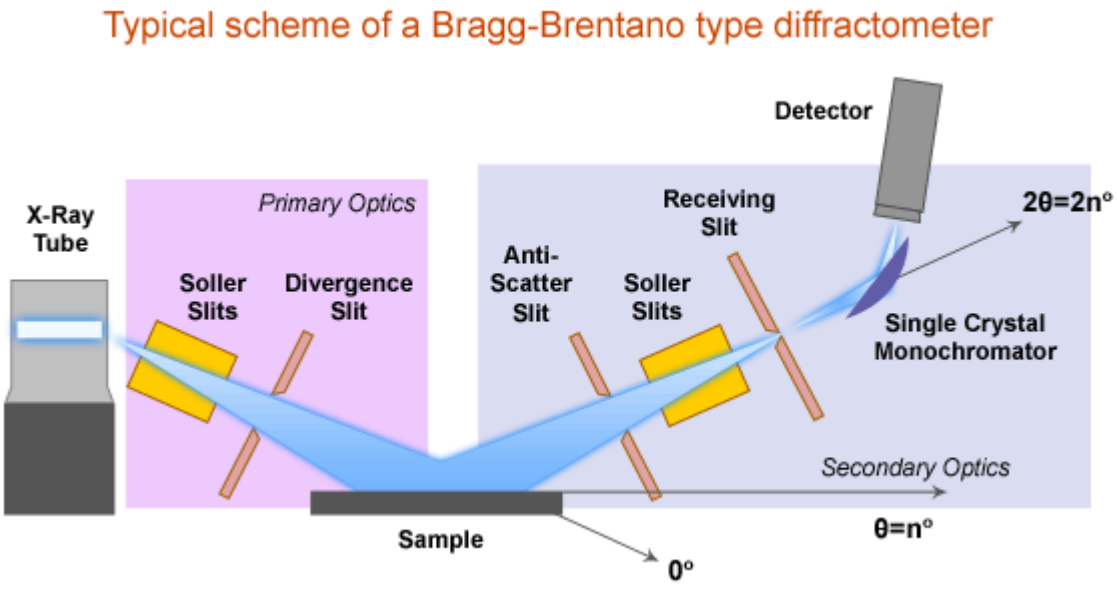

Figure.4: *Basic geometry representing the scheme of Bragg-Brentano diffractometer*

The x-ray goniometer assist in mounting the sample holder and detector arm in an appropriate position in order to obtain an ideal diffraction pattern. The distance between the sample to detector is same as the distance between the focal spot of x-ray to sample. Therefore, the x-ray tube is stationary, the sample rotates around the angle THETA and along with it the detector moves by the angle 2-THETA. A typical diffraction pattern consists of a series of reflected intensities against the detector angle 2-THETA depending on the goniometer configuration. The 2-THETA values of each corresponding peak are determined by the excited wavelength of the anode material within the x-ray tube. Therefore, by knowing the d-spacing, the area under the peak (intensity) and the indices h, k, l, a reflection peak can be defined and the dimension of the unit cell can be calculated.

The international Centre Diffraction Data (ICDD), duly maintains the information on d-spacing, chemical formula, relative intensity, RIR quality information and routing digit of various molecules. Therefore, by comparing the diffraction pattern of unknown substance against the database can provide detailed structural information about unknown materials.

Apart from, the resultant sharp crystalline peaks, the amorphous materials exhibit a broad background signal. This characteristic, broad signal is also exhibited by the organic and inorganic molecules. However, using XRD the degree of crystallinity can be determined by comparing the integrated intensity of the broad signal with the sharp peaks. The peak broadening is also contributed by other factors such as optics, convolution of the beam, particle size and crystal defect.

In this study, XRD (Panalytical X'Pert PRO, Bruker, Germany) coupled with Pixcel detector operating at 40 mA and 45 kV was used for experimental analysis.

2. Fourier Transform Infrared (FTIR)

An infrared spectrum represents a fingerprint of an unknown sample with distinctive absorption peaks which corresponds to the frequencies of vibrations between the bonds of the atoms that constitutes the material. Each and every material is unique in combination of atoms and no two compounds produce the exact same infrared spectrum. Therefore, infrared spectrums are considered to be positive identification (qualitative analysis) of every different kind of material. Moreover, the size of the peaks in the spectrum is a direct indication of the amount of material present. In infrared spectroscopy, IR radiation penetrates through the sample. The absorbed infrared rays are passed through (transmitter) and the resulting spectrum represents the molecular absorption and transmission, creating a molecular fingerprint of the material.

2.1 Different types of IR Absorptions

The stretching and bending of covalent bonds in molecules are recorded as absorptions and a typical IR spectrum runs from 4000 to 400 cm^{-1}. The IR absorption is associated with a stretch or bend which changes the dipole moment of the molecules. Molecules with symmetric bonds such as

N_2, O_2, or F_2 do not absorb in the infrared because the bond stretching does not change the dipole moment of the molecule. Primarily there are two modes of vibrations which can be either stretching or bending. Thus, the stretching can either be symmetric or asymmetric (Symmetric allows the

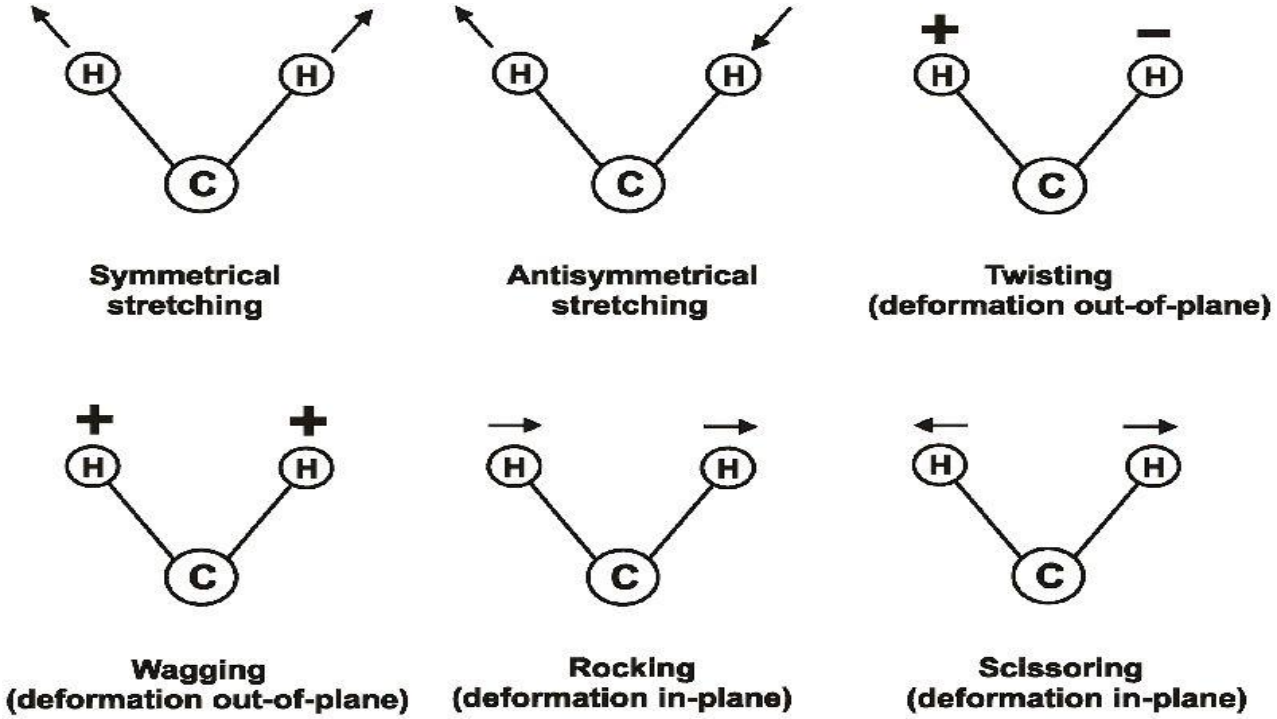

Figure.5: *Molecular vibrations in infrared spectroscopy*

molecules to move through space whereas the asymmetric increases or decreases the bond length). A molecule with more than three atoms can experience a bending vibration, a vibrational mode where the angle between atoms changes (Fig.5). Under the influence of certain frequency, the molecule is excited to the vibrational state. For a bond to be excited, it must be exposed to certain radiation of the exact same frequency as the energy difference between ground and excited states (ΔE). Thus, deceiving these frequencies and representing them provides information on the bonds that exist in a molecule. These frequencies, fit within the infrared region of the electromagnetic region. Therefore, in an IR spectrometer, the detector portraits the plot percent transmission of the radiation through the molecule versus the wave number of the radiation. A downward peak on the plot represents the absorption at a specific wave number. Thus, obtained IR spectrum can be divided into two regions which is namely the functional group region and the fingerprint region.

The fingerprint region is unique for each and every individual molecule, whereas the functional groups region can be the same for two different molecules because of the similar functional groups in their structure.

2.3 Intensity and Position of Absorption bands

The change in dipole moment of the bond determines the intensity of an absorption band. The change in dipole moment can be for two reasons, (i) the bond length and (ii) the charge difference between the two atoms. When a photon is absorbed, it undergoes stretching and the bond length changes. So, when there are two different atoms, there exist an electronegativity difference and a photon will be absorbed. In case, there is no electronegativity difference, (for e.g., O_2 or an N_2 molecule) then a photon is not absorbed and there is no molecule excitation at higher level.

So, the larger is the electronegativity difference, the more intense the absorption. Additionally, the number of the specific bond also determines the intensity of a peak. For e.g., the IR spectra of octane molecule will have a much more intense C-H peak because it has many more C-H bonds than methane.

FTIR spectroscopy has more advantages and it is preferred over dispersive or filter methods due to the following benefits (i) it is a non-destructive technique, (ii) robust and precise measurement, (iii) no external calibration, (iv) increased sensitivity and greater optical throughput and (v) mechanically simple. The sample preparation for FTIR includes grinding the sample finely using a mortar and pestle along with potassium bromide (reference material used to remove scattering effects). Thus obtained, ground powder is pressed at 8000 psi to produce transparent discs or pellet and used for analysis.

In this study, the functional group analysis was carried out using Nicolet 380 FT-IR spectrometer (Thermo Fisher Scientific Inc, Waltham, USA).

3. Inductively Couple Plasma Atomic Emission Spectroscopy (ICP-AES)

ICP-AES is one of the most widely used technique for elemental analysis. The working principle involves the use of plasma source to dissociate the sample into its constituent atoms or

ions and then excite them to produce photons of characteristic wavelength is while returning to the ground state depending on the element. The emitted light is recorded by the optical spectrometer using a detector and the quantitative element analysis of the sample can be determined from the calibrated standards.

(A) (B)

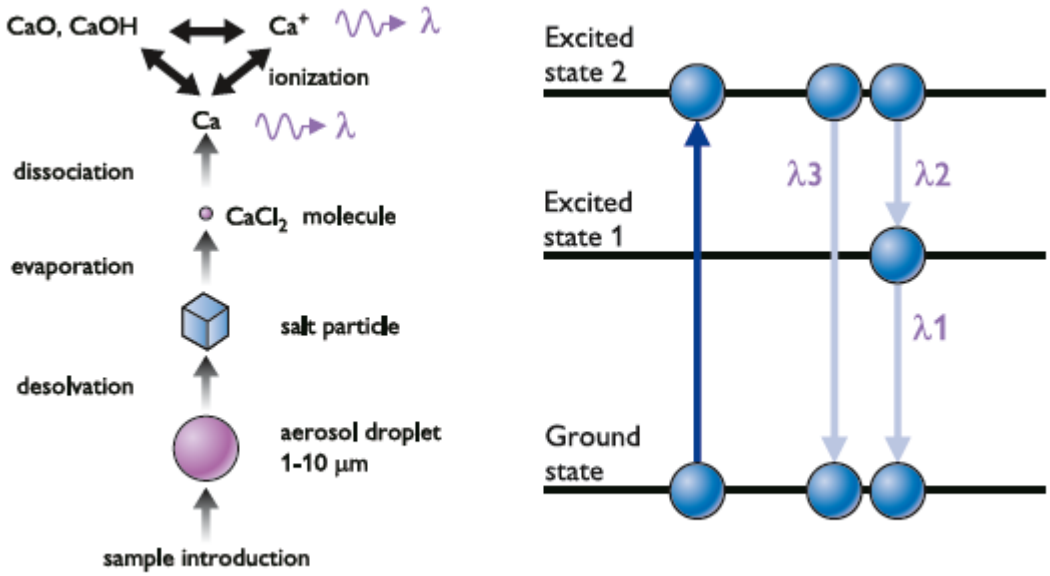

Figure 6: *(A); Sample volatilization and atomization under plasma (B); Atom excitation and wavelength emission*

Briefly, prior to analysis the sample is subjected to nitric acid (65 wt.%) digestion followed by subsequent sonication and dilution. The diluted sample solution is transformed into an aerosol by a nebuliser. The bigger droplets are separated from the smallest in a specialized spray chamber. Only smallest droplets (1-10 µm) are transferred by an argon flow into the ICP-AES, the argon plasma. The bigger droplets (>90%) are pumped out as waste. Considerably high temperature is highly essential in order to attain a strong atomic emission from all chemical elements. The highest amount of atomic emission is reached at temperatures in the range of 7,000 K to 10,000 K. Such high temperature can be obtained through inert-gas plasma. A highly gaseous state of matter is known as plasma which contains major concentrations of essential free electrons and highly charged ions.

Plasma is considered to be an effective medium for volatilization and atomization of liquid droplets. When the aerosol droplets are in direct contact with the hot area of the plasma they are transformed into salt particles by desolvation (Fig.(A)). These salt particles are segregated into individual molecules that will subsequently fall apart to atoms and ions. Most elements get ionized very efficiently (> 90%).

When these excited atoms and ions return to their ground state or to lower excitation states they will emit electromagnetic radiation in the ultra-violet/visible range of the spectrum (Fig.6(B)). Each excited element emits specific wavelengths which has a typical emission spectrum. The intensity of the radiation is proportional to the element concentration.

Commercially available element standards can be used to calibrate the ICP-AES, which helps in precise quantitative analysis. The spectrometer separates the specific wavelengths and the detector measures the elements. The resultant emission spectrum is a plot of the radiation intensity (y-axis) versus the wavelength (x-axis). Predominantly in plasma the single charged ions are abundant, but free atoms are also present. Both of these ions will be excited and then emit radiation. So, there is a possibility of the many different transitions from various excited states. For e.g., sodium has six excited states which produce fifteen wavelengths, so an emission spectrum can be complicated. Moreover, there is also the overlapping of wavelengths produced by the other elements. For each element, the natural emitted wavelengths are constant in nature. Therefore, overlap of emission from different elements can be predicted and taken into account.

In this study, ICP-OES, Agilent Technologies 5100 ICP-OES, (Santa Clara, USA) was used for the quantitative determination of ions.

4. Scanning Electron Microscopy

A Scanning Electron Microscope (SEM) is an electron microscope that utilizes the electrons instead of light source to create a magnified image. SEM can be used to produce high resolution images of the sample surface with the ability to magnify well above 100,000 times (3 nm resolution) whereas the light microscopes are only able to magnify approximately 1000 times. SEM

can be used to observe the surface properties of various natural and synthetic materials, biological tissues, microorganisms and plant specimens.

1.4 Working principle

The metallic filament generates electrons which is also called as the electron gun. The emitted electrons then form the beam which is accelerated down the column towards the specimen. The beam is more focused and guided by electromagnetic lenses as it travels down the column. On reaching the specimen, the electrons are knocked loose from the surface of the specimen. These electrons are called as secondary electrons. The secondary electrons are detected and amplified as the signals hit the monitor screen. The electron beam scans the entire sample by moving front and back aiming to build an image from the number of electrons emitted from each spot on the sample (Fig.7). This entire process takes place inside a vacuum chamber, ensuring the interference of air is avoided and the electron beam interacts with the sample alone.

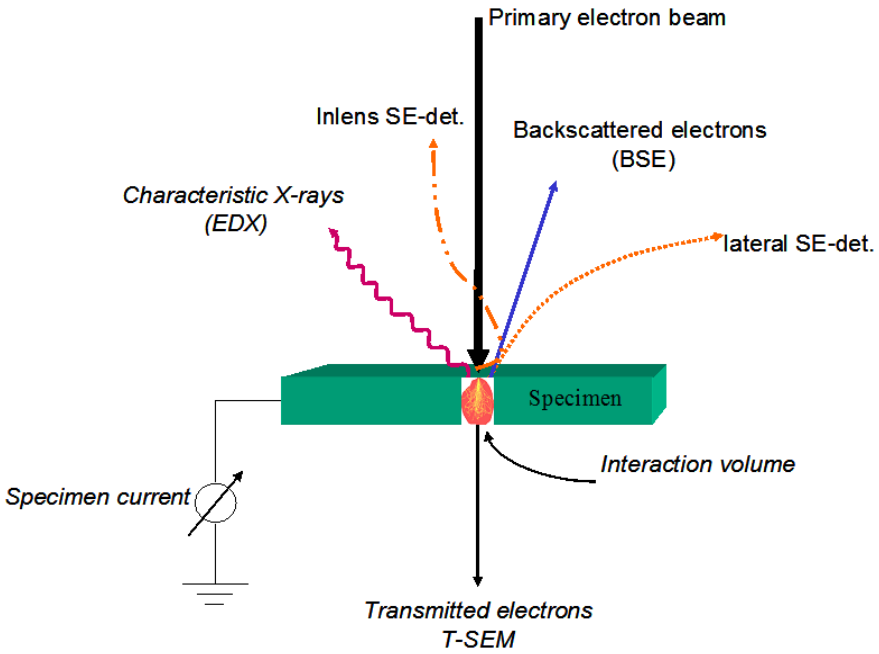

Figure.7: *Interaction of electron beam with sample*

4.2 Components of SEM

The principal components of a typical SEM are (i) electron column, (ii) scanning system, (iv) detector(s), (v) display, (vi) vacuum system and (vii) electronics controls (Fig.8). The electron

column of the SEM contains an electron filament with two or more electromagnetic lenses. The electron gun or filament generates the free electrons and accelerates these electrons to energies in the range 1-40 keV. The need of the electron lenses is to create a small, focused electron beam on the specimen. The generated electron beam hits the specimen surface with spot size less than 10 nm in diameter with a capacity to form an image.

To produce an image the electron beam is focused into a probe, which is scanned across the surface of the specimen with the help of scanning coils. The region of the specimen that is struck by the accelerated electrons emits signal in the form of electromagnetic radiation. The resultant radiations, are usually secondary electrons and/or backscattered electrons which is collected by a detector and the final signal is amplified and displayed on the computer monitor.

The electron beam can interact with the specimen surface with approximately depth of 1 μm.

The beam electrons with the atoms of the specimen produce wide variety of radiation resulting in complex interactions. When the need of high-magnification imaging is required, the sufficient knowledge of electron optics, beam-specimen interactions, detection, and visualization processes is highly essential in order to better understand the complex interactions the resultant image.

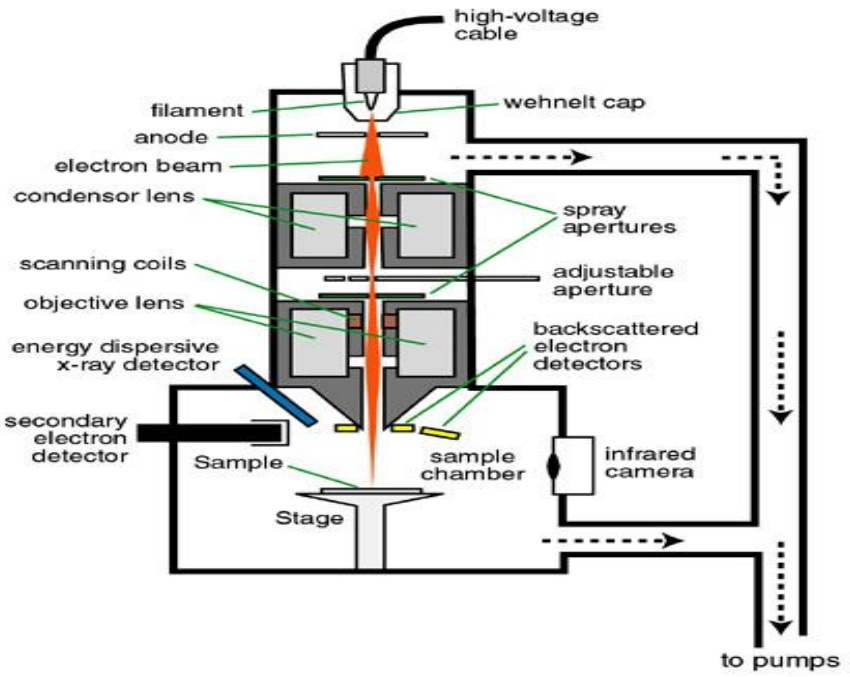

Figure.8: *Fundamentals components of a typical SEM equipment*

4.3 Lenses of SEM

The electron lens serves to produce a convergent electron beam with desired cross-over diameter. The lenses are metal made with cylindrical hole, within the lenses the magnetic field is generated, which in turn is subjected to focus or defocus the electron beam passing through the hole of the lens. There are three condenser lenses to de-magnify the electron-beam in the electron gun to a smaller size. The first and second condenser lenses control the amount of demagnification. The third lens in the column is called as “objective” which primarily focuses the probe on the sample. The design of the lenses, usually includes a space for the scanning coils, the stigmator, and the beam limiting aperture. Since the high current flows through the lenses which apparently generates excessive heat and they are cooled by circulating water.

4.4 Interaction volume

For the valuable interpretation of the SEM images, the concept of interaction volume of the primary beam electrons and the sampling volume of the emitted secondary radiation are important. The detailed image quantification and the resolution of the images are determined not only by the size of the electron probe but also by the size and characteristics of the interaction volume.

The penetration of the electron beam into the solid is controlled by the joint effect of elastic and in-elastic scattering. The region, where the incident electrons interact with the sample is called as interaction volume. The interaction volume has several important characteristics, which determine the quality of imaging in the SEM. The interaction volume increases with increasing incident beam energy and decreases with increasing average atomic number of the specimen.

4.5 Issues with SEM

Contamination is a common problem in SEM analysis, because the presence or interference of foreign material can affect the signal at high-resolution imaging. Hydrocarbon molecules are attracted to the beam location and form build-up, which can disrupt the fine-detail imaging features. Contamination can be avoided by maintaining appropriate vacuum within the specimen chamber and another possibility is UV (Ultraviolet) exposure of the specimen before analysis so the UV

crosslinking can reduce the contamination build-ups. Another important problem is charging, this is more often observed whenever a specimen or portion of it is an insulator. The charges injected by the beam cannot readily flow to ground, therefore there is an accumulation of charges. The specimen is in a continually changing state of surface potential due to the accumulation and discharge of electrons. The charging effect can be avoided or minimized by coating the sample with conductive film, adopting rapid scanning, by imaging using back scattered electrons and using low accelerating voltage.

In this study, the surface morphology was studied using SEM (FEI, Quanta 200, UK) and gold sputter coater (Q150TES, Quorum, Italy).

5. Thermogravimetric Analysis (TGA)

The weight changes in a material as a function of temperature or time under a controlled gaseous atmosphere can be measured precisely using a TGA. Using TGA, the material thermal stability, filler content in polymers, moisture and solvent content, decomposition temperature and the percentage composition of components in a compound can be measured.

The basic working principle lies on gradually raising the temperature of a sample in a gaseous furnace as its weight loss is monitored on an analytical balance that remains outside of the furnace. The main components of a TGA instrument is the temperature controlled cylindrical chamber, sample pan furnace and a purge gas supply system. During the analysis, the sample specimen is heated up in a controlled environment chamber which provides a stable temperature environment for a consistent measurement. Purging gas is provided from both horizontal and vertical directions. In horizontal flow, 60ml/min can be either air or nitrogen depending on the type of decomposition and the specific testing purposes. The vertical flow, 40 ml/min is always nitrogen, to prevent oxidative degradation of the balance elements. The mass loss of the sample is measured with a photodiode balance using a null-balance principle which measures the current required to return the meter to the null position.

The typical results of TGA includes, (i) thermal reactions causes mass loss as the result of loss of a volatile component and (ii) chemical reactions included combustion which again involves the mass loss of sample. The characteristic result of a TGA graph elaborates the weight of the sample plotted against temperature or time to illustrate the thermal transitions in the material – such as loss of solvent and plasticizers in polymers, water of hydration in inorganic materials, and final decomposition of the material.

In this study, the pyrolytic pattern of the scaffolds was determined using Thermo Gravimetric Analyser (TGA) (STA 449/C Jupiter, Netzsch Germany).

6. Dynamic mechanical analysis (DMA)

DMA is a simple mechanical analyser where an oscillating force is applied on to a sample and the material's response to force is measured. From the resultant mechanical behaviour, the tendency to flow (viscosity) from the phase lag and the stiffness (modulus) from the sample response can be calculated. Basically, the visco-elastic properties of the materials under certain oscillating force is measured which is referred as the ability to lose energy as heat (damping) and the ability to recover from deformation (elasticity).

The DMA mechanical response provides information of elastic or Hookean behaviour and viscous or Newtonian behaviour. The Hooke's law states that the deformation or strain of the spring is linearly related to the constant force or stress (Fig.9). Which can be mathematically expressed as,

$$\sigma = k * \gamma$$

where *k* is the spring constant. As the spring constant increases, the material becomes stiffer due to increase in the slope of the stress–strain curve thereby eventually the young's modulus also increases. The material's stiffness can be defined from the ratio of stress to strain. In an extension system, the modulus (*E)* can be expressed as mathematically as,

$$E = d\sigma\ d\varepsilon$$

For example, if the test is under the shear, the modulus is denoted by (*G)* and in bulk as *(B)* by knowing the Poisson's ratio (ν) which is the measure of material volume in regard to changes with deformation under extension, where it can be denoted for isotropic material as,

$E = 2G(1- \nu) = 3B(1- 2\nu)$

Whereas for an elastic material, the inverse of modulus is the compliance (*J).* The compliance is a measure of a material's willingness to yield. The relationship can be expressed as

$E = 1 / J$

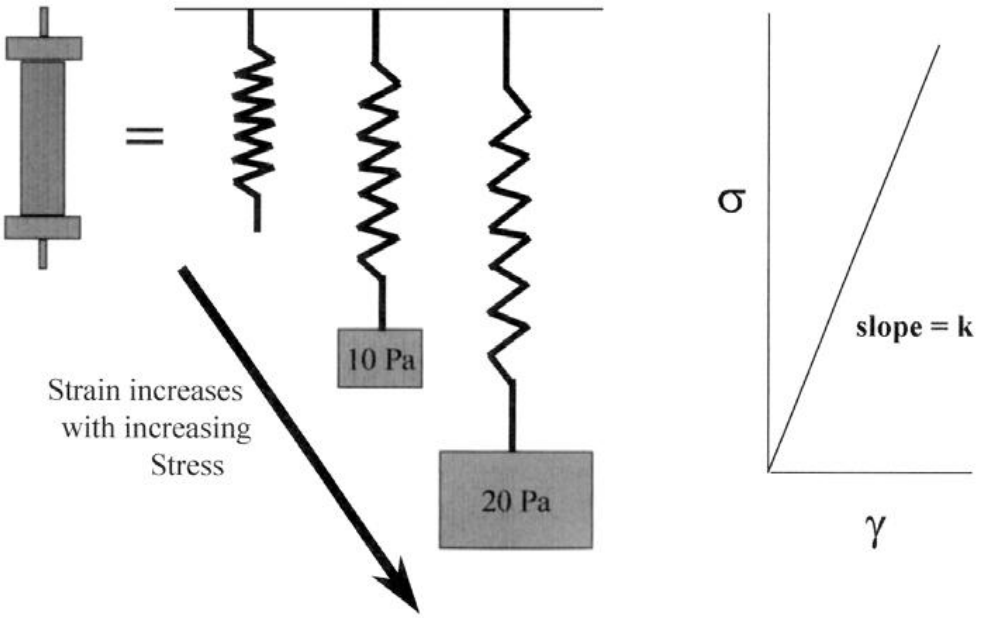

Figure.9: *Hooke's law and stress-strain curve with slope representing the linear region to determine the young's modulus*

An elastic material provides a linear response where the modulus is independent of load and of loading rate. Unfortunately, most materials are not truly elastic, for example the polymeric material in extension, the stress–strain curve isn't linear instead there is curvature due to sample deformation. This phenomenon becomes more evident as the stress increases and the material deforms. In such cases, the curve has the initial linear region immediately followed by a nonlinear region. This characteristic feature is due to the sample necking and subsequent failure, here it is difficult to identify and calculate the young's modulus due to the limited linear portion.

However, in such difficulties, the yield point of the material can be calculated which is defined as the maximum stress required for the sample failure. Therefore, at the some load the material will fail (break) and this is called as the ultimate strength. After the sample reaches the yield strength there is an immediate deformation of the sample. The area under the curve is proportional to the energy needed to fracture the sample. Therefore, the shape of this curve and its area defines whether the polymer is tough or brittle and strong or weak.

6.1 Working principle

The basic operating principle of the DMA is based on the oscillatory force which causes the sinusoidal stress to be applied to the sample, which eventually creates a sinusoidal strain. Upon measuring both the amplitude of the deformation at the peak of the sine wave and the lag between the stress and strain sine waves, the material response like the modulus, the viscosity, and the damping can be calculated. The ratio between stress to strain is the modulus (*E*), which provides information about the material's stiffness, or its ability to resist deformation. The slope (initial linear portion) of the stress–strain curve is known as the young's modulus a typical indicator of material behaviour. The advantage of using DMA is that, a modulus value at each time is obtainable when a sine wave is applied, allowing us to sweep across a temperature or frequency range. For example, if an experiment at 1 Hz or 1 cycle/second is initiated, it is possible to record a modulus value every second. Similarly, as a function of time or temperature the modulus can be recorded.

Also, wide frequency or shear rate range of 0.01 to 100 Hz in less than 2 hours can be obtained.

However, the modulus measured from the DMA stress-strain curve is not exactly the same as the Young's modulus of the classic stress–strain curve. In DMA, a complex modulus (*E**), an elastic modulus (*E*′), and an imaginary (loss) modulus (*E''*) are measured from the material behaviour to the sine wave. This helps in better characterization of the material, because with these different moduli it is possible to calculate the ability of the material to return or store energy (*E*′), to its ability to lose energy (*E''*) and the ratio of these effects (tan delta), which is also called as damping.

In this study, the both static compression test and dynamic mechanical test were performed in compression clamp using Q800 DMTA analyser (USA)

7. Reverse time – Polymerase chain reaction (RT-PCR)

RT-PCR is a molecular biology technique where the DNA is amplified to qualitatively detect the gene expression. Quantitative reverse transcription PCR (RT-qPCR) is employed when RNA is the starting material. During the initial process the RNA is first transcribed into complementary DNA (cDNA) by reverse transcriptase from total RNA or messenger RNA (mRNA). Then cDNA serves as a template for the qPCR reaction. RT-qPCR is considered widely in several applications which includes gene expression analysis, RNAi validation, microarray validation, pathogen detection, genetic testing, and disease research.

RT-qPCR is either performed as one-step or a two-step assay.

(i) One-step assays: PCR reactions is done in a single tube with reverse transcriptase along with a DNA polymerase. This reaction utilizes sequence-specific primers.

(ii) Two-step assays: The reverse transcription and PCR steps are carried out in separate tubes, with different optimized buffers, reaction conditions, and priming strategies (Fig.10)

The template for reverse transcription needs to be either total RNA or purified mRNA. Usually using total RNA is more advantageous than the mRNA because of high sensitivity, limited purification steps, enhanced quantitative recovery of the template and a better ability to normalize the results to the starting number of cells. In addition, the skewed results due to different recovery yields for different mRNAs can be avoided. Collectively, total RNA is more suitable than the purified mRNA because the relative quantification of the targets is more important for most applications than the absolute sensitivity of detection.

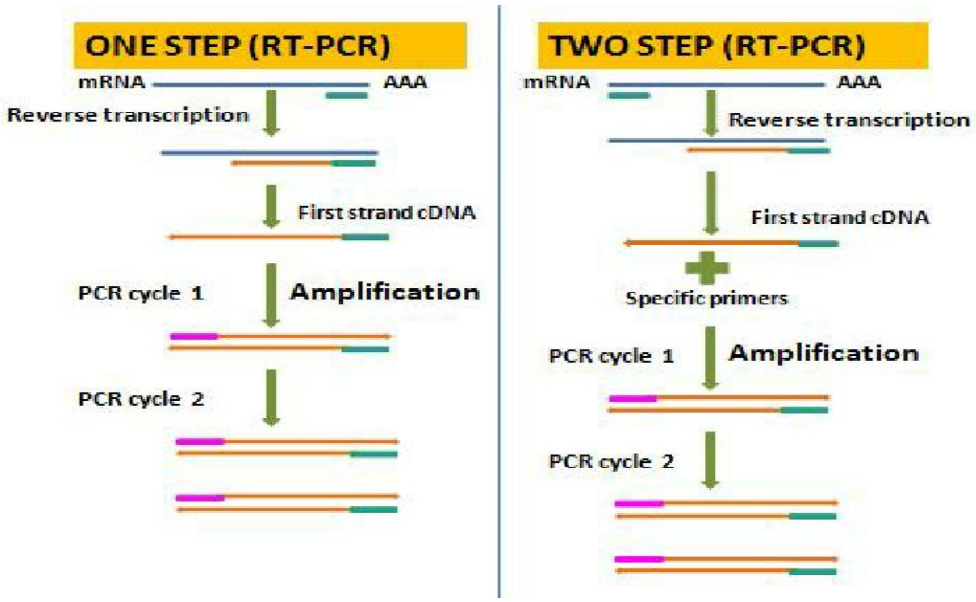

Figure.10: *Difference between 1-step and 2-step PCR reactions*

The enzyme reverse Transcriptase builds DNA from RNA. Few enzymes possess the inherent RNase activity to degrade the RNA strand in the RNA-DNA hybrid after transcription. However, if an enzyme does not possess RNase activity, an RNaseH is be added for better qPCR efficiency. The most widely used enzymes are Moloney murine leukemia virus reverse transcriptase and Avian myeloblastosis virus reverse transcriptase. It is highly essential to choose a reverse transcriptase with high thermal stability, because this ensures cDNA synthesis to be performed at higher temperatures and successful transcription of RNA with high levels of secondary structure, while preserving their full activity to yield high cDNA throughout at the end cycle. In RT-PCR, the priming of cDNA reactions in two-step assays includes oligo (dT) primers, random primers, or sequence specific primers. However, a mixture of oligo (dT)s and random primers are often used. These primers anneal to the template mRNA strand and provide reverse transcriptase enzymes a starting point for synthesis (Fig.11)

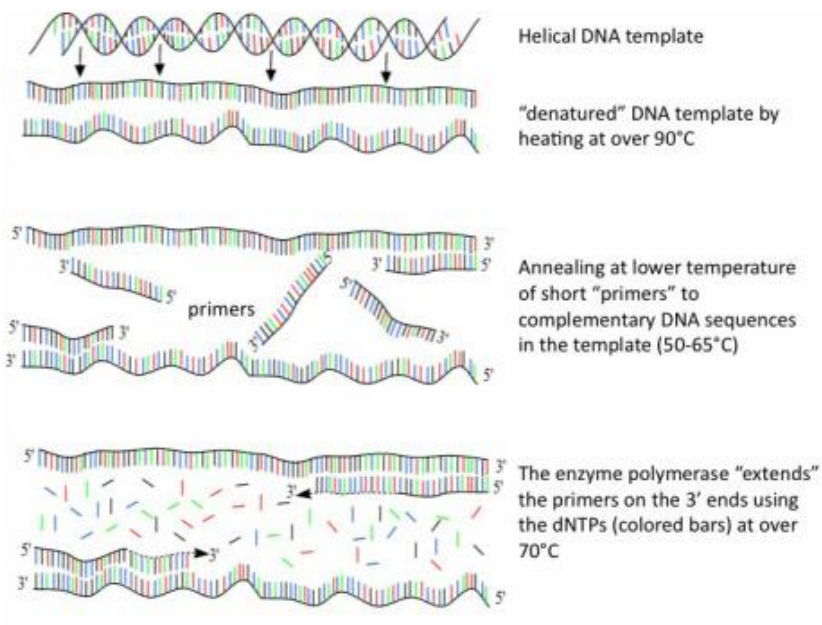

Figure.11: *Different cycles in the RT-PCR reaction*

The efficient synthesis of double-stranded DNA is initiated by the RNase H which allows the degradation of RNA from RNA-DNA duplexes. However, with long mRNA templates, RNA may be degraded prematurely resulting in truncated cDNA. It is generally essential to minimize RNase H activity when producing long transcripts for cDNA cloning. But, the intrinsic RNase H activity is best preferred in qPCR applications because they can accelerate the melting of RNA-DNA duplex during the first cycles of PCR. PCR primers should be designed to span an exon-exon junction, with one of the amplification primers potentially spanning the actual exon-intron boundary. This avoids the risk of false positives from amplification of any contaminating genomic DNA, since the intron-containing genomic DNA sequence will not be amplified.

A minus Reverse Transcription control (-RT control) should be included in all RT-qPCR experiments to test contaminated DNA (such as genomic DNA or PCR product from a previous run). In minus RT control, all the reaction components are present, except the reverse transcriptase. Reverse transcription should not occur in this control, so if PCR amplification is observed, then this is due to the contaminating DNA.

In this study, gene expression studies were assessed by StepOne Real-Time PCR System (Applied Biosystems, USA).

8. Fluorescence microscopy

George Gabriel Stokes coined the word "fluorescence" in 1852 as reported in his article [On the change of refrangibility of light, Philosophical Transactions of the Royal Society of London 142:463-562 (1852)]. He describes fluorescence as a form of quantum mechanical process termed as "photoluminescence", which is a visible optical radiation, leading to emission of photon during the energy transition from an excited (higher energy) state to its (lower energy) ground state. Depending on the lifetime of the excited state, fluorescence (~ 10^{-9}...10^{-6} s) and phosphorescence (~ 10^{-3}...1000 s) can be distinguished.

The spontaneous emission of light during energy transition (lowest vibrational energy level s_1 to ground state s_0) is known as fluorescence. The selection rule ($\Delta S = 0$) is obeyed in the spin-allowed process, in contrast to phosphorescence, where a forbidden non-radiative transition into an iso-energetic vibrational level of a triplet state T_1 with change of multiplicity occurs (inter system crossing). As a result of the Franck-Condon principle as well as inner non-radiative de-excitation (internal conversion), an increase of the wavelength of absorbed and emitted photon occurs (Stokes shift), $\Delta\lambda = \lambda_{em} - \lambda_{abs} > 0$ (Fig.12(A)). Fluorescence microscopy emerged to be an essential investigating tool in biology and materials science due to its beneficial features that are not readily available in other optical microscopy techniques. The potent usefulness of fluorochromes have offered the possibility of identify cells and their sub-microscopic cellular components with a high degree of specificity. The fluorescence microscope can be used to identify the presence of a single or multiple fluorescing molecule using different molecular probes recognizing precisely the target molecules.

(A) (B)

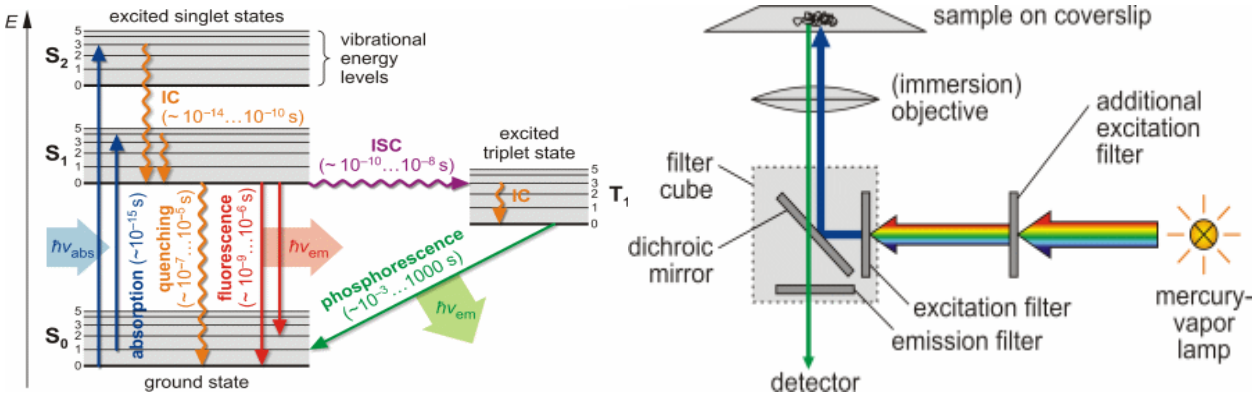

Figure.12:*(A):Quantum mechanical processes of fluorescence and phosphorescence, (B):Schematic working principle of fluorescence microscopy*

August Köhler and Henry Siedentopf developed jointly the fluorescence microscopy at Carl Zeiss AG in Jena and in April 1908, they presented to the public on the occasion of a microscopy course at the botanical institute in Vienna. Originating from the reflected light microscopy, it is more specifically termed epi-fluorescence microscopy. The basic working principle of the fluorescence microscope is based upon the irradiation of the sample specimen with the required wavelength and later to separate the emitted (fluorescent) light from the excitation light. Through the detectors, only the emitted light reaches the eye showing the fluorescent sample with dark background. The exciting light is typically 10^5 or 10^6 times brighter than the emitted light. The graphical representation of a fluorescence microscope with its essential parts are illustrated in Fig.12(B). A light source is generated from the lamp, with a specific wavelength or set of wavelengths within the UV range through a wavelength selective exciter filter. The required wavelength light passes through the sample specimen and reflects off a dichromatic mirror using the objective lens. If the sample specimen fluoresces, the emission light is collected and moves through the dichromatic mirror and finally percolates through a barrier filter that prevents the excitation wavelengths. Despite of the direction of the exciting light, the emitted light re-radiates spherically in all directions.

8.1. Issues with fluorescence microscopy

Photobleaching: A natural permanent loss of the ability of a fluorophore to fluoresce due to photochemical destruction of the fluorophore when exposed to the excitation light is known as photobleaching. The average number of excitation-emission-cycles is largely dependent on the intensity and energy of the excitation light and mainly the molecular structure of the fluorophore and its chemical environment. Bleaching can affect the fluorophore even after emission, therefore photobleaching is more a serious problem and a way to avoid this phenomenon is to reduce the intensity or duration of light exposure. Furthermore, the illumination can be controlled by focussing only the region of interest. Additionally, the number of fluorophores can be increased but there are also issues of toxicity due to high concentration in living cells.

Phototoxicity: Selective cell death of the living cells due to fluorophore illumination. Though the phenomenon is not yet fully understood, the formation of oxygen radicals due to non-radiative energy transfer seems to be the main causative factor. This toxicity is greatly dependent on the kind of fluorescent molecule used, therefore reducing intensity and time of illumination can prevent cell damage during fluorescent imaging.

In this study, inverted Ti-E fluorescence microscope (Nikon, Japan) was used for cell imaging.

PART III – EXPERIMENTAL WORK

Chapter I: To evaluate the different crosslinking strategies on functional modification of gelatin for tissue engineering applications

1. Introduction

Gelatin is a denatured derivative of collagen which is bestowed with advantageous properties such as low cost, non-immunogenicity, high biocompatibility and good biodegradability, thereby making it an exemplary scaffold material for tissue engineering application. [1,2]

The thermal denaturation of collagen leads to the collapse of triple helical structure and to form random coils. This disordered coils of collagen are known as gelatin. This protein is abundant in nature and usually derived from mammalian connective tissues of skin, tendon and bone. [3] Gelatin is generally used in food industry (gelling agents), pharmaceuticals (soft capsules) and in biomedical applications (vascular prostheses and wound dressings). When compared to collagen, gelatin does not elicit any immunogenic response in physiological condition and it is readily resorbable under in vivo conditions. [4] Moreover, the most attractive feature of gelatin is the affordability and economical aspects, which can be easily obtained and processed in large volumes.

The gelatin molecules undergo a sol-gel transformation which is temperature dependent. At temperature >40°C the aqueous gelatin solution is in the sol state, whereas when cooled at room temperature they change into gel. So, this transformation of sol-gel transition is due the conformational disorders within the gelatin chains. This apparently causes the formation of thermo-reversible networks by the adjacent helices through the hydrogen bonds. This unique sol-gel transition property of gelatin has been greatly exploited in tissue engineering application for producing mechanically stable biomaterials. [5-7]

In contempt of its attractive characteristics and as a template for tissue remodelling, gelatin possess few disadvantages such as low mechanical strength and high solubility in aqueous solution. So, in order to confront and the improve the physical and mechanical parameters, the gelatin moieties are often crosslinked by stabilizing agents. [8,9]

The main objective of this study is to use different crosslinking strategies such as physical (DHT), chemical (1, 4-butanediol diglycidyl ether (BDDGE)) and natural (Genipin) methods to develop an ideal scaffold from gelatin for tissue engineering application. In this work, we tend to investigate the feasibility of choosing different crosslinkers and controlling their crosslinking ratio to produce biocompatible and mechanically stable gelatin scaffolds for tissue engineering applications. Thus, porous gelatin crosslinked with various reactive groups were prepared and characterized with the objective to compare their physio-chemical and biological features. To this aim, a comparative evaluation was performed on different scaffolds to determine the effect of porosity, water uptake, degradation and mechanical performance. Additionally, the in vitro biocompatibility was evaluated using human chondrocytes to assess the cell viability, proliferation and differentiation. The chondrogenic gene expression for specific markers were estimated by real time quantitative-Polymerase chain reaction (qPCR) and western blot analysis.

2. Preparation of scaffolds

3D porous scaffolds were prepared from commercial pig skin gelatin (Type A, Bloom number: 280)**.** Briefly, the gelatin was dissolved in demineralised water (dH2O) at 40° C to obtain a 5 % (w/v) aqueous solution. Accordingly, the following procedure was used to prepare the crosslinked scaffolds.

(i) DHT crosslinked scaffolds were prepared by pouring the 5% (w/v) gelatin solution to a polystyrene multi-plate (12-wells) and allowed to cool at 25±2° C to form a gel.

(ii) BDDGE (Sigma Aldrich, USA) crosslinked scaffolds were prepared by adding appropriate amount of BDDGE (10% (w/w), pH.10) to 5% (w/v) gelatin solution. The resulting solution was mixed homogenously under stirring condition at 40° C for 15 min. Later, the aqueous mixture was poured on to polystyrene multi-plate (12-wells) and the crosslinking reaction was carried at 25±2° C for 48 h.

(iii) Genipin (Wako, Germany) crosslinked scaffolds were prepared by adding appropriate amount of BDDGE (1.5% (w/w), pH.6) to 5% (w/v) gelatin solution. The resulting solution was mixed

homogenously under stirring condition at 40° C for 15 min. Later, the aqueous mixture was poured on to polystyrene multi-plate (12-wells) and the crosslinking reaction was carried at 25±2° C for 48 h. Subsequently after crosslinking all the scaffolds were freeze-dried (5 Pascal, LIO 3000 PLT, Italy) at - 40° C for 48 h to obtain porous 3-D matrices. Whereas, the DHT scaffolds after freeze drying were subjected to high temperature of 160° C under vaccum (0.1 Pa) for 48 h. All crosslinked scaffolds were labelled as G-DHT (DHT crosslinked samples), G-BDD (BDDGE crosslinked samples) and G-GEN (Genipin crosslinked samples).

3. Results and discussion - Characterization of scaffolds

3.1. Fluid uptake test

Under physiological conditions, the water sorption ability and permeability of the scaffolds were evaluated by observing the fluid uptake ability. Briefly, the scaffolds were immersed in phosphate buffer saline (PBS), pH.7.4 at 37 °C. After 1, 3, 6, 24, 32, 48 and 72 h, the scaffolds were taken, blotted in filter paper and wet weight was noted. The swelling ability was expressed as percentage of swelling ability and calculated as ((wet weight) – (dry weight) X 100) / (dry weight). The results, show that fluid binding capacity is an important characteristic feature of the scaffold which determines the structural and mechanical properties. In Fig.1.A, the increasing fluid uptake ability of the scaffolds is illustrated with increase in incubation time which indicates the suitable time-dependent swelling nature of the scaffolds. G-GEN scaffold showed the highest swelling percentage, i.e. 644 ± 16% and 1111 ± 1% at 1 and 72 h respectively. Whereas, other scaffolds such as G-DHT and G-BDD showed 609 ± 6% and 658 ± 26% respectively at 72 h. Nevertheless, fluid uptake index for G-DHT was comparatively minimum, this material can absorb more PBS rapidly than other scaffolds by representing a 3-fold increase in fluid-retention ability between 1 h and 72 h of incubation. Whereas, the fluid-retention ability was 1.8 and 1.7 X for G-BDD and G-GEN respectively. The fluid uptake result shows that the scaffolds were hydrophilic in nature with capacity to hold equitable water molecules for biological performance. Moreover, any proteinous scaffolds with the ability to assimilate adequate water can have analogous properties to living

tissues in terms physiological stability and permeability of the biomolecules. Moreover, the high degree of water holding capacity provides larger surface area/volume ratio which augments cellular proliferation and infiltration into the porous scaffolds. Therefore, the ability of the material to interact and hold the water molecule within its network is greater dependent upon the micro-architecture of the scaffolds. Since the gelatin macromolecule can rapidly hydrate, this moist saturation helps in maintaining the 3D porous structure under the biological condition without the collapse of the network. It can also well have explained that the crosslinking can reduce the hydrophilicity of the material due to the reduction of amino and carboxylic groups. [10] However, our results show that the crosslinking mechanism employed in this study didn't reduce the hydrophilicity instead it has immensely enhanced the structural stability and eventually alleviated the water-retention of the scaffolds. Moreover, it is highly essential to maintain an appreciable swelling property of the scaffolds because this distinct parameter facilities the metabolic exchanges between the cell and the scaffold. However, the G-GEN scaffolds showed the highest swelling ability than the other scaffolds, nevertheless all the scaffolds represented a favorable swelling property.

3.2. In-vitro degradation test

The resistance to rapid degradation of the scaffolds were assessed by monitoring the degradation rate at scheduled time-points. Briefly, the scaffolds were immersed in PBS, pH.7.4 at 37° C for 21 days and at regular intervals the PBS solution was refreshed. After 3, 7, 14, 21 days, three samples from each scaffold type was removed and washed in fresh PBS, pH.7.4 and dried at 40° C. The percentage of weight loss was expressed as ((initial dry weight – final dry weight)/initial dry weight) X 100. An important parameter to monitor is the structural stability and integrity of the scaffolds to avoid rapid degradation of the material under physiological conditions. From the macroscopic observation, there was no loss of shape or weakening of structural architecture of the scaffolds when compared to the non-crosslinked scaffolds which rapidly dissolved within 1 h of PBS incubation at 37° C. The highest weight loss was observed for G-GEN which had a dissolution

level of 37 ± 1.23% at day 21. (Fig.1.B). Whereas in G-DHT there was an acceptable trend with increase in mass loss with increase in time with maximum dissolution level of 19 ± 1.87 % at day 21. Whereas, the overall mass loss of G-BDD was very low (2 ± 0.5 % at day 21) which can be good indication of scaffold solid integrity under physiological conditions, however the low dissolution rate of the G-BDD can also be associated to the high heterogeneity of the material. It is well known that gelatin macromolecule is highly hydrophilic and it is more susceptible to rapid degradation. This results can be correlated with the crosslinking degree data, which shows the highest degree of crosslinking for G-BDD (73 ± 0.44%**)** which shows the least dissolution level. Therefore, it is evident that the effective crosslinking provides strong covalent bridges through hydroxyl group bonding which is less accessible to dissolution. Whereas, the influence of genipin and DTH on bio-stability was similar and comparable to the other previous literature reports because these treatments always resulted in less availability of surface energy which eventually resulted in lower crosslinking degree which ultimately caused higher dissolution rate. Even though there were dissimilarities in the dissolution rates among the groups, regardless after 21 days of incubation all scaffolds maintained a good solid integrity with a homogenous micro-structure, which is essential for cartilage regeneration.

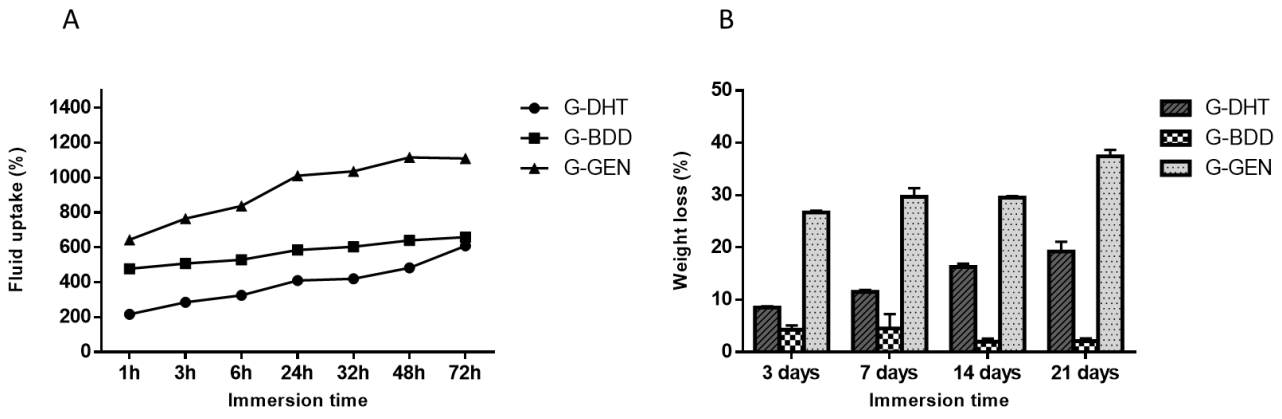

Figure 1. *(A) Fluid uptake and (B) in vitro degradation as a function of time of G-DHT, G-BDD and G-GEN scaffolds in PBS at 37° C.*

3.3 *Extent of Crosslinking*

The extent of crosslinking was measured by Picrylsulfonic acid [2, 4, 6-Trinitrobenzene sulfonic acid]-TNBS assay according to the procedure of Bubnis et al. [11] In brief, the crosslinked and un-crosslinked scaffolds were immersed in 2 ml of solution containing (1 ml of 4% (w/v) di-sodium hydrogen orthophosphate (Sigma Aldrich, USA) and 1 ml of 0.5 % (v/v) TNBS reagent (Sigma Aldrich, USA) and incubated at 37° C for 3 hrs. The reaction was suspended by addition of 3 ml of HCL and the incubation was continued for overnight at 37° C. After appropriate dilution, the absorbance of the resulting solution was measured at 345 nm using UV-Visible spectrophotometer (7315 Jenway, UK). The degree of crosslinking of gelatin scaffolds has been calculated from the moles of free amino groups per gram of gelatin.

The results as illustrated in Table.1, shows that the concentration of coupling agents was a major determinant of crosslinking degree. The G-BDD scaffolds had the highest degree of crosslinking owing to the fact that the presence of several functional side groups within the gelatin backbone which readily undergoes chemical modification. While, the G-GEN and G-DHT had similar crosslinking degree with no significant difference in their values. The possible explanation for the lower degree of crosslinking in G-DHT group can be contributed due to the higher temperature treatment. This particular treatment tends to completely remove the bound water from the material with less surface energy available for crosslinking. [12] Whereas in G-GEN group, we found that increasing the genipin concentration more amino groups were crosslinked which eventually led to higher degree of crosslinking. However, minimum genipin concentration was used in order to evade any cytotoxic response, moreover the crosslinking degree observed for G-DHT and G-GEN were in accordance with the literature report which was highly sufficient and suitable for tissue engineering application. [1]

3.4 Surface Morphology Analysis

The scaffold surface morphology and micro-architecture was evaluated by scanning electron microscopy (SEM) performed on specimens mounted onto aluminium stubs using black carbon tapes and sputter coated with gold (Sputter Coater Q150TES, Quorum, Italy). The specimen surface was examined using high resolution SEM (FEI, Quanta 200, UK) at a pressure of 0.1 m Torr at an accelerating voltage of 15 kV. The pore size and distribution in the wet scaffolds were evaluated by observation of thin slices (20 μm thickness) under a bright field microscope (Nikon). The slices were obtained by using a cryostat (Histo-line, 5000 MC) to cut scaffolds previously soaked in PBS (pH 7.4) for 24 h then embedded in OCT and subsequently quenched into liquid nitrogen.

All the scaffolds had a highly porous surface with the typical foam like morphology with difference in texture and coloration. The G-DHT appeared to be yellow in color, G-BDD appeared to be white in color and G-GEN in greenish-blue due to pigmentation of genipin. The surface of all scaffolds had a highly interconnected micro-architecture with heterogeneous pore size distribution as seen in Fig.2(A, B, C). On observing the cross-section of the scaffolds, the porous morphology was also well maintained within the walls of the scaffold due to effective freeze-drying Fig.2(D, E, F). Average pore size (μm) were measured after 24 h of swelling in PBS at 37° C in order to obtain pore size of swollen scaffolds reflecting the physiological conditions (n=50 data are mean ± SEM). The range of average pore size were between 354±17 μm for G-BDD scaffold, 390±14 μm for G-DHT and 368±10 μm for G- GEN as illustrated in Table 1. The scaffold morphology with adequate porosity and pore size are considered to be indispensable elements of the biomaterials for biological activity. The homogeneity and the porous patterning of the scaffolds are highly influenced by the concentration of the crosslinking agent. All scaffolds represented a porous morphology with presence of several macro and micro pores. However, there were slight difference in the homogeneity or pore size distribution in all the scaffold groups due to the

concentration dependent crosslinker effect. However, all the scaffolds had sufficient porosity for the effective biological performance of the cells.

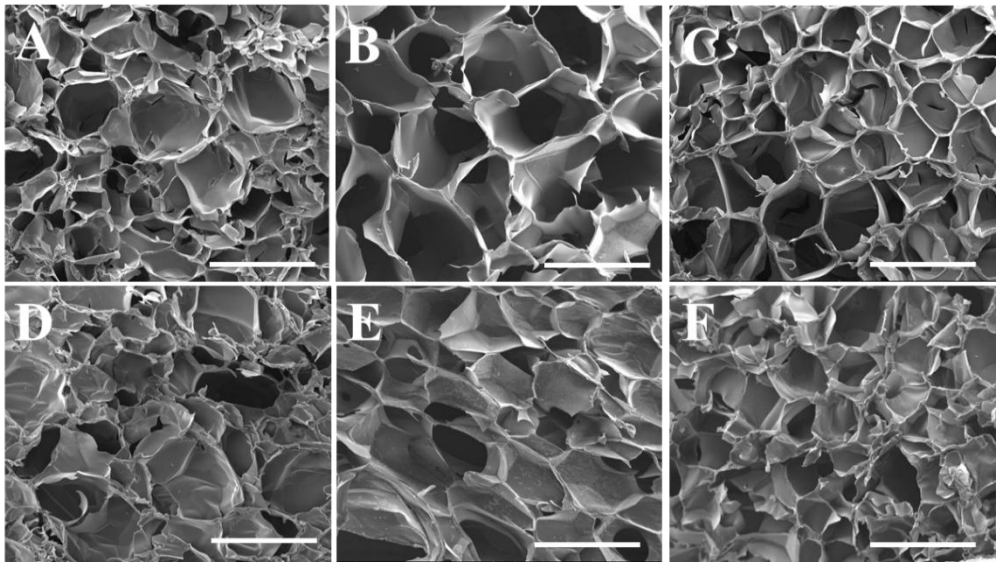

Figure 2. *Surface morphology of (A): G-DHT, (B): G-BDD, (C):G-GEN and Cross-sectional morphology of (D): G-DHT, (E): G-BDD, (F):G-GEN.*

Scaffold Type	Average pore size (µm)	Crosslinking degree (%)	Maximum mass loss (%)
G-DHT	390 ± 14	31 ± 2	19 ± 2
G-BDD	354 ± 17	73 ± 0.4	2.0 ± 0.5
G-GEN	368 ± 10	30 ± 2	37 ± 1

Table 1. *Summary of morphological characteristics of scaffolds. Average pore size (µm) of scaffolds (50 pores in total ± SEM). Percentage of crosslinking degree express as a free amine group content per scaffold (n=3 data are mean ± SEM). Percentage of mass loss at 21 day measured by degradation test in PBS at 37°C (n=3 data are mean ± SEM).*

3.5 Fourier Transform Infrared Spectroscopy (FTIR)

The FTIR patterns of the scaffolds were measured using Nicolet 380 FT-IR spectrometer (Thermo Fisher Scientific Inc, Waltham, USA). Briefly, 2 mg of the scaffold was mixed with 100 mg of anhydrous KBr and then power pressed at 8000 psi into 7 mm diameter discs. The infrared

spectra were collected in the wavelength ranging from 400 to 4000 cm^{-1} with 2 cm^{-1} of resolution. To assess the effect of crosslinking mechanism on the primary structure of the gelatin, the FTIR measurements were analysed as described in Fig.3.A. The gelatin molecule showed typical band assignments corresponding to Amide I at 1690 cm-^{1} due to C-O stretching, Amide II at 1560 cm^{-1} due to N-H deformation and Amide III at 1250 cm^{-1} due to C-N stretching vibrations. The G-GEN and G-DHT exhibited no visible changes in the IR chemical structure, this may be attributed to the low presence of genipin concentration (1.5 wt.%) within the gelatin macromolecule and also probably due to low crosslinking degree. Whereas the G-BDD represented vibrational modification between the wave-number 2950-2890 cm-1. Therefore this specific spectral peak modification confirms the reaction mechanism taking place at alkaline pH which facilities the opening of oxirane rings in BDDGE through the nucleophilic attack of amino side chain groups of gelatin with the concomitant appearance of secondary hydroxyl groups. [13] Therefore the reaction of crosslinking mechanism has an effect on modifying the primary structure of the gelatin backbone moieties.

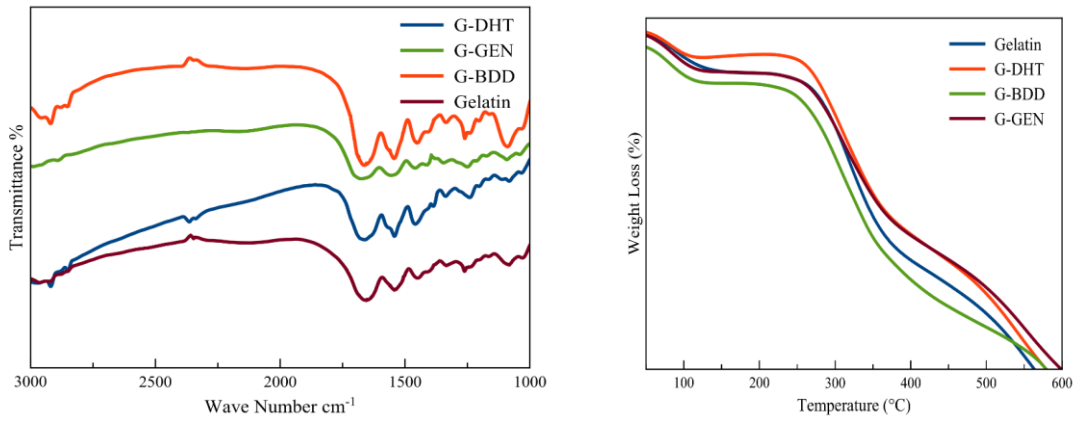

Figure 3. *(A):FTIR spectra and (B): of G-DHT, G-BDD, G-GEN and non-cross linked gelatin scaffolds.*

3.6. Thermal characteristics

The pyrolytic pattern of the scaffolds was determined using Thermo gravimetric (TGA) analyser (STA 449/C Jupiter, Netzsch Germany). In brief, 10 mg samples were placed in aluminium crucible and crushed and press sealed for complete contact with the crucible. The experiment was

carried in a temperature range of 30-600° C at a heating rate of 10°C/min in an atmosphere of nitrogen. The results demonstrate the changes in weight in relation to temperature of the material. There was a rapid degradation after 600 °C, as seen in the pyrolytic pattern (Fig.3.B). The first phase of the degradation prolife attributes to the initial weight loss between 50-90 °C, mainly due to loss of water molecules. The second phase of weight loss was between 250-300 °C is mainly due to destabilization of macromolecule, eventually inducing the thermal degradation of the gelatin helices. However, all scaffolds (G-DHT, G-BDD and G-GEN) behaved similarly with very little differences in their degradation profile. The TGA peaks demonstrates that the presence of crosslinkers did attribute to the increase in thermal durability of the material, by increasing the length of gelatin molecule thereby ensuring better thermal stability [14].

3.7 Dynamic Mechanical analysis (*DMTA*)

Cylindrical scaffolds (8 mm in diameter and 5 mm thickness) were soaked in PBS at 37 °C for 24 h prior to measurement. A minimum preload force was applied to each sample to ensure complete contact between the scaffold's surface and the compression plates. All samples were uniaxially compressed using controlled-force DMA test with a force ramp from 0.5 to 5 N and a speed of 0.5 N/min. From the linear part of the obtained stress-strain curve the compressive modulus was calculated up to 10% strain. Using Multi-Frequency DMA test, under compressive mode the visco-elastic response of the scaffolds was measured with frequency scan from 0.1 until 10 Hz measurements and with a constant strain amplitude of 75 μm. The respective material response can be observed in the stress strain curves regarding different crosslinkers as seen in (Fig.4.A). G-DHT scaffolds showed the highest compressive modulus of (54.4 ± 3.8 kPa) followed by G-BDD (46.0 ± 2.8 kPa) and G-GEN (16.2 ± 0.3 kPa) (Fig.4.B). G-GEN scaffolds showed significant decrease in compressive modulus respect to G-DHT and G-BDD ($p \leq 0.0001$). The storage modulus (E') of all the scaffolds increased with oscillating frequency (Fig.5.A). G-DHT showed the highest storage modulus that increased from 41.6 ± 3.1 kPa at the frequency 0.1 Hz to

58.8 ± 6.0 kPa at 10 Hz. For G-BDD and G-GEN storage moduli increased at lower rates, giving rise from 36.4 ± 1.2 to 44.4 ± 1.2 kPa for G-BDD and from 17.9 ± 0.8 to 24.0 ± 1.4 kPa in case of G-GEN. This study elucidates that, G-DHT promotes the stiffness of the scaffolds in a higher extent in respect to two other groups. The loss factor (tan δ) of G-DHT and G-BDD increased up to certain frequency (3.4 Hz and 4.5 Hz respectively) and after started dropping till 10 Hz, which indicates that these scaffolds at particular point became more elastic than viscous (Fig.5.B). For G-GEN tan δ is decreasing from the beginning of test, showing only its elastic response upon increasing frequencies. The mechanical test results demonstrate that at oscillating frequencies, the differences in stiffness and visco-elastic behaviour was observed. Moreover, it is reported that scaffold's stiffness and compressive modulus decrease with increasing pore size [16]. In our study the highest values of moduli was observed in G-DHT sample which apparently has the biggest pore size (Table 1), however this effect can counterbalanced by the hydrostatic interaction of the water molecules within the large pores which prevents material deformation and eventually results in higher E'[17]. This apart, another important parameter of viscoelasticity is the loss factor. Loss factor (tan δ) is a ratio of the amount of energy dissipated, representing the viscous portion to energy stored, representing the elastic portion [17,18]. At low frequencies, the loss factor of G-DHT and G-BDD increased demonstrating their higher damping capabilities than G-GEN. Moreover, G-DHT is able to store energy maintaining viscous response up to higher frequency than G-BDD. G-GEN represents mostly elastic behavior without suitable viscosity and stiffness which is necessary in resisting compressive loading in cartilage [15,17]. However, the compressive moduli of our scaffolds were greatly higher than those found in the literature regarding cartilage tissue application [19,20].

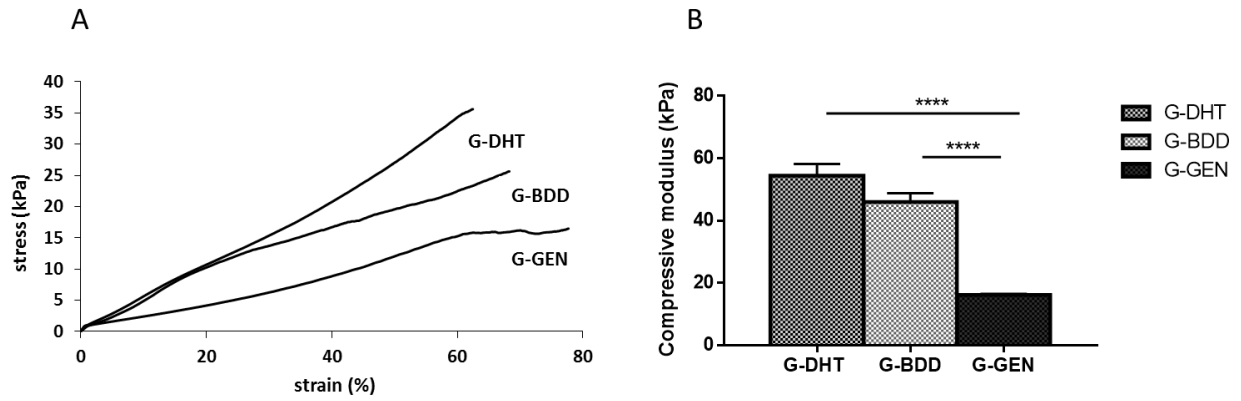

Figure 4. *Mechanical properties of gelatin scaffolds. (A) Representative stress-strain curves and (B) Compressive moduli of G-DHT, G-BDD and G-GEN scaffolds hydrated in PBS at 37° C for 24h; tested at force 0,5 N/min; Data are mean ± SEM from 5 samples each type of scaffold. Statistically significant differences between G-DHT and G-GEN (****p ≤ 0.0001) and between G-BDD and G-GEN (****p ≤ 0.0001).*

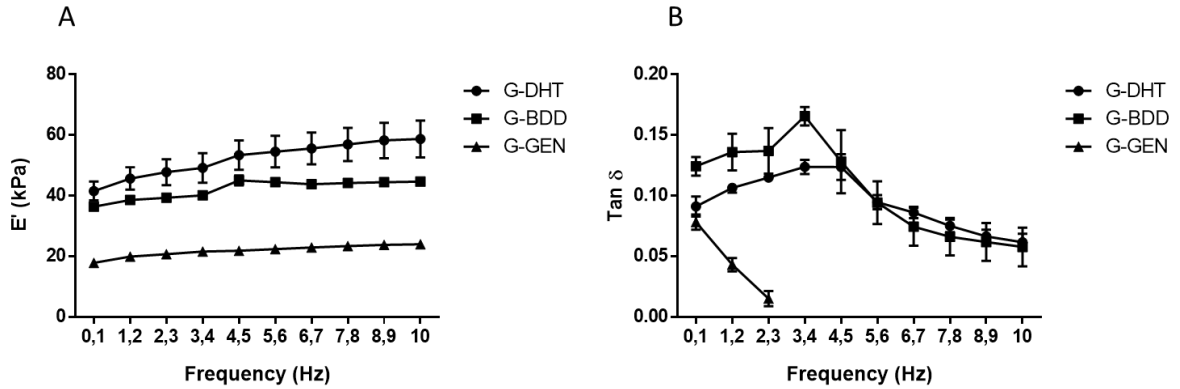

Figure 5. *Viscoelastic properties of gelatin scaffolds. (A) Storage modulus (E') and (B) loss factor (tan δ) of G-DHT, G-BDD and G-GEN scaffolds hydrated in PBS at 37° C for 24h; tested at varying frequencies; Data are mean ± SEM from 5 samples each type of scaffold.*

3.8 Cell Culture

Human chondrocytes (CHON-002) were supplied by ATCC® (CRL -2847™, Italy) and used to assess the cell/material interaction. According to the ATCC® protocol (cell line data sheet) the chondrocytes were infected by the defective retrovirus containing human telomerase reverse

transcriptase gene under G418 selection. The chondrocytes were cultured in Dulbecco Modified Eagle's Medium (DMEM, PAA, Austria) supplemented with 10% Fetal Bovine Serum (FBS) and 1% penicillin/streptomycin (100 U/ml/100 l g/ml) and incubated at 37 °C with 5% CO_2 atmosphere. The cells were cultured in T-75 flasks until 80% confluence and detached by trypsinization and centrifugation, later the cell number and viability was assessed by trypan blue dye exclusion test. The experimental scaffolds were cut out from punching machine with dimensions of 8 mm in diameter and 3 mm in thickness and were sterilized by 25 kGy gamma-ray radiation. Prior to experimentation, all scaffolds were pre-incubated with 1 ml of culture media for 24 h at room temperature (RT). Samples were placed one per well in a 24-well plate and a drop of 20 µl containing 5.0 x 10^4 cells was added onto the upper layer of the scaffold for initial cell attachment. After 30 mins, 1.5 ml of cell culture media was added and incubated at 37 °C, 5% CO_2 for 21 days. All cell handling procedures were performed in a sterile laminar flow hood. At regular time intervals of 1, 3, 7 and 14 days the scaffolds of G-DTH and G-BDD were harvested and Live/Dead assay (Invitrogen, USA) was performed. Briefly, the harvested scaffolds were washed in 1X PBS for 5 mins and stained with Calcein acetoxymethyl (Calcein AM) 2 µM and Ethidium homodimer-1 (EthD-1) 4 µM for 15 min at 37°C. Later the scaffolds were again washed in 1X PBS for 5 mins and viewed under inverted Ti-E fluorescence microscopy (Nikon). Due to technical difficulty live/dead assay could not be performed on the G-GEN scaffolds, instead the viability of the chondrocytes was evaluated using fluorescent dye. At individual time points, one scaffold was harvested and rinsed in PBS (pH 7.4) and stained with 4',6-diamidino-2-phenylindole (DAPI) and immediately viewed under inverted Ti-E fluorescence microscopy (Nikon).

At regular time intervals of 1, 3, 7 and 14 days of cell cultivation, 10% 3-(4,5-dimethylthiazol-2-yl)-2,5-diphenyltetrazolium bromide (MTT) solution of the total volume of the well was added and incubated for 2 h at 37 °C. After incubation, the scaffolds were transferred to centrifuge tubes and 1ml of dimethyl sulfoxide (DMSO) was added. The scaffolds were crushed using the pestle and vortexed subsequently to release the inter-located cells and incubated at RT for 15 mins and later

centrifuged at 1000 rpm for 1 min. Later 200 µl of the supernatant was transferred to 96 wells and read using a spectrophotometer (Multiskan FC Microplate photometer, Thermo Scientific, USA) at optical density of 570 nm to measure the metabolically active cells which reacts with MTT to produce a formazan dye. Three parallel scaffolds were measured at individual time points.

The attachment and morphology of the chondrocytes on the scaffolds were visualized using SEM. Briefly, after 7 days, the cell-seeded scaffolds were washed in PBS (pH 7.4) and then fixed in 2.5% glutaraldehyde for 2 hrs at 4°C. Later, the specimens were mounted onto the aluminium stubs using black carbon tapes and they were sputter coated with gold particles (Sputter Coater Q150TES, Quorum, Italy). The cells on the scaffold surface was then examined using high resolution SEM (FEI, Quanta 200, UK) to view the distinct sections of the scaffolds.

After regular time intervals of 7 and 14 days of cell cultivation, the scaffolds were harvested for sulphated glycosaminoglycan (GAG) assay. At the end of each time point the scaffolds were solubilized at 65 °C for 3 hrs using lysis buffer (5 mg/ml papain in 50 mmol sodium phosphate buffer (pH 6.4) containing 5 mmol EDTA and 5 mmol cysteine). The digestive solution was collected, centrifuged and analysed for GAG using dimethylmethylene blue (DMMB) dye and read using a spectrophotometer (Multiskan FC Microplate photometer, Thermo Scientific, USA) at optical density of 530 nm. Shark chondroitin sulphate with concentration gradient of 0 to 5 µg/ml was used as a standard and scaffolds without cells were used as controls and three parallel scaffolds were measured at individual time points. Total RNA was isolated from the harvested scaffolds at day 7 and 14 using TriFast® reagent (EuroClone, USA). In brief, the samples were lysed in 1 ml of TriFast, crushed and centrifuged at 12,000 x g for 5 min; supernatant was collected for RNA purification using Direct-Zol™ RNA MiniKit (Zymo Research, USA). The purified RNA was quantified using Qubit® RNA BR assay kit and Qubit® fluorimeter. The integrity of the RNA was analysed using native agarose gel electrophoresis. Reverse transcriptase was carried out on purified RNA (500 ng) to produce cDNA using high capacity cDNA reverse transcriptase kit with RNase inhibitor, according to manufacturer's instructions (Applied Biosytems, USA). Relative

quantification of gene expression, using Taqman assays (Applied Biosystems), for transcription factor SOX-9 (SOX-9, HS01001343), and glyceraldehyde 3-phosphate dehydrogenase, used as housekeeping gene, (GAPDH, HS99999905) was performed by use of the StepOne Real-Time PCR System (Applied Biosystems). Three technical replicates for each sample was used and data were collected using the OneStep Software (v.2.2.2) and relative quantification was performed using the comparative threshold (Ct) method (ΔΔCt), where relative gene expression level equals $2^{-\Delta\Delta Ct}$ [21]. The cell viability of the chondrocytes on the porous scaffolds was visualized by live/dead assay. The fluorescence of the live/dead cells were only visible in G-DTH and G-BDD scaffolds, whereas the G-GEN displayed a brighter background in TRITC filter (578 nm) leading to difficulties in visualizing the dead cells. Therefore, the cell viability and colonization on the G-GEN scaffolds were examined through DAPI staining. As represented in Fig.6, the G-BDD and G-DHT scaffold demonstrate high cell viability representing good cytocompatibility at each time point. With the increase in culture time there was increase in cell density especially on day 7 and 14 and the cells appeared to be equally distributed in both the scaffolds surface. Moreover, DAPI staining of the G-GEN showed proper round cell nuclei morphology visualized in dark blue and along the time there was increase in cell colonization of the material (Fig. 7 A-C). Both the live/dead and DAPI images shows the gradual increase in cellularity with respect to increase in culture time indicating the absence of cytotoxicity of the studied material. There was no difference in terms of cell viability amongst the scaffolds and the presence of crosslinkers did not impede the chondrocytes expansion and scaffold colonization.

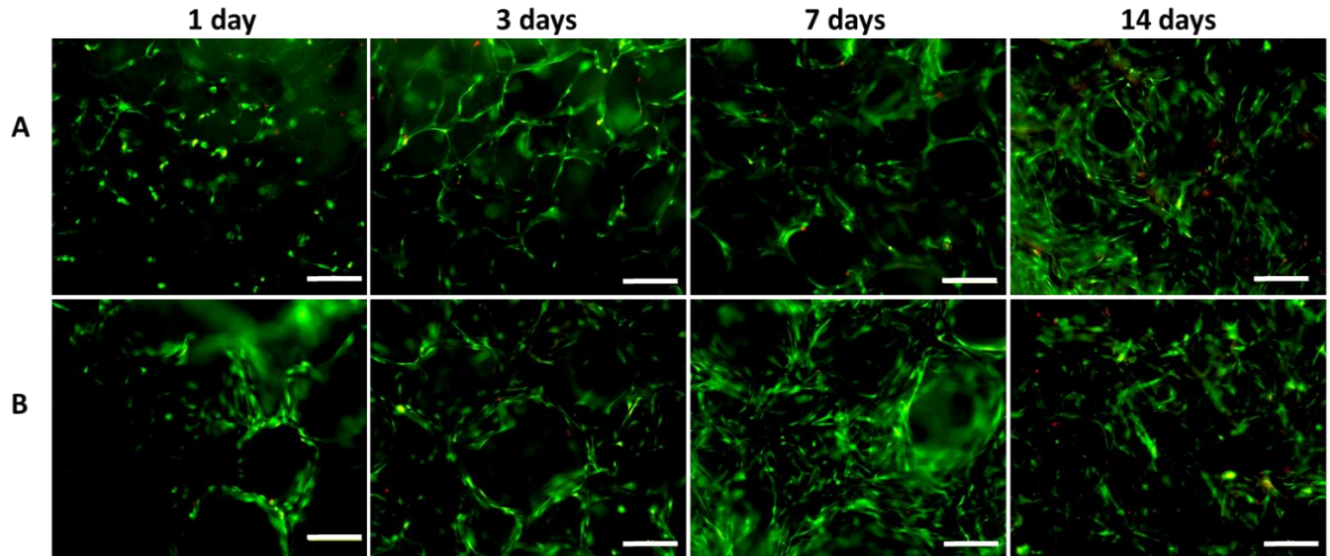

Figure 6. *Cell viability analyzed by the live/dead assay (Calcein stains live cells in green, Ethidium homodimer-1 stains dead cells in red). Panel A. presents G-DHT scaffold and panel B. G-BDD scaffold at time points: 1 day, 3 days, 7 days and 14 days. Scale bars: (A, B) 200 µm.*

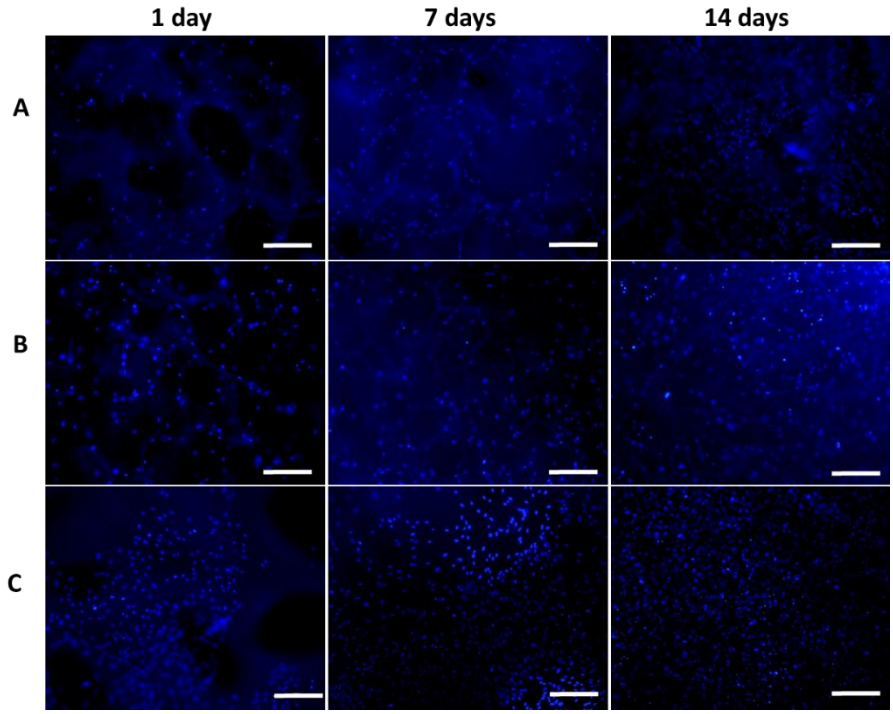

Figure 7. *Cell colonization of G-DHT (A), G-BDD (B) and G-GEN (C) scaffolds analyzed by DAPI staining at day 1, 7 and 14. Cell nucleus stained in blue. Scale bars: (A,B,C,) 200 µm.*

Cell proliferation was evaluated by the MTT assay showing the increase in cell growth with time for all the scaffolds (Fig. 8). The highest proliferation was observed for G-DHT which was

statistically significant when compared to G-GEN at day 7 and 14 ($p \leq 0.05$; $p \leq 0.0001$) and to G-BDD at day 7 and 14 ($p \leq 0.05$; $p \leq 0.01$). Comparing the G-BDD and G-GEN, the higher cell proliferation rate was observed for G-BDD with statistically significant difference at day 7 and 14 ($p \leq 0.05$; $p \leq 0.0001$). The cell viability was observed to be in the order: G-DHT> G-BDD> G-GEN as the culture time is prolonged.

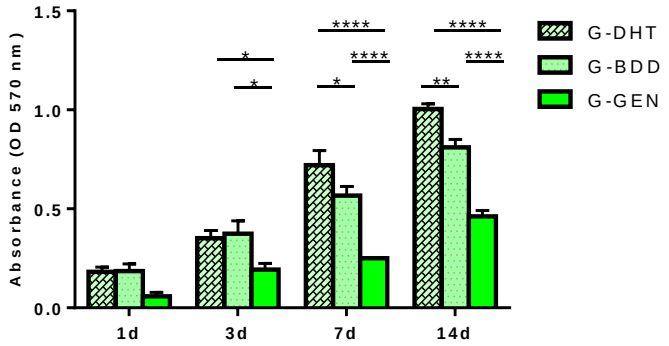

Figure 8. *Analysis of cell proliferation by the MTT assay after 1, 3, 7 and 14 days of cell seeding (n = 3). Cells seeded on G-DHT and G-BDD scaffolds proliferate in a higher extent compared to cells growing in G-GEN scaffold. *p ≤ 0.05; **p ≤ 0.01; ****p ≤ 0.0001.*

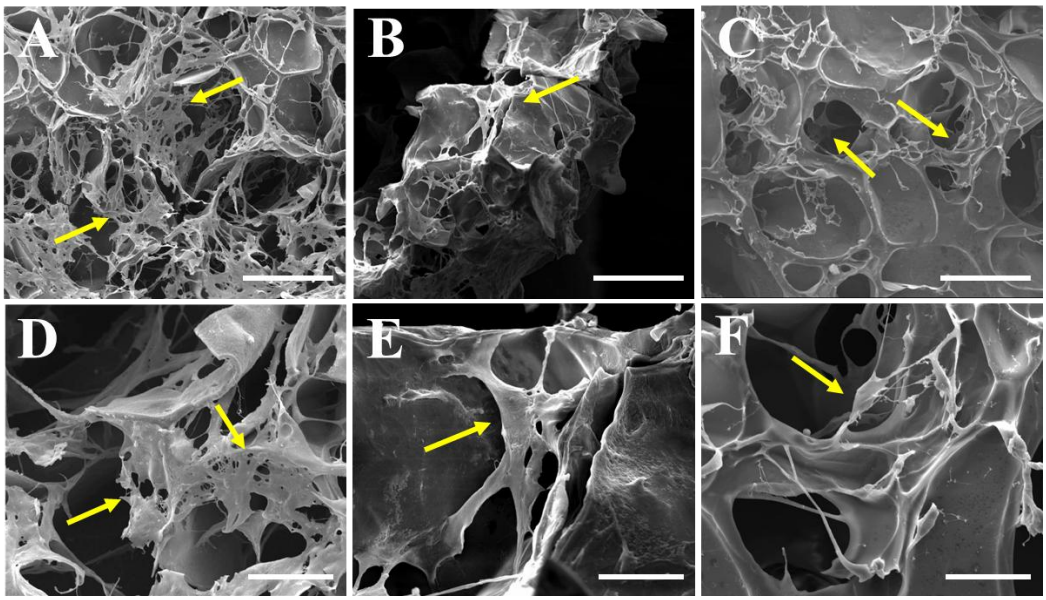

Figure 9. *Morphology of cell-seeded scaffolds at day 7. (A,D): G-DHT, (B,E): G-BDD and (C,F): G-GEN. (D,E,F) Detailed morphology of cell-seeded scaffolds at day 7. Scale bars: (A,B,C) 200 µm; (D,E,F) 50 µm.*

The DAPI staining results can be correlated with the MTT assay. The results elucidate a significant increase in number of viable cells in all the scaffold groups as the culture time is prolonged. But, when compared to other scaffolds, G-GEN scaffold exhibited slower growth rate and recovered in the later stage of culture time. The possible explanation that can contribute to the slower growth rate can be the reaction of genipin with the primary amine groups of arginine residues of gelatin leading to reduction of adhesion promoting RGD-like sequence. Another explanation could be that the large pores of the G-GEN can accommodate more cells for penetration, so that they grow on crevices and later find an increased surface area of contact to grow [12,23]. Moreover, previously several authors have reported the toxicity of genipin and they have speculated to be cell and dose dependent [24,25]. However, the observations of the culture studies also provide the evidence that the crosslinking mechanism assists in providing a more suitable micro-environment for the overall cellular activity which in turn benefitted their proliferation as well.

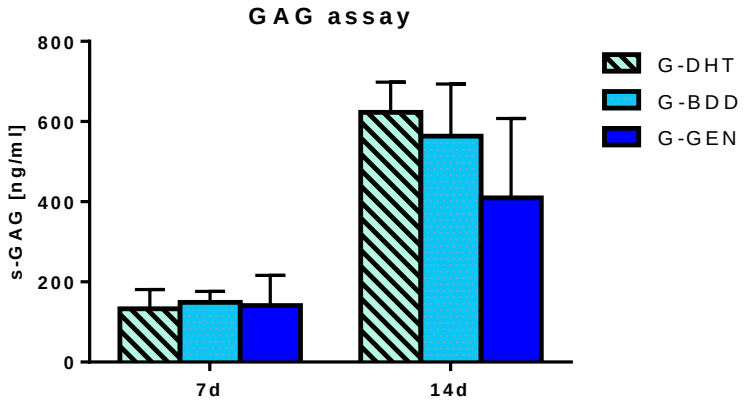

Figure 10. *GAG deposition by chondrocytes on G-DHT, G-BDD and G-GEN scaffolds after 7 and 14 days of culture. No statistically significant differences noticed*

The micro-environment quality and the compatibility of scaffolds for cellular infiltration was evaluated using SEM. After 7 days of cell culture, the human chondrocytes were able to adhere, grow and penetrate into the porous material as seen in Fig.9 (A-F). Moreover, the chondrocytes exhibited their typical fibroblast-like morphology. The porous nature of the scaffold enabled easy cell attachment and infiltration. There was no difference in the cell morphology on different

scaffolds, all the scaffolds accommodated the chondrocytes to expand and grow with a branched spindle shaped morphology. From the SEM images, it can be seen that the crosslinking mechanism of different coupling agents at 25 ° C ± 2 would modulate a porous micro-structure to have an average pore size above 350 µm. The presence of interconnecting porous texture characterized by the presence of heterogeneous macro and micro pores would facilitate easy cell adhesion and pores scaffold penetration. The chondrocytes were able to attach and spread over the scaffolds forming multiple protrusions without any polarization or aggregation.

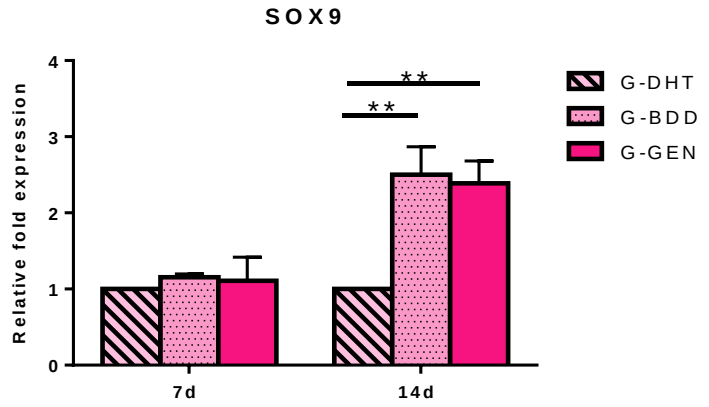

Figure 11. *Gene expression analysis of SOX-9 gene. Relative quantification of gene expression after 7 and 14 days of chondrocytes culture on the gelatin scaffolds. G-DHT scaffold was taken as a control. Results were normalized to GAPDH and presented as fold change respect to G-DHT control group. **$p \leq 0.01$.*

The amount of GAGs produced by the cells in correspondence to the culturing time was increased between day 7 and 14 for all the scaffolds without any significant differences (Fig. 10). Therefore, the higher level of glycosaminoglycans produced by the cells shows the rich deposition of cartilage extra cellular matrix components by the chondrocytes. Proteoglycans are considered to be the major ECM component of cartilage synthesized by chondrocytes. Since the proteoglycans are composed of 95% GAGs and 5% protein, it is always essential to measure the GAG content in order to understand the metabolic activity of the cells [26]. Accordingly, the cells in all the scaffolds were able to secrete more ECM as the culture time prolonged. These results can

be coordinated with the scaffold morphology and pore size distribution. The results of GAG quantification suggest that the average pore size of 350 μm helps the chondrocytes to infiltrate and secrete their ECM components through efficient transport of the nutrients or metabolites. Moreover, the good hydration properties of the scaffolds also helped in providing the required microenvironment for cell migration and proliferation. Furthermore, the yield of GAG content was considerable and comparable to results reported in the literature [27]. A preliminary qPCR analysis was performed on all three scaffolds and G-DHT scaffolds were used as controls. The chondrogenic gene expression includes the transcription factor SOX-9 and the mRNA analysis was performed on day 7 and 14 of the culture time. The mRNA level of SOX-9 was increasing in a time dependent manner for both G-BDD and G-GEN scaffold with statistically significant difference with respect to the control at day 14 ($p \leq 0.01$) as seen in Fig.11. The quantitative gene expression of the chondrocytes marker shows the up regulation of SOX-9 mRNA level induced by G-GEN and G-BDD respect to G-DHT after 14 days. This transcription factor is highly essential for the cartilage formation and also important in maintaining the chondrocytes phenotype and also guides the chondrocytes in expressing hyaline cartilage specific genes. The induction and regulation of SOX-9 gene observed in both the scaffolds could be attributed to the structural suitability of the scaffolds induced by the GEN and BDD crosslinkers.

4. Conclusion

This study, we demonstrated a comparative analysis of using various coupling agents in modifying the gelatin macromolecule for tissue engineering application. To conclude, on evaluating the influence of thermal, chemical and natural coupling agents on crosslinking the gelatin, we found that G-DHT a thermally crosslinked was more appropriate with suitable physical-chemical and biological features. We believe that thermal dehydration of the gelatin improves the overall characteristics without affecting the biocompatibility of the G-DHT. Moreover, the absence of any chemical residues within the protein network would absolutely avoid the antigenicity in

physiological conditions. Similarly, the G-BDD a chemically crosslinked scaffold showed good surface properties with acceptable chemical composition, topography, hydrophilicity and satisfying biological properties. Whereas, the G-GEN scaffolds also showed good morphological features however lower biocompatibility was observe when compared to other scaffolds but there was slow recovery in the biocompatibility in the later days of culture due to the cell and dose dependent effect of genipin. Taken collectively, our results suggest that, of the three-crosslinking mechanism, G-DHT treated scaffolds are the most favourable and reasonable scaffolds for bone or cartilage tissue engineering.

5. References

1) Islam MM, Khan MA, Rahman MM . Mater Sci Eng C Mater Biol Appl. 2015;49:648-55.

2) Whu SW, Hung KC, Hsieh KH, Chen CH, Tsai CL, Hsu SH. Mater Sci Eng C Mater Biol Appl. 2013;33(5):2855-63.

3) Rose PJ, Mark HF, Bikales NM, Overberger CG, Menges G, Kroschwitz JI. Encyclopedia of polymer science and engineering, 2nd ed., Vol. 7. New York: Wiley Interscience, 1987.

4) Bigi A, Cojazzi G, Panzavolta S, Roveri N, Rubini K. Biomaterials. 2002;23(24):4827-32.

5) Ross-Murphy SB. Polymer 1992;33:2622–7.

6) Maquet J, Th!eveneau H, Djabourov M, Leblond J, Papon P. Polymer 1986;27:1103–10.

7) Michon C, Cuvelier G, Relkin P, Launay B. Int J Biol Macromol 1997;20:259–64.

8) Ostrovidov S, Shi X, Zhang L, Liang X, Kim SB, Fujie T, Ramalingam M, Chen M, Nakajima K, Al-Hazmi F, Bae H, Memic A, Khademhosseini A. Biomaterials. 2014;35(24):6268-77.

9) Hodde J. Tissue Eng. 2002 Apr;8(2):295-308.

10**)** Yan LP, Wang YJ, Ren L, Wu G, Caridade SG, Fan JB, Wang LY, Ji PH, Oliveira JM, Oliveira JT, Mano JF, Reis RL. J Biomed Mater Res A. 2010;95(2):465-75.

11) Bubnis WA and Ofner CM. Analytical Biochemistry. 1992; 207(1):129-133.

12) I.Prasertsung, R.Mongkolnavin, S.Damrongsakkul, C.S.Wong. Surface and Coatings Technology. 2010;205(1):133-138.

13) C.R. Correia, L.S. Moreira-Teixeira, L. Moroni, R.L. Reis, C.A. van Blitterswijk, M. Karperien, J.F. Mano, Tissue. Eng. Part C Methods 17(7) (2011) 717-730.

14) A. Arora, A. Kothari, D.S. Katti, J. Mech. Behav. Biomed. Mater. 51 (2015) 169-183.

15) A.J. Sophia Fox, A. Bedi, S.A. Rodeo, Sports Health 1(6) (2009) 461-468.

16) P. Gentile, M. Mattioli-Belmonte, V. Chiono, C. Ferretti, F. Baino, C. Tonda-Turo, C. Vitale-Brovarone, I. Pashkuleva, R.L. Reis, G. Ciardelli, J. Biomed. Mater. Res. A 100(10) (2012) 2654-2667.

17) L.P. Yan, J.M. Oliveira, A.L. Oliveira, S.G. Caridade, J.F. Mano, R.L. Reis. Acta Biomater. 1 (2012) 289-301.

18) L.P. Yan, Y.J. Wang, L. Ren, G. Wu, S.G. Caridade, J.B. Fan, L.Y. Wang, P.H. Ji, J.M. Oliveira, J.T. Oliveira, J.F. Mano, R.L. Reis, J. Biomed. Mater. Res. A 95(2) 2010 465-475.

19) C.R. Correia, L.S. Moreira-Teixeira, L. Moroni, R.L. Reis, C.A. van Blitterswijk, M. Karperien, J.F. Mano, Tissue. Eng. Part C Methods 17(7) (2011) 717-730.

.

20) A. Arora, A. Kothari, D.S. Katti, J. Mech. Behav. Biomed. Mater. 51 (2015) 169-183.

21) K.J. Livak, T.D. Schmittgen, Method. Methods. 25(4) (2001) 402-408.

22) J.H. Ko, H.Y. Yin, J. An, D. J. Chung, J.H. Kim, S.B. Lee, D.G. Pyun, Macromol. Res. 18 (2010) 137-143.

23) H.G. Sundararaghavan, G.A. Monteiro, N.A. Lapin, Y.J. Chabal, J.R. Miksan, D.I. Shreiber, J. Biomed. Mater. Res. A 87(2) (2008) 308-320.

24) C. Wang, T.T. Lau, W.L. Loh, K. Su, D.A. Wang, J. Biomed. Mater. Res. B Appl. Biomater. 97(1) (2011) 58-65.

25) S.M. Lien, L.Y. Ko, T.J. Huang, Acta. Biomater. 5(2) (2009) 670-679.

26) N. Bhardwaj, Q.T. Nguyen, A.C. Chen, D.L. Kaplan, R.L. Sah, S.C. Kundu. Biomaterials 32(25) (2011) 5773-5781.

27) S.R. Tew, T.E. Hardingham J. Biol. Chem. 281 (2006) 39471-39479

CHAPTER II: Reinforcement of mineralized collagen through ribose glycation

1. Introduction

The concept of bone tissue engineering (BTE) was developed to challenge the conventional autologous bone grafting (ABG) treatment method which includes drawbacks such as longer operating time, dearth of material and significant morbidity. The typical paradigm of BTE is the four biological factors which includes the (osteogenic cells, osteoinductive stimulus, osteoconductive matrix scaffolds and a suitable mechanical environment) which is also known as the diamond concept. The BTE strategy heavily depends upon the diamond concept, where the synergic coordination and interaction of the above mentioned biological factors is highly essential in developing a rationale bone scaffold material [1-3]. Over the last decades, the idea of BTE has gained significant interest in tissue engineering leading to development of plethora of biomaterials with suitable biocompatibility, competent micro-architecture, controlled degradability and enhanced osteoinductive properties [4-6]. Currently, developing tailor-made, tissue-specific scaffolds with the capacity to fine-tune osteogenesis is of significant importance in BTE. The fine-tuning of scaffolds is usually achieved through identifying the key osteogenic cues and adopting the biomimicry strategy to obtain hierarchically organized structures similar to the anatomical bone with the ability to activate mechano-transduction processes and to yield regeneration of well organized bone [7]. In bone, the extracellular matrix (ECM) consists of organic (35%) and inorganic (65%) phases, where the predominant organic protein (collagen) allows the inorganic nano hydroxyapatite (HA) crystals to precipitate on the collagen fibrils to form a mineralized structural unit of bone. The active interaction between the organic and inorganic phases results in a natural composite material (bone) with high resiliently and compressive strength [8,9]. Developing biomimetic scaffolds using the biomimicry strategy has been a successful approach with proven results. Bone-like composite obtained through the direct nucleation of HA nano-crystals on the self assembling collagen fibrils showed structural, compositional and morphological similarities to the mineral component of the

natural bone [10]. Similarly, graded biomimetic osteochondrol composite scaffolds were developed with a differentially ability to support cartilage and bone tissue regeneration [11]. The simulation of synthetic substitutes with the HA-crystal structure has shown to have significant positive effect on bone formation and remodelling [12]. In particular, magnesium (Mg^{2+}) are bivalent ions largely present in the young or newly formed bone. The substitution of calcium by magnesium in the surface crystal site increases the chemical-physical likeness of HA nano particles to biologic HA eventually with a beneficial impact on protein adsorption and cell adhesion to the scaffold [13]. Incorporation of Mg^{2+} ions in the HA lattice has also highly improved the osteoconductive activity with enhanced bone repair in *in-vivo* studies [14].

However, obtaining biomimetic, highly organized and mineralized bone-like scaffolds is still a laborious task, because achieving the similar mechanical features of the native bone is still a challenge. The recent advances in material science offers the innovative concept of crosslinking of macromolecules which allows to develop and obtain bone-like scaffolds with analogous mechanical and resorption properties of the native bone. Accordingly, there are numerous crosslinking agents such as glutaraldehyde (GA), dehydrothermal (DHT), 1,4-butanediol diglycidyl ether (BDDGE), 1-ethyl-3-(3-dimethylamino propyl) carbodiimide hydrochloride (EDC) and genipin which offers advantages in developing mechanical stable scaffolds [15]. An alternative crosslinking paradigm is the, non-enzymatic crosslinking, which is of greater interest in BTE applications in order to understand the effect of reducing sugars in enhancing the ECM stiffness and rigidity. Non-enzymatic crosslinking is a simple and natural glycation reaction, where the reducing sugars (glucose or ribose) interacts with the amino group of proteins to create chemical alteration in protein structure which is known as Schiff's base alteration. This Schiff's base rearranges to form a Amadori product, which allows the protein-to-protein crosslinking to occur, eventually leading to the formation of advanced glycation products (AGEs) through Maillard reaction [16,17]. The formation of AGEs attribute to the increased matrix stiffness, decreased solubility and high enzymatic resistivity of the crosslinked tissue [18-20]. This glycation process is a normal

biochemical reaction happening in the living system as result of natural ageing, usually AGEs are considered to be detrimental to diabetes and other degenerative diseases. However, adopting this interesting glycation technique under *in-vitro* and *in-vivo* conditions is widely investigated nowadays to improve tissue functionality in tissue engineering applications. The rationale use of this glycation reaction is to confront the existing challenges in scaffold processing such as poor mechanical property and high susceptibility to enzymatic degradation. Accordingly, several, *in-vitro* studies have demonstrated that ribose glycation has a significant role in modifying the mechanical properties of cortical bone [21-23]. In particular, studies have shown that minimal concentration of ribose (30 mM) has a significant effect on intermolecular crosslinking of collagen [24]. Similarly, glucose modified gelatin/collagen matrix, demonstrated to be a safe and effective biomaterial with excellent biocompatibility [25]. Besides this, *in-vivo* studies have successfully used ribose-crosslinked-collagen as dermal fillers in rabbit model, where the results demonstrated increased functional longevity with better soft-tissue augmentation [26]. In addition, the clinical evidence also suggests that ribose crosslinking is safe and effective in supporting guided tooth bone regeneration [27,28]. Thus, from the available literature, it is speculated that reducing sugars can cause possible alterations in the protein structure with enhanced functionality in terms of mechanical and biodegradability aspects. Therefore, in this study, we investigate the feasibility in developing bone-like scaffold with magnesium-doped hydroxyapatite/type I collagen (MgHA/Coll) scaffold through a bio-inspired, pH driven, self-assembling process. The developed MgHA/Coll were crosslinked with D-ribose under physiological conditions and was physico-chemically characterized. The biocompatibility and cell material interaction was evaluated using mouse pre-osteoblast (MC3T3) cells under *in-vitro* conditions which showed favourable cell adhesion and proliferation. To best of our knowledge, this is the first study to investigate the effect of ribose glycation as crosslinking agent in biominerlarized collagen. As a proof of concept, we have demonstrated that this cost-effective, biological crosslinking approach has led to develop

mechanically stable MgHA/Coll with promising and encouraging results and also offers new insights and opportunities in developing better scaffolds for BTE application.

2. Synthesis of MgHA/Coll hybrid composite

Type I collagen from equine tendon (1 wt.% in acetic buffered solution (pH 3.5) was supplied by Opocrin SpA, (Italy) and was used as organic matrix to synthesis MgHA/Coll hybrid composite. Briefly, two aqueous suspensions were prepared: (i) acidic suspension: 2.4 g of H_3PO_4 was diluted with 500 ml of milli-Q water and added to 150 g of 1 wt.% collagen gel to obtain an aqueous homogenous suspension. (ii) basic suspension: 2.7 g of $Ca(OH)_2$ and 0.35 g of $MgCl_2.6H_2O$ were dispersed in 500 ml of milli-Q water to obtain an aqueous homogenous suspension. Later, the acidic suspension was added drop-wise to the basic suspension at 25° C under continuous stirring. The biomineralization process is a slow pH-driven process, where the neutralization reaction causes the MgHA nanocrystals formation on collagen fibres and the simultaneous self-assembling of collagen fibrils with the consequent precipitation of the hybrid composite MgHA/Coll. The reaction product was kept at static condition for 2 h at 25° C to mature. The final synthesized composite slurry had a HA/Coll nominal ratio of (70/30 wt.%) mimicking the natural bone composition. After the biomineralization process, the composite slurry was washed three times in milli-Q water and filtered through metallic sieve (150 μm) to eliminate any un-react product and counter-ions. The final recovered composite slurry is referred as MgHA/Coll and was used to produce ribose crosslinked scaffolds.

2.1 Ribose glycation of MgHA/Coll scaffolds

In this study two different crosslinking strategies were employed to investigate the effect of ribose glycation in three-dimensional (3D) MgHA/Coll scaffolds which as follows,

(i) Pre-glycation: Biomineralized MgHA/Coll recovered as slurry was crosslinked in ethanol and PBS solution (70:30 vol.%) with 30 mM of ribose under intermittent shaking condition at 37° C for 5 days. Then, the slurry was washed in milli-Q water three times to remove unbound ribose and residual solvents. Later the slurry was filled onto a polystyrene well-plate and freeze-

dried by freezing at – 40° C and drying at 25° C (5 Pascal, LIO 3000 PLT, Italy) for 48 h under a constant vacuum of 0.1 mbar to obtain 3D porous scaffolds and hereafter referred as MgHA/$Coll_{Pre}$ scaffolds.

(ii) Post-glycation: Biomineralized MgHA/Coll recovered as slurry was filled onto a polystyrene well-plate and freeze-dried using the same above-mentioned conditions. Thus, obtain 3D porous scaffolds were crosslinked in ethanol and PBS solution (70:30 vol.%) with 30 mM of ribose under intermittent shaking condition at 37 °C for 5 days. Later the scaffolds were washed in milli-Q water three times to remove unbound ribose and residual solvents and later freeze-dried again using the same above-mentioned conditions. The final 3D porous scaffolds were hereafter referred as MgHA/$Coll_{Post}$ scaffolds.

3D Porous non-crosslinked MgHA/Coll scaffolds served as reference material where ever needed in this study.

Bone biomineralization occurs through a series of electrostatic and stereo-chemical interaction between the inorganic and organic phase [30]. Biomineralized MgHA/Coll is synthesised through an innovative, bioinspired, pH-driven process, initiated by the PO_3^{-4} ions provided by the H_3PO_4 in aqueous solution. Under the alkaline pH conditions, the self-assembling of collagen fibrils occurs which serves as a template for mineralization. Upon further decrease in pH (~ 8), while the fibrils are still self-assembling, the precipitation of amorphous HA nanoparticles occurs on the collagen fibrils. On arriving at a neutral pH, two distinct processes synergies to conclude biomineralization which is namely the collagen fibres organisation into 3D network and HA nucleation [31]. Undoubtedly, the Mg^{2+} ions are key bivalent ions associated with biological apatite. Therefore, during the process of developing bone-like scaffolds, the incorporation of Mg^{2+} ions can stabilize the amorphous calcium phosphate precursor and control the qualitative changes of the bone [32]. Furthermore, collagen glycation causes inter-molecular crosslinking between the triple-helical regions of adjacent collagen molecule. These sugar-induced changes can significantly increase tissue stiffness and decrease

enzymatic solubility. In this experiment, we aim to study the influence of ribose in functional crosslinking of MgHA/Coll by following two different methodologies (pre-and-post glycation). The detailed schematic illustration of scaffold synthesis and crosslinking mechanism is depicted in Fig.1.

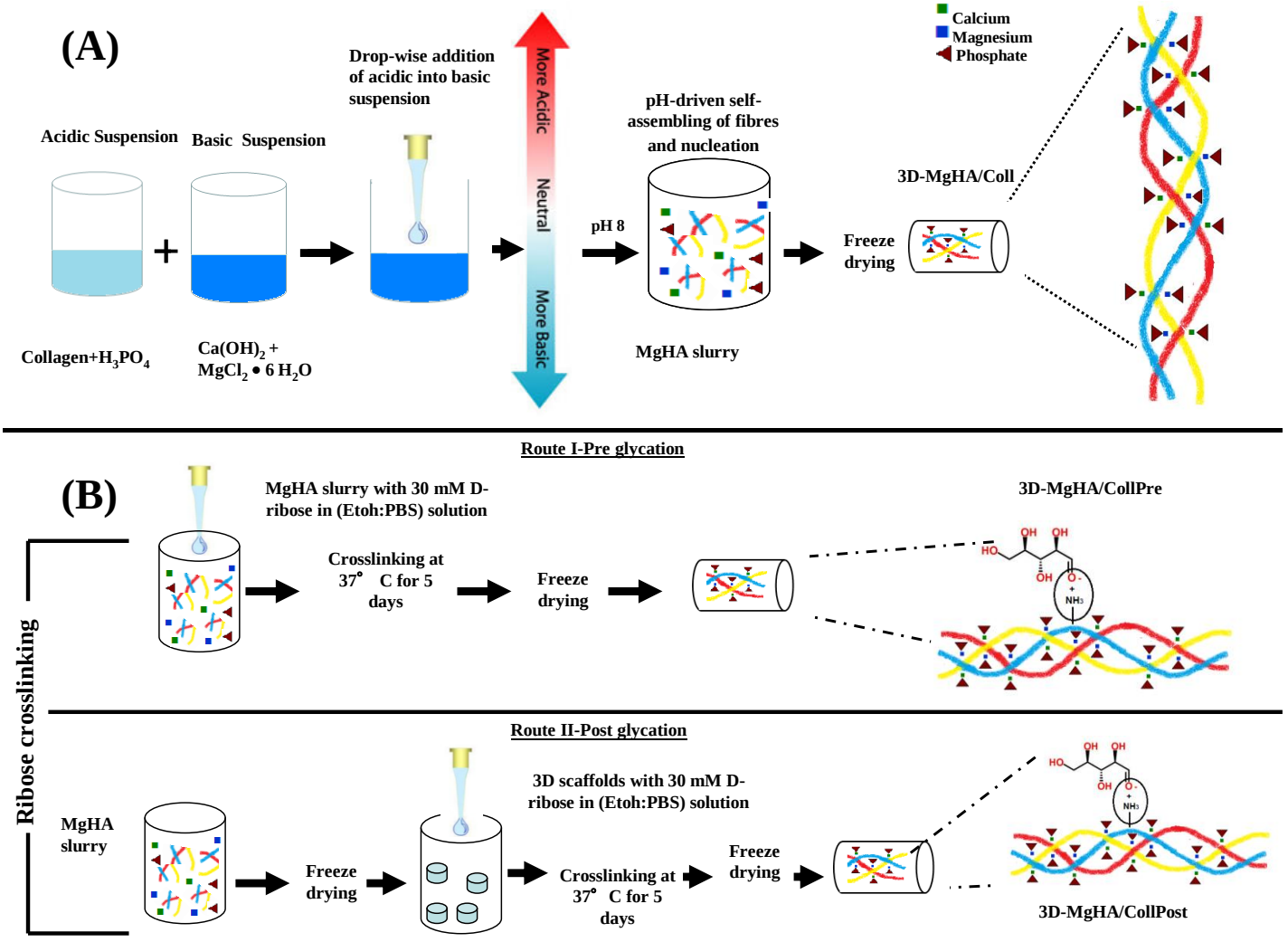

Figure.1: *Detailed schematic illustration of MgHA/Coll hybrid scaffold development, (A) pH-driven, bioinspired biomineralization process, (B) MgHA/Coll crosslinking with ribose scaffolds in pre and post glycation processes.*

3. Results and discussion - Characterization of the MgHA/Coll composites

3.1 Swelling behaviour

The fluid uptake ability was monitored by the water sorption study under physiological conditions. Cylindrical samples (diameter: 8 mm, height: 5 mm) were immersed in PBS solution at 37° C until the scaffolds reached a swelling saturation. At regular time intervals of (1, 2, 4, 6, 8 h) the scaffolds were withdrawn and the surface wetness was removed using a filter paper and the weight was measured. The equilibrium swelling ratio was calculated as: [(wet weight – dry weight)/wet weight] x 100.

The result elucidates that, the high degree of swelling was observed immediately after immersion in PBS solution at the initial stage for both the scaffolds. The equilibrium saturation was observed after 8 h with swelling percentage of 437.8 ± 20 %, 670.8 ± 52 % and 550.1 ± 46 % for MgHA/Coll, MgHA/$Coll_{Pre}$ and MgHA/$Coll_{Post}$ scaffolds respectively, with significantly higher values for ribose glycated scaffolds ($p<0.001$), as shown in Fig.2.A. The fast-swelling response is the characteristic feature attributed to the high hydrophilicity and porosity of MgHA/Coll scaffolds. Moreover, it is highly important for the polymer matrix to imbibe adequate water content in order to function similar to the living tissue with the ability to maintain physiological stability, low interfacial tension and allow the permeability of other biomolecules [33]. In addition, the incorporation of ribose enhanced the swelling behaviour with a favourable large surface/volume ratio which is beneficial for cell attachment and infiltration.

3.2. In-vitro collagenase assay

The structural integrity of the scaffolds is an important variable to monitor while developing long-term scaffolds. Osteoclasts release the collagenase enzyme in order to break down the collagenous networks during bone resorption [34]. To partially, biomimic the *in-vivo* conditions, the developed scaffolds were incubated in collagenase solution. Briefly, known weight of sample was incubated in 0.1 M Tris-HCl (pH 7.4) containing collagenase enzyme (100

units/ml) for 24 h at 37° C. Then, the samples were removed and washed with milli-Q water and the final dry weight was noted after freeze drying. The degradation rate was estimated through percentage of weight loss and calculated as: [(initial dry weight – final dry weight)/initial dry weight] x 100.

The results show that the treatment with ribose of MgHA/Coll composite has a positive effect in modulating its degradation kinetics. The not treated MgHA/Coll composite had the highest weight loss of 17.2 ± 0.84 %, whereas the MgHA/Coll$_{Pre}$ and MgHA/Coll$_{Post}$ had the lowest weight loss of 4.05 ± 0.45 % and 3.5 ± 0.36 % as seen in Fig.2.B. The enhanced resistance to rapid enzymatic degradation of MgHA/Coll$_{Pre}$ and MgHA/Coll$_{Post}$ crosslinked scaffolds is strongly due to chemical reaction of ribose used as reticulating agent. The newly formed crosslinks between collagen molecules due to ribose interaction helps in masking of collagenase recognition sites and increases the resistance to enzymatic degradation [35].

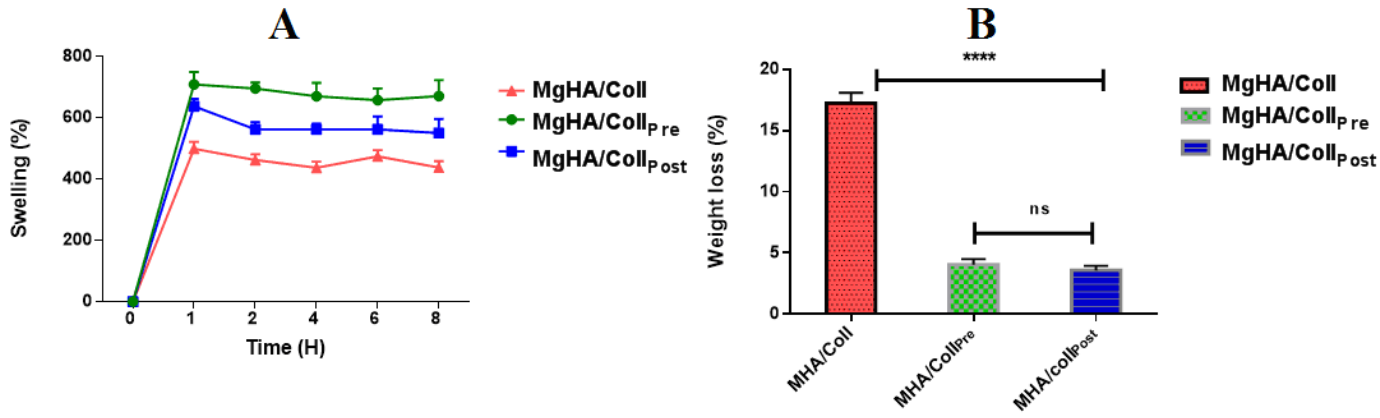

Figure.2: *(A) Water uptake capacity as function of time, (B) Enzymatic resistivity as function of time of MgHA/Coll, MgHA/Coll$_{Pre}$ and MgHA/Coll$_{Post}$ scaffolds. Data are mean ± SEM from 3 samples each type of scaffold. Statistically significant differences between MgHA/Coll respect to MgHA/Coll$_{Pre}$ and MgHA/Coll$_{Post}$ (****$p \leq 0.001$) and ns represents not significant.*

3.3 Scaffold dimensional properties

The surface and the topographical micro-architecture of the scaffolds were examined by high resolution scanning electron microscopy (SEM: FEI, Quanta 200, UK) at a pressure of 0.1 m Torr at an accelerating voltage of 15 kV performed on sample specimens mounted onto aluminium stubs using black carbon tapes and sputter coated with gold (Sputter Coater Q150TES, Quorum, (Italy)).

The pore size distribution in the wet scaffolds was evaluated by observing thin sections (20 μm) of the scaffold specimen under a bright field microscope (Nikon). The thin sections were obtained by soaking the scaffolds in PBS solution for 24 h and later embedding in OCT medium and subsequently quenched in liquid nitrogen. The frozen OCT blocks were cut horizontally using a cryostat (Histo-line, 5000 MC, Italy) to obtain thin sections. The pore diameter was measured using NIS Elements Imaging Software (3.22.1, Nikon). The relative density of the scaffolds was calculated from measuring the dry density of the samples using the equation ($\boldsymbol{\rho}^* = m/v$), where m and v indicates the mass and volume of the 3D scaffolds. The known dry density of collagen ($\boldsymbol{\rho}s$) was assumed to be 1.3 g/ml as reported elsewhere [29]. The percentage of porosity is calculated from the relative density values and calculated as: $(1- \boldsymbol{\rho}^*/ \boldsymbol{\rho}s) \times 100$. The measure was repeated three times on different samples.

The scaffolds morphology was observed using the SEM (Fig.3), which revealed fibrous micro-architectures with very small nanocrystals closely bound to the collagen fibres thereby giving the material a highly porous structure with micro/macro porosities. At lower magnification, the MgHA/Coll appeared to be more fibrous, whereas the both glycated MgHA/Coll showed more random distribution of anisotropic pores. At higher magnification, it was possible to view a single or bundles of collagen fibres being completely covered by the amorphous mineral phase as depicted in Fig.3. However, all the scaffolds represented a morphology and structure significantly similar to human trabecular bone [14]. In terms of porosity, all scaffolds exhibited a high level of porosity, above 80%, as shown in Fig.4.A, nevertheless when compared with MgHA/Coll the both pre-and-post glycated MgHA/Coll had significant higher porosity ($p \leq 0.001$). This can be correlated with

water uptake capacity, which demonstrated higher swelling ratio for glycated scaffolds (Fig.2.A). Therefore, the influence of ribose as a coupling agent helped additionally in achieving well desired porosity to promote cell invasion and subsequent vascularisation [36]. The average pore size was within the range of 0-200 µm, with presence of large and small pores as illustrated in the Fig.4.B. The small pores (< 200 µm) can be due to the alcoholic solvent treatment during crosslinking reaction which often leads to protein hydrophobicity, shrinkage and collapse of the final structure with reduced pore size [37]. Nonetheless, the obtained pore size in these scaffolds was sufficiently high to enable cellular infiltration and exchange of metabolic products, which is also confirmed from the cell-material interaction study.

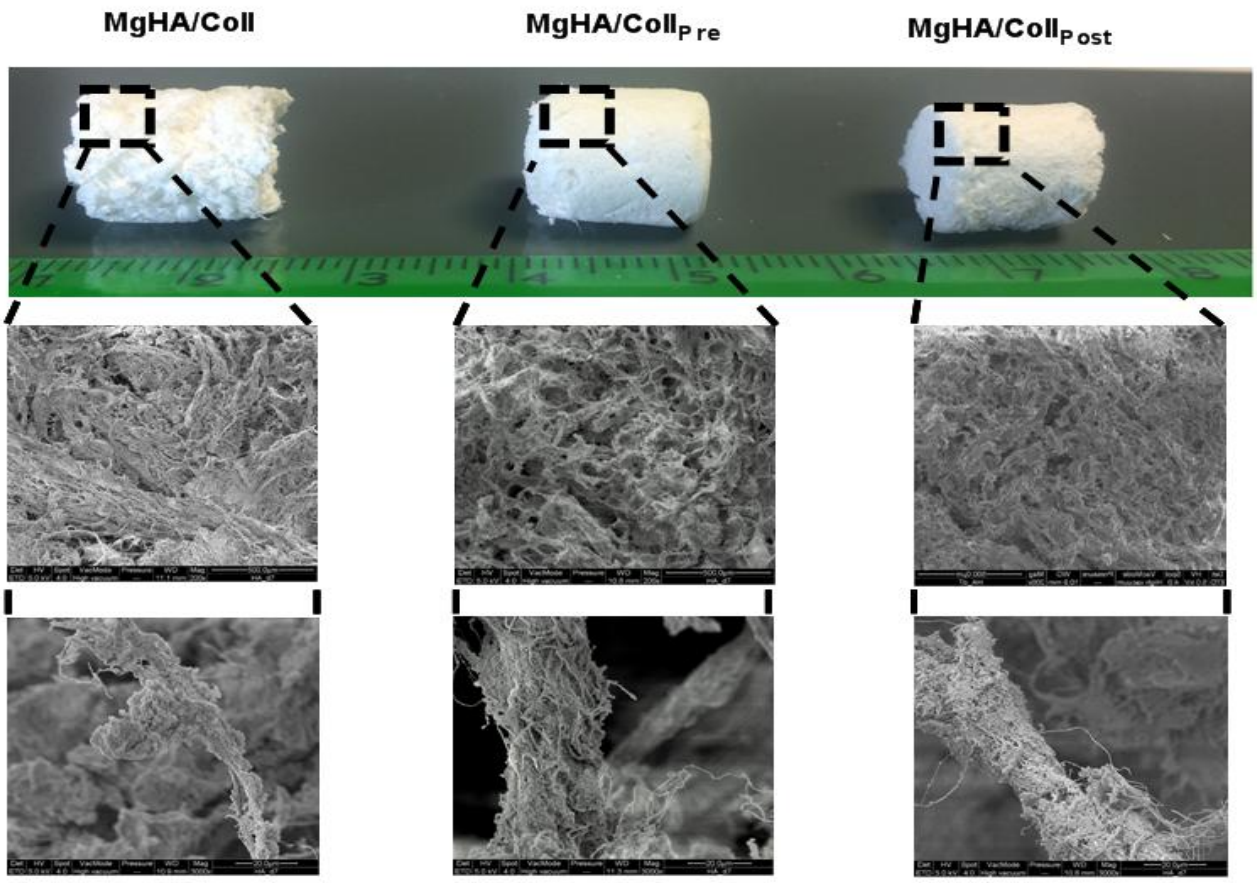

Figure.3: *Surface morphology of MgHA/Coll, MgHA/Coll$_{Pre}$ and MgHA/Coll$_{Post}$ scaffolds at respective magnification. (Panel A – 200 X and Panel B – 2500 X)*

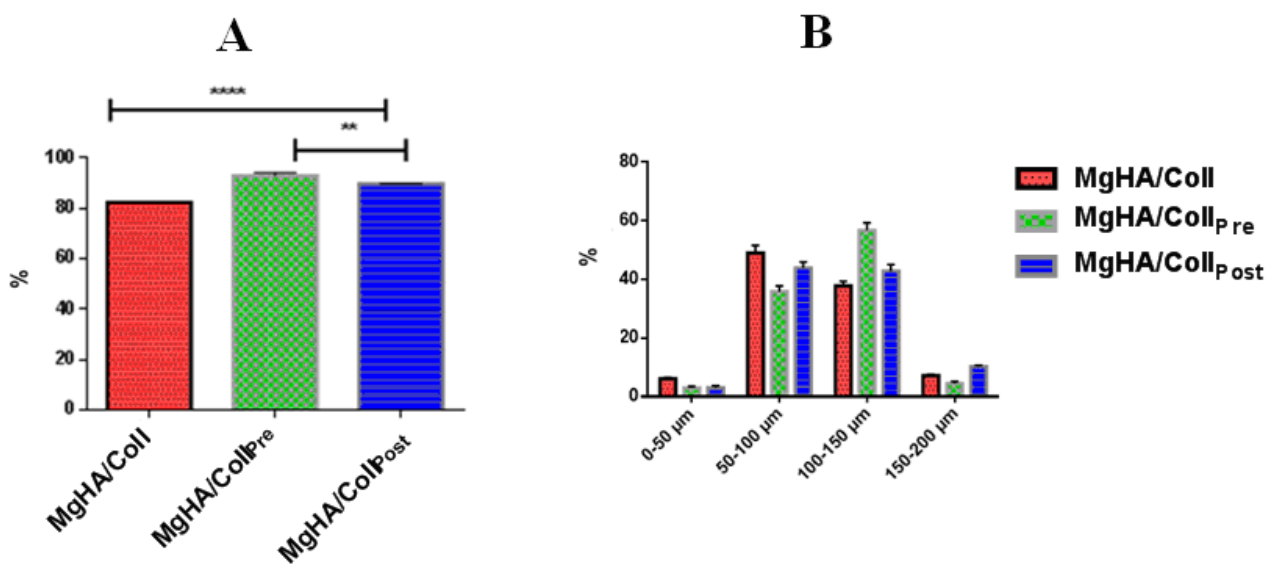

Figure.4: *Dimensional properties of the scaffolds, (A) Porosity, (B) Wide spectrum of pore size distribution in the MgHA/Coll, MgHA/Coll$_{Pre}$ and MgHA/Coll$_{Post}$ scaffolds. Data are mean ± SEM from 3 samples each type of scaffold. Statistically significant differences between MgHA/Coll respect to MgHA/Coll$_{Pre}$ and MgHA/Coll$_{Post}$ (****$p \leq 0.001$) and between MgHA/Coll$_{Pre}$ and MgHA/Coll$_{Post}$ (**$p \leq 0.01$).*

3.4 Physical-Chemical characterization

3.4.1 ICP Analysis

Inductively coupled plasma-optical emission spectrometry (ICP-OES, Agilent Technologies 5100 ICP-OES, Santa Clara, USA) was used for the quantitative determination of Mg^{2+}, Ca^{2+} and PO_3^{-4} ions that constitutes the inorganic mineral component. Briefly, 40 mg of sample was dissolved with 2 ml nitric acid (65 wt.%) followed by subsequent sonication and dilution with 100 ml of milli-Q water. The following analytical emission wavelengths were used for Ca (422 nm), Mg (279 nm) and P (214 nm) ions.

The chemical mimesis of the natural bone was achieved by the addition of Mg^{2+} ions in the apatite lattice of the scaffolds during the biomineralization process. The ICP analysis demonstrates that the values of (Ca+Mg)/P ratio were 1.54 ± 0.013, 1.57 ± 0.040 and 1.56 ± 0.004 for MgHA/Coll, MgHA/Coll$_{Pre}$ and MgHA/Coll$_{Post}$ respectively as illustrated in Table.1. These values construe the

typical low crystalline apatite (1.45 – 1.60) range which is mainly due to the presence of HPO_2^{-4} ions [38]. The evidence for magnesium substitution of calcium was found to be of 3.1 ± 0.03 %, 3.2 ± 0.03 % and 3.6 ± 0.03 % for MgHA/Coll, MgHA/$Coll_{Pre}$ and MgHA/$Coll_{Post}$ respectively. This result confirms that the mineral phase was preserved during the glycation process with the magnesium substitution of calcium ratio comparable to the MgHA/Coll scaffolds with high biomimetic mineral phase.

	Ca/P (mol)	**Mg/Ca (mol%)**	**(Ca+Mg)/P (mol)**
MgHA/Coll	1.49 ± 0.013	3.19 ± 0.031	1.54 ± 0.013
MgHA/CollPre	1.53 ± 0.028	3.20 ± 0.027	1.57 ± 0.040
MgHA/CollPost	1.50 ± 0.004	3.68 ± 0.036	1.56 ± 0.004

Table.1: *Chemical composition of MgHA/Coll, MgHA/$Coll_{Pre}$ and MgHA/$Coll_{Post}$ scaffolds obtained from ICP analysis.*

3.4.2 FTIR Analysis

The infrared spectres were collected using Nicolet 380 FT-IR spectrometer (Thermo Fisher Scientific Inc, Waltham, USA). Briefly, 2 mg of sample was mixed with 100 mg of anhydrous potassium bromide and then pressed at 8000 psi into 7 mm diameter discs. The spectrums were collected in the wavelength ranging from 400 to 4000 cm^{-1} with 2 cm^{-1} of resolution.

The chemical interaction between the mineral phase MgHA and collagen fibres can be observed in the FTIR spectral peaks Fig.5. The shift from 1340 to 1337 cm^{-1} indicates the stretching of COO^- groups of collagen which typically represents the active interaction of collagen functional groups with the positively charged apatite crystals. The typical spectra at 873 cm^{-1} indicates the carbonation of the MgHA nucleation on the collagen fibrils. The carbonation was visible in both pre and post glycated collagen which clearly indicates that the glycation of collagen with ribose did not affect the carbonation of the inorganic phase Fig.5.A. Moreover, the three carbonation peaks in the B position of the HA was visualized at 1540, 1455 and 1413 cm^{-1}. The peak corresponding to acid

phosphate (HPO_2^{-4}) in the mineral lattice was visible between 550 to 560 cm^{-1}. These distinctive peaks of MgHA/Coll scaffolds are similar to the FTIR pattern of young bone [14]. Due to the complex structure of the scaffolds, there exist an overlapping of many spectral peaks of Coll, HA and ribose, thereby making it harder to determine then spectral changes brought due to collagen-sugar interaction. However, the slight spectral changes observed between 1035 and 1081 cm^{-1} for the ribose crosslinked scaffolds Fig.5.B shows the C-O, C-C stretching and C-O-H and C-C-O bending vibrations mainly due to the collagen-sugar interaction between the carbonyl group of ribose and the amine group of collagen [39]. Therefore, these spectral changes confirm (i) the nucleation of Mg^{2+} ions in the collagen template, which is exceptionally amorphous and non-stoichiometric with evidence of high level biomimicry analogous to the natural bone mineral and (ii) the active interaction and presence of ribose as crosslinker within the collagen and MgHA heteromolecular networking.

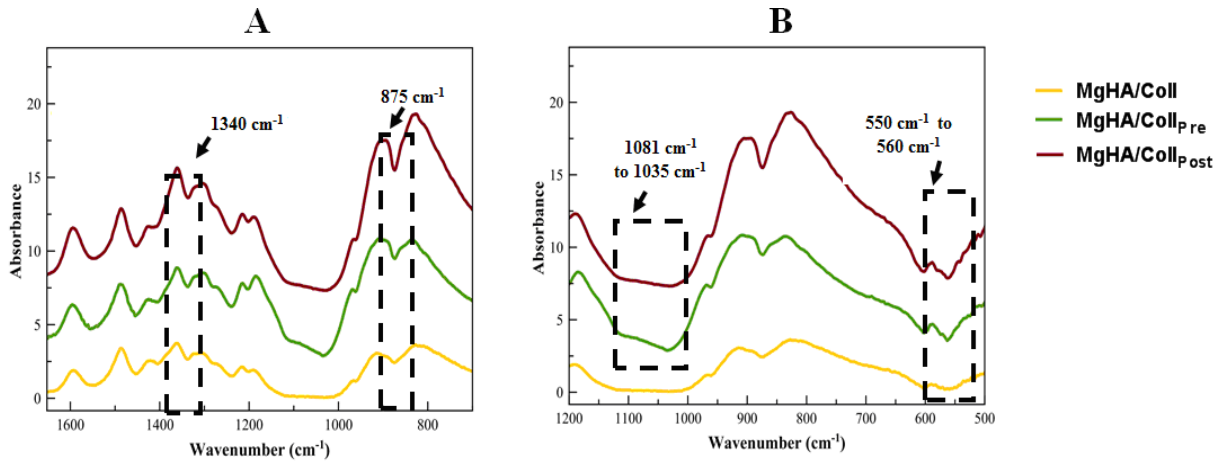

Figure.5: *FTIR spectral peaks, (A) Functional interaction of collagen and HA crystals with* evidence of MgHA carbonation in MgHA/Coll, MgHA/$Coll_{Pre}$ and MgHA/$Coll_{Post}$ scaffolds (B) The peaks contributing to D-ribose interaction in MgHA/$Coll_{Pre}$ and MgHA/$Coll_{Post}$ scaffolds.

3.4.3 XRD Analysis

X-ray diffraction patterns (XRD) were performed using D8 Advance diffractometer (Bruker, Germany) with Cu Kα radiation (λ = 1.5418 Å) in the 2θ range 20°-80° with step angle of 0.013° and scan time of 0.5s.

The direct nucleation of the MgHA crystals on the collagen fibrils results in a composite material (MgHA/Coll) which displayed a low crystalline pattern. Both the pre and post glycated MgHA/Coll displayed a very similar band patterning with broad peaks as seen in Fig.6.A. Moreover, the composite synthesis at 25° C highly influenced in obtaining an amorphous phase without any long-range periodic regularities. The large broadening of reflections in the XRD pattern shows that during the nucleation process, the nano-sized dimensions of crystallites were growing along the collagen fibrils with preferential *c*-axis orientation [40]. Moreover, in this study the theoretical HA/Coll ratio was (70/30 wt %) which is identical to the natural bone. It is well understood that there exists a competition in between the magnesium and calcium ions in occupying the crystal lattice which is mainly modulated during the nucleation and crystallization kinetics which apparently also determines the crystallinity of the mineral phase [11]. In addition, the decreased crystallinity can also be attributed to the presence of foreign ions (Mg^{2+}, CO_2^{-3} and HPO_2^{-4}) in the apatite lattice as analogous to the natural bone niche, where these multitude of ions play a crucial role in maintaining bone metabolism which also directly corresponds to high reactivity under *in-vivo* conditions and determines the rate of bone formation and remodelling [12].

3.4.4 TGA Analysis

The pyrolytic curves were determined using Thermo Gravimetric Analyser (TGA) (STA 449/C Jupiter, Netzsch Germany). Briefly, 20 mg of sample was placed in aluminium crucible and then crushed and press sealed for complete contact with the crucible. The experiment was carried in the temperature range of 30-1000° C at a heating rate of 10° C/min in nitrogen atmosphere.

The nucleation of the mineral phase on the collagen was quantified by TGA. Initially, all scaffolds had a nominal composition of MgHA/Coll of 70/30 wt %, the amount of inorganic phase was calculated as residual mass of the sample at 1000° C from the TGA curves. The residual mass was 50 wt % for MgHA/Coll and MgHA/$Coll_{Post}$ and whereas in MgHA/$Coll_{Pre}$ it was found to be 53 wt % as seen in Fig.6.B. It is note worthy to mention the role of temperature in the reaction yield as studied by others which reports that low temperature synthesis greatly enhances the availability of

nucleation sites on the collagen and greatly avoids the partial denaturation of polymers [41]. However, the both pre and post glycated MgHA/Coll scaffolds were synthesised at 25° C (low temperature) and crosslinked at 37° C (high temperature) in presence of ribose. Therefore, this result as an evidence shows that high temperature crosslinking reaction does not disturb the nucleation of the mineral phase and also helps in producing an equivalent reaction yield similar to the non-crosslinked MgHA/Coll.

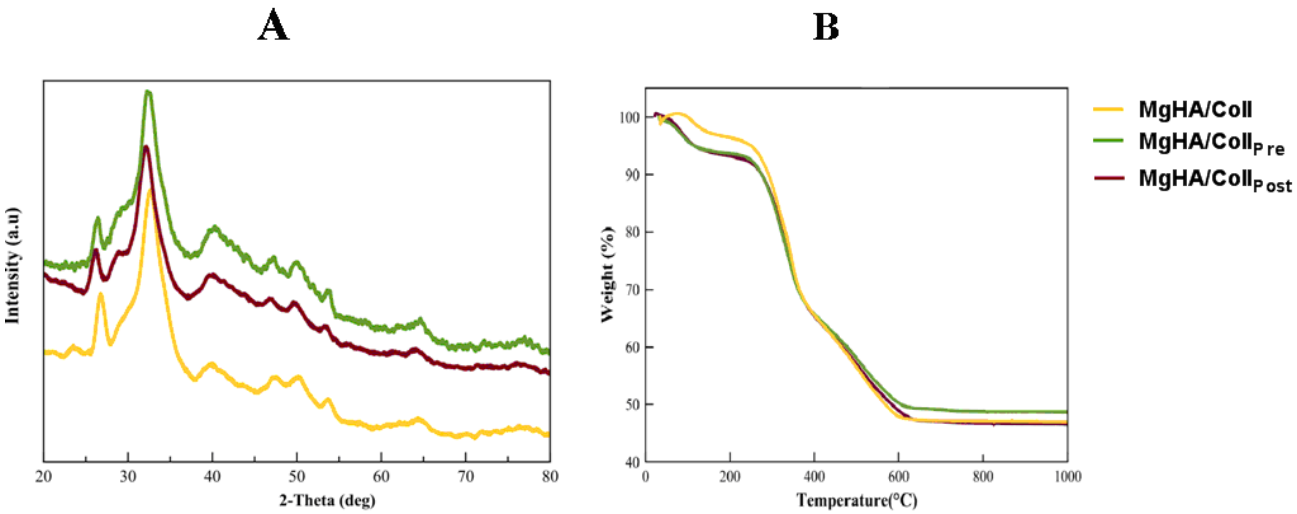

Figure.6: *(A) XRD patterns, (B) TGA curves of MgHA/Coll, MgHA/Coll$_{Pre}$ and MgHA/Coll$_{Post}$ scaffolds.*

3.5 Mechanical Characterization

For the dynamic mechanical analysis (DMTA), cylindrical scaffolds with dimensions of 10 mm in diameter and 10 mm in thickness were prepared and hydrated for 24 h prior to testing in PBS solution. Both static compression test and dynamic mechanical test were performed in compression clamp using Q800 DMTA analyser (USA). To mimic the physiological conditions, every test was performed at 37 ° C and initially preloaded at 0.01N to ensure the complete contact between the end-plates of the scaffolds and the compression plates and then compressed in force control at a force ramp rate of 0.5 N/min to the upper force limit of 5 N. The compressive moduli were calculated as the slope of the initial linear part of the stress-strain curve up to 10% strain. The viscoelastic properties of the scaffolds were also measured by applying an initial strain of 75 µm,

followed by frequency sweep from 0.1 Hz to 10 Hz. The storage modulus (E'), loss modulus (E") and tan δ (=E"/E') were calculated. Six samples were tested for each formulation.

Under adequate hydration, the scaffold mechanical behaviour can fluctuate depending on the swelling ability and porosity of the scaffolds. The drastic swelling response of scaffolds due to high degree of hydrophilicity can make the scaffolds more elastic and less stiff, eventually causing significant reduction in compressive modulus [42]. However, it is more important to biomimic the biological conditions, all kinds of mechanical analyses were performed on completely swollen scaffolds. The catastrophic failure plateau and the densification regions of the scaffolds can be observed from the typical stress-strain curve as seen in Fig.7.A. Identifying and determining the initial linear region (elastic zone) was truly difficult due to the micro-fractures of the collagen fibrils at initial stress which is likely due to strut buckling and collapsing of the fibrils. In order to standardise the results, the compressive modulus was calculated between 1-10 % strain values.

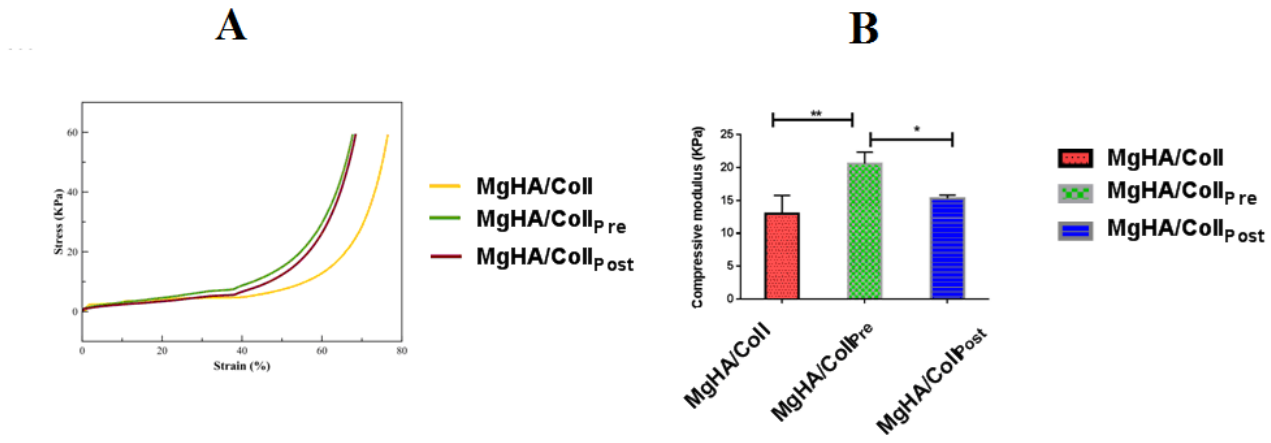

Figure.7: *Mechanical analysis, (A) The typical stress-strain curve (B) Compressive modulus of MgHA/Coll, MgHA/Coll$_{Pre}$ and MgHA/Coll$_{Post}$ scaffolds. Data are mean ± SEM from 6 samples each type of scaffold. Statistically significant differences between MgHA/Coll and MgHA/Coll$_{Pre}$ (**$p \leq 0.01$) and between MgHA/Coll$_{Pre}$ and MgHA/Coll$_{Post}$ (*$p \leq 0.05$).*

The modulus and the strength of the MgHA/Coll scaffolds were improved greatly due to ribose crosslinking. The MgHA/Coll$_{Pre}$ represented to be the strongest material with highest compressive modulus of (20.6 ± 1.7 KPa) followed by MgHA/Coll$_{Post}$ (15.3 ± 0.51 KPa) and MgHA/Coll (13.9 ± 2.7 KPa) as seen in Fig.7.B.

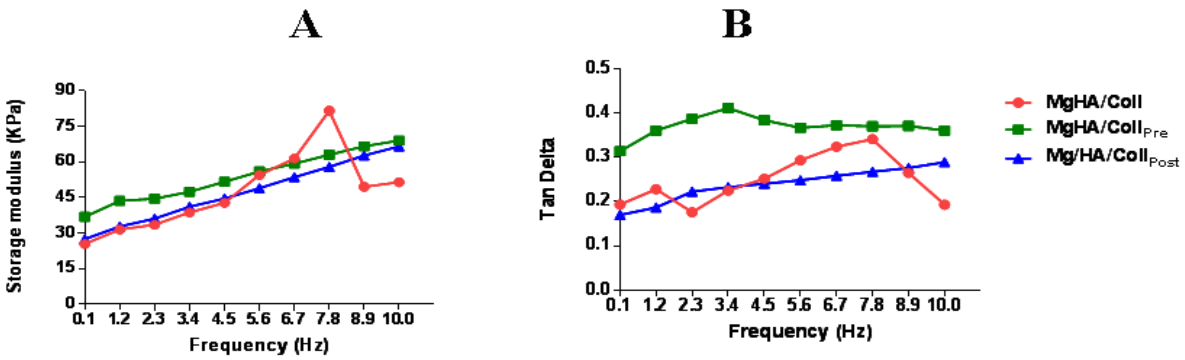

Figure. 8:*Viscoelastic properties, (A) Storage modulus (B) Tan delta of MgHA/Coll, MgHA/Coll$_{Pre}$ and MgHA/Coll$_{Post}$ scaffolds. Data are mean ± SEM from 6 samples each type of scaffold.*

The viscoelastic behaviour of any bone-like scaffold needs to demonstrate satisfactory biomechanical property for a successful long-term *in-vivo* application. Accordingly, all scaffolds showed significant variation in storage modulus (E') in response to oscillating frequencies. The MgHA/Coll$_{Pre}$ scaffolds showed the highest E' value followed by MgHA/Coll$_{Post}$ and MgHA/Coll as depicted in Fig.8.A. Therefore, the increased E' values in ribose glycated samples is a good indictor illustrating the capacity of the material to store energy during deformation [43]. Similarly the loss factor (tan δ) was increasing in all scaffolds as the frequency fluctuated as seen in Fig.8.B. The loss factor represents the ratio between the amount of energy dissipated by the viscous portion and the energy stored in the elastic portion. Therefore, the increasing tan δ values as function of increase in frequency suggests that all scaffolds represented to be more viscous and less elastic [44]. The increased tan δ values for ribose glycated samples is ascribed due to the adequate pore size and porosity of the scaffolds which assists in achieving sufficient water retention within the pore wall

due to hydrostatic effect. This indicates the higher damping capabilities of the ribose glycated samples, therefore such scaffolds under weight bearing conditions can provide the sufficient mechanical support to tolerate the *in-vivo* stress and load [45]. Overall, the performed mechanical characterization shows that the presence of ribose did have a significant effect in ameliorating the mechanical resistance of the MgHA/Coll scaffolds.

3.6 Cell Culture

Mouse pre-osteoblast cell line (MC3T3-E1) was supplied by ATCC® (USA) and was used to investigate the cell-scaffold interaction. MC3T3-E1 cells were cultured in α-MEM containing ribonucleosides, deoxyribonucleosides, L-glutamine, supplemented with 10 % FBS and 1 % penicillin/streptomycin (100 U ml^{-1}/100 µg ml^{-1}) and incubated at 37° C with 5 % CO_2 atmosphere. The cells were cultured until 85 % confluence and detached by trypsinization and centrifugation, later the cell number and viability were assessed by trypan blue dye exclusion test. The experimental scaffolds were obtained in dimensions of 5 mm in diameter and 6 mm in thickness and were sterilized by 25 kGy gamma-ray radiation. Prior to experimentation, all scaffolds were pre-incubated with 1 ml of culture media for 48 h at 37° C to swell the scaffolds and to remove any residues. The pre-incubated samples were placed one per well in a 24-well plate and a drop of 20 µl containing 7.5 x 10^4 cells suspension in culture media was added on upper-surface of the scaffolds for initial cell attachment. After 30 min, 1.5 ml of cell culture media supplemented with 50 µg/mL ascorbic acid and 10 mM β-glycerophosphate was added for cell proliferation and differentiation and incubated at 37° C, 5 % CO_2 for 7 days. Considering the issues of instability and vulnerability to degradation under physiological conditions due to lack of crosslinking, the cell culture experiments on the non-crosslinked MgHA/Coll scaffolds were not studied. Therefore, only ribose glycated MgHA/$Coll_{Pre}$ and MgHA/$Coll_{Post}$ scaffolds were studied and compared in all cell culture experiments. All cell handling procedures were performed in a sterile laminar flow hood.

Cell viability was assessed by Live/Dead assay which is based on the simultaneous detection of live and dead cells with two probes, Calcein and Ethidium homodimer-1, that measures the recognized parameters of cell viability: intracellular esterase activity and plasma membrane integrity respectively. Briefly, at 1, 3 and 7 days of cell culture the scaffolds were washed in PBS solution for 5 min and stained with Calcein acetoxymethyl 2 µM and Ethidium homodimer-1 4 µM for 15 min at 37° C. Later the scaffolds were again washed in PBS for 5 min and viewed under inverted Ti-E fluorescence microscopy (Nikon). Two scaffolds at each time point were analysed. The cell viability was quantified by counting the total number of cells from five random fields of view per sample at 10 X magnification using Image J (1.6.0) software and is reported as of percentage of live cells respect to the total number of cells.

The morphology of the osteoblasts grown on the scaffolds was visualized using SEM. Briefly, after 1 and 7 days, the cell-seeded scaffolds were washed with 0.1 M sodium cacodylate buffer (pH 7.4) and later fixed in the same buffer with 2.5 % glutaraldehyde for 2 h at 4° C. Later, the freeze-dried specimens were mounted onto the aluminium stubs using black carbon tapes and they were sputter coated with gold particles (Sputter Coater Q150TES, Quorum, Italy). The cells on the scaffold surface were then examined using high resolution SEM (FEI, Quanta 200, UK).

The actin cytoskeleton organisation and morphology of the cells on the scaffolds was visualized by actin-DAPI staining. After 3 days of cell culture, the scaffolds were removed and rinsed in PBS and fixed in 4 % paraformaldehyde solution for 10 min at room temperature. Then the samples were permeabilzed with 0.1 % Triton in PBS for 10 min followed by FITC-conjugated Phalloidin staining for 20 min and subsequent DAPI staining for 5 min and visualized immediately with an inverted Ti-E fluorescence microscope (Nikon).

The cytocompatibility of the low-cost, mineralized scaffolds in terms of cell colonization and adhesion was evaluated by MC3T3-E1 cells. The cell viability of the pre-osteoblasts cultured on the porous scaffolds was observed using the Live/Dead assay, which demonstrated high viability representing good cytocompatibility at each time point. With the increase in culture time there was

increase in cell density especially on day 7 and cells appeared to be homogenously distributed in both the scaffold surfaces as shown in Fig.9. The cell proliferation was evaluated by counting the total number of cells at each time point and was reported as percentage of live cells, which again demonstrated a high level of cell viability as the culture time prolonged as illustrated in Fig.10.

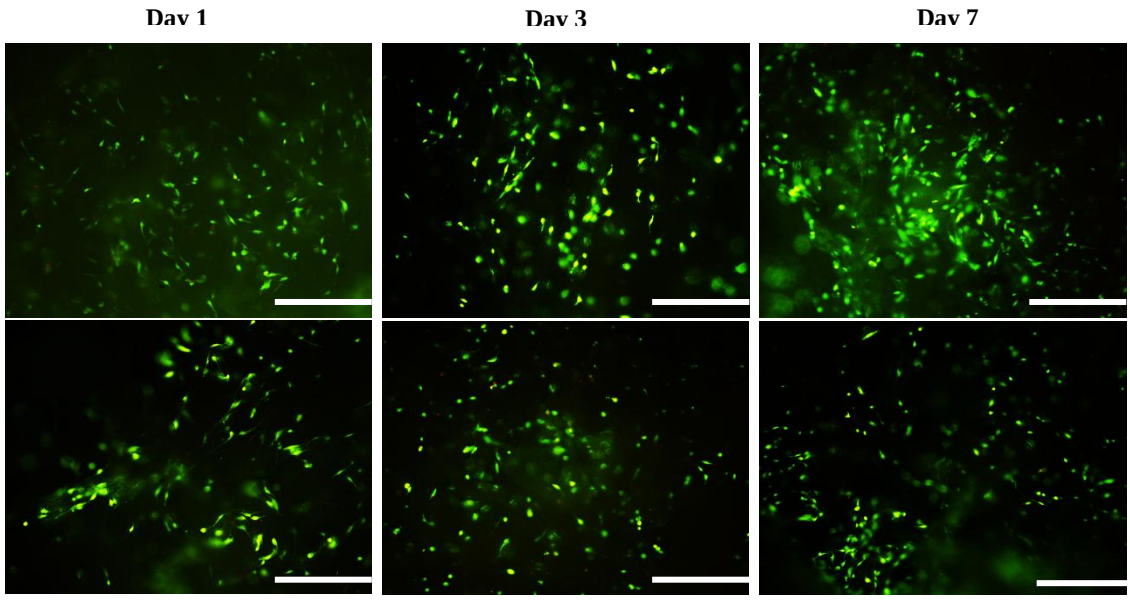

Figure.9: *Cell viability analyzed by the live/dead assay (Calcein stains live cells in green, Ethidium homodimer-1 stains dead cells in red) of MgHA/Coll$_{Pre}$ and MgHA/Coll$_{Post}$ scaffolds on 1 day, 3 days and 7 days. Scale bar: 100 µm.*

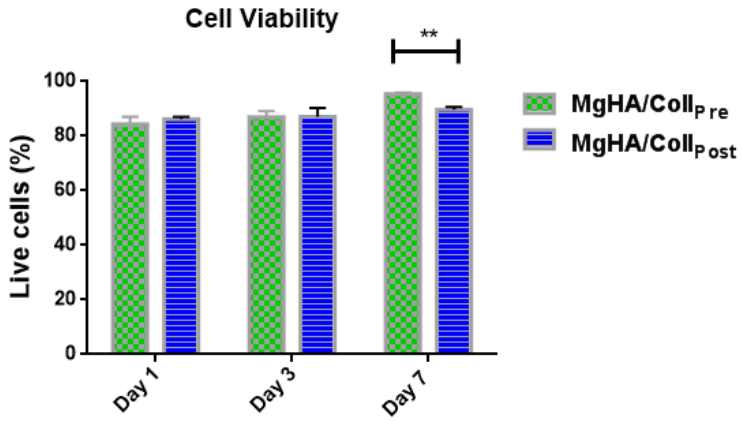

Figure.10: *Cell proliferation of MgHA/Coll$_{Pre}$ and MgHA/Coll$_{Post}$ scaffolds on 1 day, 3 days and 7 days. (**$p \leq 0.01$).*

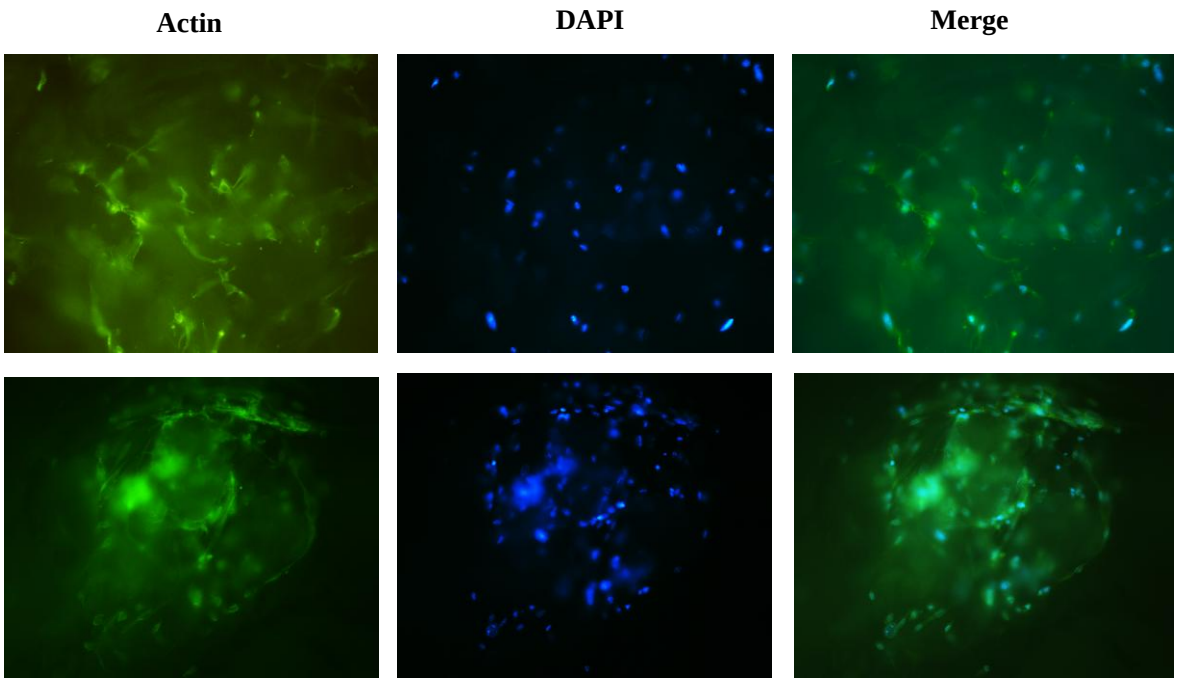

Figure.11: *Cell morphology analysed by the Actin-DAPI staining (Phalloidin stains exoskeleton actin filaments in green and DAPI stains cell nuclei in blue) of MgHA/Coll$_{Pre}$ and MgHA/Coll$_{Post}$ scaffolds on day 3. Scale bar: 50 µm.*

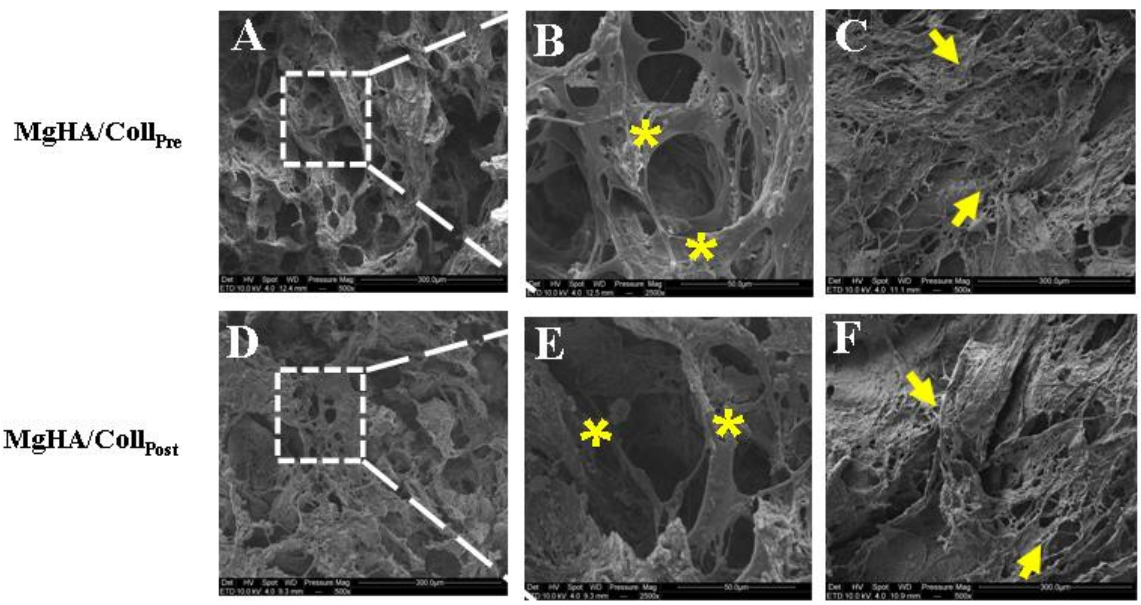

Figure.12: *Morphology of cell-seeded scaffolds at day 1 of MgHA/Coll$_{Pre}$ (A, B) and MgHA/Coll$_{Post}$ scaffolds (D, E) analysed by SEM. Morphology of cell-seeded scaffolds at day 7 of MgHA/Coll$_{Pre}$ (C) and MgHA/Coll$_{Post}$ (F). Asterisk and arrow marks indicates the cells spreadability over the scaffold at respective time points.*

However, on comparing the MgHA/$Coll_{Pre}$ and MgHA/$Coll_{Post}$ there was no statistical significant difference in their viability outcomes at all time points. From the cytoskeleton structure staining, the proper presence of extended actin filaments with cell nuclei manifests the cell survival with rational cell-material interaction under the influence of ribose in both pre and post glycated samples as seen in Fig.11. The detailed cell morphology, as observed from the SEM analysis shows the strong scaffold colonization with the characteristics osteoblast morphology without any abnormal alterations as depicted in Fig.12. At 7 days of cell culture, there is a presence of cell layers over the scaffolds showing the good spreadability of osteoblasts as evident in Fig.12 (C, F).

This preliminary *in-vitro* study was performed to assess the functional utility of this novel, low-cost crosslinker in MgHA/Coll scaffolds in terms of cell-material interaction. Overall, the presence of ribose can collectively strength the matrix stiffness which greatly influences cell proliferation and adhesion. Previous studies have shown, that the use of nominal concentration of ribose (30 mM) has a strong effect in accelerating the cellular activities without any toxic response [21,23]. Accordingly, in this study our scaffolds also behaved similarly with a favourable cellular response. In addition, the presence of HA within the collagen networking has greatly helped in obtaining good surface properties (suitable roughness) and opportune hydrophilicity which greatly improves the biocompatibility of the scaffolds [46]. Moreover, the presence of Mg^{2+} ions in the scaffolds, can improve osteoconductivty and osteogenesis [47]. Therefore, when the reputability of HA and Mg^{2+} ions is highly ratified in BTE applications, adding an inexpensive ribose as an alternative reticulating agent, can be more economical and feasible in BTE application for producing functional scaffolds. This *in-vitro* study strongly supports this hypothesis, that the minimum concentration of ribose with nominal ratio of HA helps in obtaining highly desirable crosslinking with opportune surface roughness that collectively benefits the overall biocompatibility of these scaffolds.

4. Conclusion

On comparing, the physical-chemical features of MgHA/$Coll_{Pre}$ and MgHA/$Coll_{Post}$, there was no significant difference in their performance. Both scaffolds exhibited similar chemical, physical and morphological characteristics analogous to the control MgHA/Coll scaffolds. The mechanical behaviour was more favourable for MgHA/$Coll_{Pre}$ scaffold and represented to be the strongest material. In terms of biological performance, there was no significant difference in cell proliferation and viability. Both the scaffolds demonstrated good compatibility without any toxic response. Therefore, irrespective of their mode of action (pre or post glycation) both scaffolds demonstrated good cell adherence and proliferation.

Taken collectively, based on evident results, we consider that MgHA/$Coll_{Pre}$ scaffolds produced through pre glycation of ribose mechanism is more favourable and beneficial for BTE applications due to the following reasons, (i) pre glycation mechanism is facile, robust, cost-effective and less time consuming process, (ii) pre glycation causes *in-situ* crosslinking, which means there is a direct local interaction of fibrous collagen with ribose to form the necessary essential crosslinks, (iii) the final 3D production of MgHA/$Coll_{Pre}$ scaffold is less time consuming, which is highly supportive in preventing deterioration of mineral phase during scaffold synthesis, (iv) MgHA/$Coll_{Pre}$ scaffolds demonstrated significantly higher compressive modulus, (v) pre glycation mechanism is more beneficial, when there is a need to incubate the cells before collagen polymerization, because under such reactions, the cells can reside within the active sites of collagen fibrils before polymerization to avoid any osmotic imbalances [48]. Therefore, the ribose glycation of collagen can serve as a value tool to study, (i) altered tissue mechanical properties due to glycation, (ii) cell behaviour in response to glycation, (iii) as *in-vitro* model to study extra cellular matrix changes in age-related bone pathologies. Moreover, this study also offers new insights and opportunities in developing promising scaffolds for bone tissue engineering.

5. References

1) Giannoudis PV, Einhorn TA, Marsh D. Injury. 2007, 38 Suppl 4:S3-6. Review.

2) Zhi W, Zhang C, Duan K, Li X, Qu S, Wang J, Zhu Z, Huang P, Xia T, Liao G, Weng J. J Biomed Mater Res A. 2014, 102(8):2491-501.

3) Fan H, Zeng X, Wang X, Zhu R, Pei G. Biomaterials. 2014, 35(26):7407-15.

4) Smith EL, Kanczler JM, Gothard D, Roberts CA, Wells JA, White LJ, Qutachi O, Sawkins MJ, Peto H, Rashidi H, Rojo L, Stevens MM, El Haj AJ, Rose FR, Shakesheff KM, Oreffo RO. Acta Biomater. 2014, 10(10):4186-96.

5)Amorosa LF, Lee CH, Aydemir AB, Nizami S, Hsu A, Patel NR, Gardner TR, Navalgund A, Kim DG, Park SH, Mao JJ, Lee FY. Int J Nanomedicine. 2013;8:1637-43.

6) Guo Y, Tran RT, Xie D, Wang Y, Nguyen DY, Gerhard E, Guo J, Tang J, Zhang Z, Bai X, Yang J. J Biomed Mater Res A. 2015, 103(2):772-81.

7) Filardo G, Kon E, Tampieri A, Cabezas-Rodríguez R, Di Martino A, Fini M, Giavaresi G, Lelli M, Martínez-Fernández J, Martini L, Ramírez-Rico J, Salamanna F, Sandri M, Sprio S, Marcacci M. Tissue Eng Part A. 2014;20(3-4):763-73.

8) R. Havaldar, S.C. Pilli, B.B. Putti. IOSR J Dent Med Sci. 1 (2012) 12-16.

9) F. Barrère, C.A. Blitterswijk, K. Groot. Int J Nanomedicine. 1(3) (2006) 317-332.

10) Tampieri A, Celotti G, Landi E, Sandri M, Roveri N, Falini G. J Biomed Mater Res A. 2003, 67(2):618-25.

11) Tampieri A, Sandri M, Landi E, Pressato D, Francioli S, Quarto R, Martin I. Biomaterials. 2008;29(26):3539-46.

12) Landi E, Logroscino G, Proietti L, Tampieri A, Sandri M, Sprio S. J Mater Sci Mater Med. 2008;19(1):239-47.

13) Sprio S, Ruffini A, Valentini F, D'Alessandro T, Sandri M, Panseri S, Tampieri A. J Biotechnol. 201 20;156(4):347-55.

14) Minardi S, Corradetti B, Taraballi F, Sandri M, Van Eps J, Cabrera FJ, Weiner BK, Tampieri A, Tasciotti E. Biomaterials. 2015;62:128-37.

15) Shankar KG, Gostynska N, Montesi M, Panseri S, Sprio S, Kon E, Marcacci M, Tampieri A, Sandri M. Int J Biol Macromol. 2016 Nov 9. pii: S0141-8130(16)31045-5. doi: 10.1016/j.ijbiomac.2016.11.010.

16) Siimon K, Reemann P, Põder A, Pook M, Kangur T, Kingo K, Jaks V, Mäeorg U, Järvekülg M.

17) Willems NM, Langenbach GE, Stoop R, den Toonder JM, Mulder L, Zentner A, Everts V. Mater Sci Eng C Mater Biol Appl. 2014, 42:15-21.

18) Mason BN, Reinhart-King CA. Organogenesis. 2013, 9(2):70-5.

19) Francis-Sedlak ME, Uriel S, Larson JC, Greisler HP, Venerus DC, Brey EM. Biomaterials. 2009, 30(9):1851-6.

20) Francis-Sedlak ME, Moya ML, Huang JJ, Lucas SA, Chandrasekharan N, Larson JC, Cheng MH, Brey EM. Microvasc Res. 2010, 80(1):3-9.

21) Boonkaew B, Tompkins K, Manokawinchoke J, Pavasant P, Supaphol P. Biomed Mater. 2014, 9(2):025001.

22) Wang J, He C, Cheng N, Yang Q, Chen M, You L, Zhang Q. J Nanosci Nanotechnol. 2015;15(7):4844-50.

23) Vicens-Zygmunt V, Estany S, Colom A, Montes-Worboys A, Machahua C, Sanabria AJ, Llatjos R, Escobar I, Manresa F, Dorca J, Navajas D, Alcaraz J, Molina-Molina M. Respir Res. 2015, 16:82.

24) Chiue H, Yamazoye T, Matsumura S. Biochem Biophys Res Commun. 2015, 461(3):445-9.

25) Lam PL, Kok SH, Bian ZX, Lam KH, Tang JC, Lee KK, Gambari R, Chui CH. Colloids Surf B Biointerfaces. 2014, 117:277-83.

26) Pitaru S, Noff M, Blok L, Nir E, Pitaru S, Goldlust A, Savion N. Dermatol Surg. 2007, (9):1045-54; discussion 1054.

27) Zubery Y, Nir E, Goldlust A. J Periodontol. 2008, 79(6):1101-7.

28) Tal H, Kozlovsky A, Artzi Z, Nemcovsky CE, Moses O. Clin Oral Implants Res. 2008, 19(3):295-302.

29) Tertuliano OA, Greer JR. Nat Mater. 2016 Nov;15(11):1195-1202. doi: 10.1038/nmat4719.

30) Zhengwen Yang, Yinshan Jiang, Li xin Yu, Bo Wen, Fangfei Li, Shemmei Sun, Tianyi Hou. J. Mater. Chem. 15 (2005) 1807-1811.

31) A. Tampieri, S. Sprio, M. Sandri, F. Valentini. Trends Biotechnol. 29 (2011) 526-535.

32) Veronesi F, Giavaresi G, Guarino V, Raucci MG, Sandri M, Tampieri A, Ambrosio L, Fini M. J Biomed Mater Res A. 103(9) (2015) 2932-41.

33) Tonda-Turo C, Gentile P, Saracino S, Chiono V, Nandagiri VK, Muzio G, Canuto RA, Ciardelli G. Int J Biol Macromol. 49(4) (2011) 700-6.

34) Eeckhout Y, Delaisse JM. Pathol Biol (Paris). 36(9) (1988) 1139-46.

35) Charulatha V, Rajaram A. Biomaterials. 24(5) (2003) 759-67.

36) Baskin JZ, Vasanji A, McMasters J, Soenjaya Y, Barbu AM, Eppell SJ. J Biomed Mater Res A. 100(9) (2012) 2462-73.

37) Annabi N, Nichol JW, Zhong X, Ji C, Koshy S, Khademhosseini A, Dehghani F. Tissue Eng Part B Rev. 16(4) (2010) 371-83.

38) Ramírez-Rodríguez GB, Delgado-López JM, Iafisco M, Montesi M, Sandri M, Sprio S, Tampieri A. J Struct Biol. (2016) doi: 10.1016/j.jsb.2016.06.025.

39) Roy R, Boskey A, Bonassar LJ. J Biomed Mater Res A. 93(3) (2010) 843-51.

40) Roveri N, Falini G, Sidoti MC, Tampieri A, Landi E, Sandri M, Parma B. Mat Sci Eng. 23(3) (2003) 441–446.

41) Tampieri A, Iafisco M, Sandri M, Panseri S, Cunha C, Sprio S, Savini E, Uhlarz M, Herrmannsdörfer T. ACS Appl Mater Interfaces. 6(18) (2014) 15697-707.

42) Sionkowska A, Kozłowska J. Int J Biol Macromol. 52 (2013) 250-9.

43) Rodrigues SC, Salgado CL, Sahu A, Garcia MP, Fernandes MH, Monteiro FJ. J Biomed Mater Res A. 101(4) (2013) 1080-94.

44) Yan LP, Wang YJ, Ren L, Wu G, Caridade SG, Fan JB, Wang LY, Ji PH, Oliveira JM, Oliveira JT, Mano JF, Reis RL. J Biomed Mater Res A. 95(2) (2010) 465-75.

45) Ghosh S, Gutierrez V, Fernandez C, Rodriguez-Perez MA, Viana JC, Reis RL, Mano JF. Acta Biomater 4 (2008) 950–959.

46) Panseri S, Montesi M, Dozio SM, Savini E, Tampieri A, Sandri M. Front Bioeng Biotechnol. 4(48) (2016) doi: 10.3389/fbioe.2016.00048.

47) Wallach S. Magnes. Trace Elem. 9 (1990) 1–14.

48) Roy R, Boskey AL, Bonassar LJ. J Orthop Res. 26(11) (2008) 1434-9.

CHAPTER III: Evaluation of different crosslinking agents on hybrid biomimetic collagen-hydroxyapatite composites

1. Introduction

The hierarchical architecture of the natural bone is highly complex which involves the active synergism of collagen fibrils and hydroxyapatite nanocrystals. This intricacy is often difficult to perceive because of various factors such as chemical, morphological and biomechanical characteristics which contribute towards the overall functionality of the bone tissue [1]. Thus, understanding the different aspects of biological and chemical mimesis of the bone can greatly help in developing functional bone scaffolds with optimal features [2]. Bone scaffolds have been vital alternatives to autografts and allografts as these biomimetic biomaterials can support and guide to achieve hierarchically organised tissue regeneration [3].

Collagen extracted from different animal tissues has found great suitability for broad range of biomedical applications by virtue of high biocompatibility, good degradability and inherent structural architecture [4]. Similarly, synthetic hydroxyapatite has also gained significant applicability due to its high bioactivity and osteoconductive properties which are analogous to the bio-apatite of bone [5]. Accordingly, significant research has been focussed on biomimetic strategies, especially more efforts were devoted to develop hybrid composites using hydroxyapatite and biopolymers in conjugation. In the last decade, plethora of bio-composites containing ceramic-biopolymers were developed and investigated extensively to evaluate their influential role in osteoinductivity, osteoconductivty, biodegradability and mechanical resistivity [6].

There is abundant literature evidence showing several biopolymers such as collagen, gelatin, chitosan, silk and synthetic polymers such as (polylactic acid, polyglycolic acid, poly(caprolactone) and poly(vinyl alcohol)) which are deliberately copulated with hydroxyapatite to produce a bio-composites with innate features similar to the native bone tissues [7]. Despite the existence of other biological/synthetic materials, collagen is hitherto considered as the first-choice material in bone tissue engineering due to its natural biological resemblance and suitable physical-chemical

properties. New generation bone substitutes are often derived from type I collagen and hydroxyapatite in order to biomimic the native bone morphological and biological features [8]. In particular, the biomineralization process is largely being exploited in order to adapt the concept of organ-morphicity in producing biomimetic bone scaffolds through chemical or biological manipulation [9].

Correspondingly, the synthesis of bioinspired, pH-driven, bone substitutes through biomimetic mineralization was developed, where the structural and chemical control is well calibrated through an organic template (collagen) on which the amorphous inorganic mineral constitutes (hydroxyapatite) nucleates to complete the biomineralization process with three dimensional (3D) organization of collagen fibrils [10]. This approach has been extensively investigated and demonstrated in several studies to develop, (i) bi-layered, graded, osteochondral scaffolds [11], (ii) magnesium (Mg) substitution mimicking the osteogenic niche [12], (iii) biomimetic magnetic nano-structured composites [13], and (iv) biomimetic scaffolds with aligned micro-porosity [14]. Despite achieving the chemical mimesis of the bone successfully, the biomechanical and morphogical mimesis is still a challenge. This is mainly due to the weak properties of collagen, which is especially the high degradation rate and subsequent loss of mechanical performance. The use of crosslinkers has been a constructive approach to collectively strengthen the degradability and mechanical resistivity of the composites [15].

Among the diverse crosslinking mechanisms, few crosslinkers have shown exquisite results which includes dehydrothermal (DHT), ultra violet (UV) rays, glutaraldehyde, 1,4-butanediol diglycidyl ether (BDDGE), 1-ethyl-3-(3-dimethylamino propyl) carbodiimide hydrochloride/N-hydroxysuccinimide (EDC/NHS), genipin and ribose, however each of the above crosslinkers have their own limitations and disadvantages [16-18]. Accordingly, this study focuses on the development of novel bone-like scaffolds by bio-inspired, pH-driven, mineralization of type I collagen matrix with magnesium-doped hydroxyapatite nanophase (MgHA/Coll). To this aim, this study evaluates the altered modifications in the obtained composites due to different crosslinkers

such as DHT, BDDGE and ribose in terms of morphological and physical-chemical properties. Finally, the biological properties of the composites were evaluated using *in-vitro* experiment to address the cytotoxicity of the composites using mouse pre-osteoblast cells (MC3T3-E1) in terms of cell viability. To best of our knowledge, this is the first comparative study investigating the effect of different crosslinking agent in biomineralized collagen matrices.

2. Synthesis of hybrid MgHA/Coll composites

As reported previously, the MgHA/Coll composites were prepared through a bioinspired, innovative, pH-driven, self-assembling process. In brief, 150 g of (1 wt% collagen gel) was diluted with 500 ml of milli-Q water containing 2.4 g of H_3PO_4 and agitated continuously to obtain an acidic aqueous homogenous suspension. In a separate beaker, 2.7 g of $Ca(OH)_2$ and 0.35 g of $MgCl_2{\cdot}6H_2O$ were mixed in 500 ml of milli-Q water and agitated continuously to obtain a basic aqueous homogenous suspension. At 25 °C, the acidic suspension was added drop-wise to the basic suspension under continuous stirring condition. The reaction mixture was maintained at static condition for 2 h at same temperature to ripen. Later, the slurry solution was rinsed thrice in milli-Q water and filtered through metallic sieve (150 µm) to exclude any unreacted counter-ions. Thus, recovered slurry solution is henceforth termed as MgHA/Coll and was used as starting material to produce different crosslinked composites which as follows,

2.1 DHT crosslinked MgHA/Coll (MgHA/Coll$_{DHT}$)

Thus, obtained biomineralized MgHA/Coll slurry solution was filled onto a polystyrene well-plate and lyophilized by consecutive freezing at (– 40 °C) and drying at (25 °C) for 48 h under a constant vacuum of 0.1 mbar (5 Pascal, LIO 3000 PLT, Italy). Later the obtained 3D scaffolds were subjected to heat treatment of (160 °C) under vacuum of (0.001 mbar) for 48 h and thus obtained samples were henceforth termed as MgHA/Coll$_{DHT}$ composites.

2.2. BDDGE crosslinked MgHA/Coll (MgHA/Coll$_{BDD}$)

Thus obtained biomineralized MgHA/Coll slurry solution was crosslinked with 2 wt% BDDGE. The crosslinking reaction was maintained at 25 ± 2 °C for 48 h. Later the slurry solution

was rinsed thrice in milli-Q water to remove any residues and later freeze-dried using the same above-mentioned conditions. Then obtained 3D samples were henceforth termed as MgHA/$Coll_{BDD}$ composites.

2.3 Ribose crosslinked MgHA/Coll (MgHA/$Coll_{RIB}$)

Thus, obtained biomineralized MgHA/Coll slurry solution was crosslinked with 30 mM of ribose dissolved in ethanol and PBS solution (70:30 vol%) under continuous agitation for 5 days at 37 °C. Later the slurry solution was rinsed thrice in milli-Q water to remove any residues and later freeze-dried using the same above-mentioned conditions. Then obtained 3D samples were henceforth termed as MgHA/$Coll_{RIB}$ composites.

Biomineralization process is a great source of inspiration to design biomimetic materials for regenerative medicine, because this process provides greater insights on how mineral-rich tissues are created in-vivo conditions [19]. Bone mineralization is a multitude-step-reaction and a complex process thus making it extremely difficult to study under in-vivo conditions. Therefore in-vitro biomineralization experiments with close biomimicry of biological conditions have been studied extensively to understand how collagen mineralization process occurs and has consequently led to the development of plethora bioinspired biomimetic nano-structured biomaterials for tissue repair [20]. Accordingly, in this study, the biomineralized MgHA/Coll is produced through an innovative, bioinspired, pH-driven process, triggered by the PO_4^{3-} ions provided by the H_3PO_4 in aqueous solution. In alkaline pH conditions, the self-assembling of collagen fibrils occurs which serves as a template for mineralization. Around, pH (~8), while the self-assembling of fibrils is ongoing, the precipitation of amorphous HA nanoparticles occurs on the collagen fibrils. At a neutral pH, two distinctive processes, the collagen fibres organisation into 3D network and HA nucleation collaborates to accomplish biomineralization process [21]. Certainly, Mg^{2+} ions are key divalent ions associated with biological apatite. Therefore, during the process of developing bone-like scaffolds, the incorporation of Mg^{2+} ions can stabilize the amorphous calcium phosphate precursor and control the qualitative changes of the bone [22].

In this study, thus developed MgHA/Coll composites were crosslinked using different treatment methods such as DHT, BDDGE and ribose. Each of the above crosslinker has a peculiar binding affinity with collagen amine groups to form stable inter-intra-molecular hydrogen bonding thus collectively improving the degradability and mechanical features of the composites. For example, in DHT crosslinking mechanism, the thermal dehydration causes chemical bond between the amino and carboxyl groups of collagen molecules [23]. In case of BDDGE, the crosslinking occurs between the lysine or hydroxylysine residues of collagen thus forming chemical bridges between collagen molecules, that contains secondary amines and hydroxyl groups [24]. Similarly, in ribose crosslinking, the protein glycation causes irreversible chemical reaction between the free amine groups of collagen thus resulting in either side-chain modifications on collagen or links collagen fragments together through advanced glycation end products (AGEs) formation [25]. The detailed schematic illustration of various crosslinking mechanisms is depicted in Fig.1.

3. Results and discussion - Characterization of the composites

3.1 Swelling behaviour

The fluid uptake ability and imbibition properties of the 3D composites were monitored under physiological conditions. Swelling ability is an important parameter to evaluate while developing biological composites as this feature greatly influences adhesion, growth, behaviour and differentiation of the cells [23]. In brief, dried scaffolds of 8 mm in diameter and 5 mm in height were immersed in 2 ml of PBS solution at 37 °C for 1, 2, 4, 6 and 8 h. At regular time points the composites were withdrawn carefully and excess moisture was removed using a filter paper and the weight was measured. The swelling percentage was calculated as: [(wet weight – dry weight)/wet weight] x 100. The final swelling percentage value was averaged from three parallel measurements.

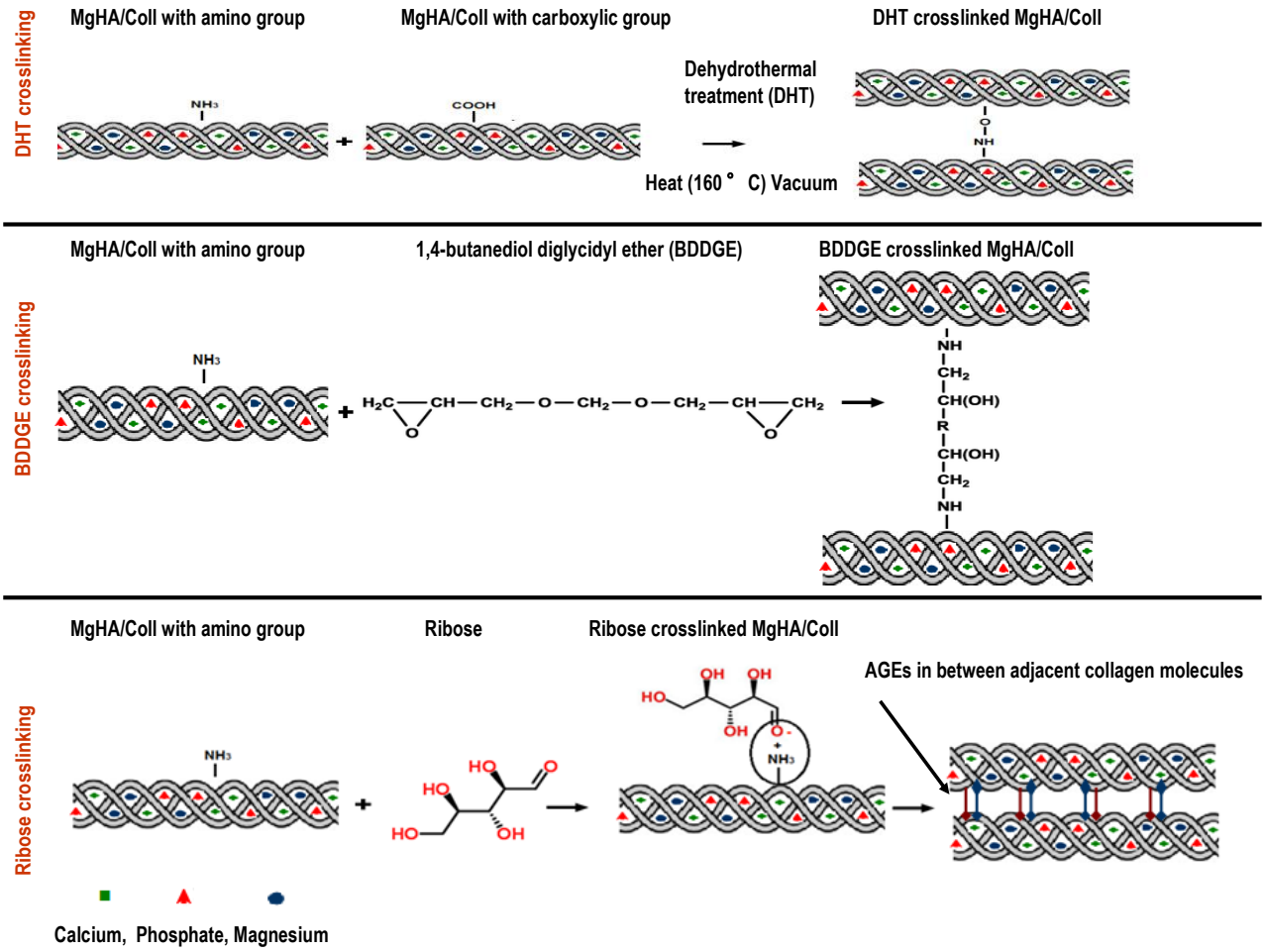

Figure 1: *Schematic illustration of various crosslinking reactions on MgHA/Coll composites.*

Swelling ability is an important parameter to evaluate while developing biological composites as this feature greatly influences adhesion, growth, behaviour and differentiation of the cells [26]. Accordingly, in this study, each composite depicted a distinctive water uptake ability in a time-dependent manner due to compositional differences and crosslinking methods as illustrated in Fig.2(A). On observing the swelling behaviour, rapid water uptake during the first hour of experiment was evident in all composites and after 2 h the swelling capacity seized completely in all composites thus maintaining the same saturation level up to 8 h. Comparing the different composites swelling behaviour at 8 h of incubation, MgHA/Coll$_{RIB}$ had the highest imbibing capacity of (670.88±52.19%) followed by MgHA/Coll$_{BDD}$ of (616.26±47.65%). Whereas, the MgHA/Coll$_{DHT}$ (339.59±56.27%) swelled more slowly than the MgHA/Coll composite (437.87±20.16%). Probably this phenomenon is likely due to the hydrophobicity that occurs during

the DHT crosslinking reaction, where more ester and amide bonds are formed with fewer free carboxyl, amine and hydroxyl moieties apparently causing significant reduction in hydrophilicity [27]. However, all composites as effect of different crosslinkers possessed sufficient water holding capacity which is significantly dependent upon both the compositional and crosslinking treatments.

3.2 Collagenase degradation assay

The enzymatic resistivity of the composites was evaluated using collagenase enzyme under physiological conditions. Degradation kinetics of biological composite is essential to monitor in a tissue reparative process, as this greatly affects cell vitality, cell growth and host response [25]. Briefly, a known weight of sample was incubated in 0.1 M Tris-HCl (pH 7.4) containing collagenase enzyme (100 units/ml) at 37 °C. After 24 h, the samples were removed and washed with milli-Q water and the final dry weight was noted after freeze-drying. The degradation rate was estimated through percentage of weight loss and calculated as: [(initial dry weight – final dry weight)/initial dry weight] x 100. The measure was repeated three times on different samples and the average percentage loss was recorded.

Degradation kinetics of biological composite is essential to monitor in a tissue reparative process, as this greatly affects cell vitality, cell growth and host response [28]. Bacterial collagenase enzyme was employed to study the rate of degradation in the composites, the action of collagenase enzyme is preferentially on the X-Gly bond in a sequence typical and specific of collagen: R-Pro-X-Gly-Pro [29]. The weight loss percentage of composites after 24 h incubation in collagenase solution is illustrated in Fig.2(B). The MgHA/Coll composite due to lack of crosslinking represented the highest weight loss of 17.24±0.84%, followed by MgHA/$Coll_{DHT}$ of 13.79±0.20% thus representing a poor resistance to enzymatic degradation. Whereas, MgHA/$Coll_{RIB}$ and MgHA/$Coll_{BDD}$ composites were more resistant to degradation with weight of loss of 4.05±0.45% and 5.8±0.50% respectively. The enhanced resistivity is largely attributed to the newly formed crosslinks between collagen molecules due to ribose and BDDGE interaction, thus masking the collagenase recognition sites and decreasing the degradation rate [30]. On comparing the

different crosslinkers, the DHT crosslinked composite represented the faster degradation rate, which is mainly due to the collagen triple helix denaturation and disorganization of collagen molecules at higher temperature thereby causing significant reduction in enzymatic resistivity [31].

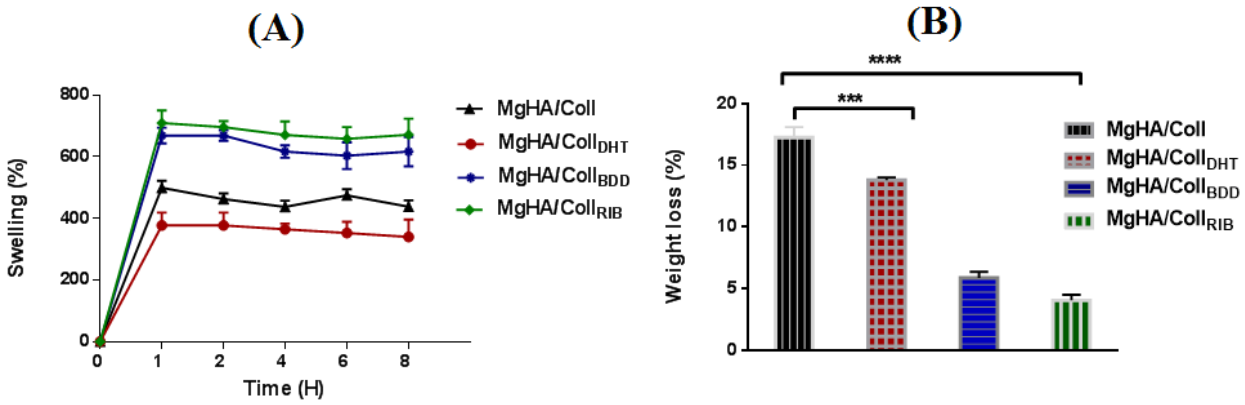

Figure. 2: *(A) Time-dependent swelling behaviour of composites, (B) In-vitro degradation of composites after 24 h of incubation in collagenous solution. Data are mean ± SEM from 3 samples each type of scaffold. Statistically significant differences between MgHA/Coll respect to MgHA/Coll$_{DHT}$ (***$p \leq 0.001$) and MgHA/Coll respect to MgHA/Coll$_{BDD}$ and MgHA/Coll$_{RIB}$ (****$p \leq 0.0001$).*

3.3 Morphogical characterization

3.3.1 Scaffold surface properties

The topographical micro-architecture of the composites was examined by scanning electron microscopy (SEM) performed on sample specimens mounted onto aluminium stubs using black carbon tapes and sputter coated with gold (Sputter Coater Q150TES, Quorum, (Italy)). The specimen surface was examined using high resolution SEM (FEI, Quanta 200, UK) at a pressure of 0.1 m Torr at an accelerating voltage of 15 kV.

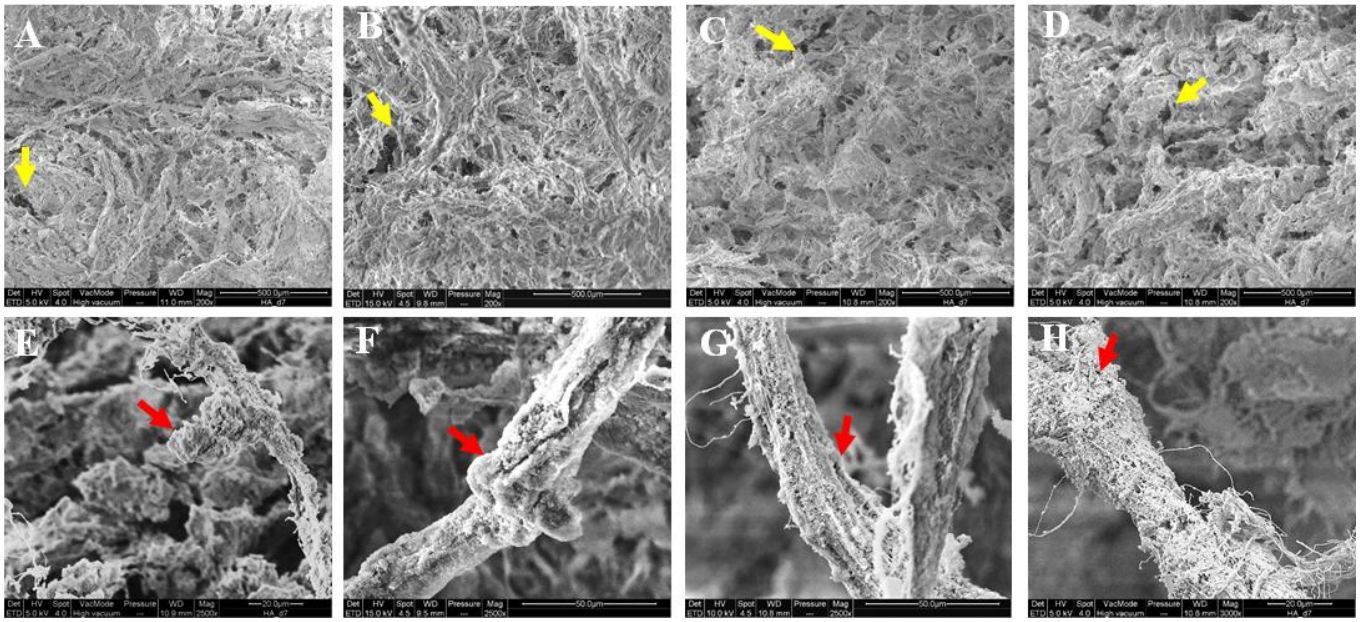

Figure. 3: *Scanning electron microscopy images of different composites. (A&E): MgHA/Coll, (B&F) MgHA/Coll$_{DHT}$, (C&G) MgHA/Coll$_{BDD}$, (D&H) MgHA/Coll$_{RIB}$. Upper panel represents fibrous composites at lower magnification and lower panel represents the respective composites at higher magnification. Yellow arrows indicate the open pores and red arrows indicate the close binding of nanocrystals on collagen fibrils.*

The composite morphology was evaluated by SEM as shown in Fig.3, which portrays a highly heterogeneous porous and fibrous arrangement with relatively large and small nanocrystals of hydroxapaptite closely bound with collagen fibres. At lower magnification, all composites represented highly anisotropic porous and fibrous pattern, however as effect of different crosslinkers the fibrous micro-structure differed with presence of micro/macro pores. At higher magnification, single or bundle of collagen fibres is more evident with complete mineralization of amorphous phase. The composite micro-structure observed in this study was in accordance with similar mineralized collagen composites studied by others [12].

3.3.2 Scaffold dimensional properties

The density and porosity of the composites was calculated from measuring the dry density of the samples using the equation ($\boldsymbol{\rho}^* = m/v$), where m and v indicates the mass and volume of the 3D composites. The known dry density of collagen ($\boldsymbol{\rho}s$) was assumed to be 1.3

g/ml as reported by Davidenko et al [18]. The percentage of porosity is calculated from the relative density values and calculated as: (1- **ρ***/ **ρ**s) x 100. The final percentage porosity value was averaged from three parallel measurements.

Under wet conditions, the composite pore size arrangement and distribution was evaluated by observing thin sections (20 μm) of the composite specimen under a bright field microscope (Nikon). Briefly, the thin sections were obtained by incubating individual composite in PBS solution for 24 h and later embedding in OCT medium followed by subsequent quenching in liquid nitrogen. The frozen OCT blocks were cut horizontally using a cryostat (Histo-line, 5000 MC, Italy) to obtain thin sections. The pore diameter was measured using NIS Elements Imaging Software (3.22.1, Nikon) and the average pore size was obtained from ten parallel section measurements.

In terms of total porosity, all composites exhibited a high level of porosity above 85% as seen in Fig.4(A). However, MgHA/Coll and MgHA/$Coll_{DHT}$ composites showed significant lower porosity when compared to MgHA/$Coll_{RIB}$ and MgHA/$Coll_{BDD}$. This aspect can be correlated with swelling behaviour results, where MgHA/Coll and MgHA/$Coll_{DHT}$ composites demonstrated a lower imbibing ability. Concerning, the pore size distribution, anisotropic distribution was evident in all composites. The average pore size was within the range of 0-200 μm, with presence of large and small pores as illustrated in the Fig.4(B). From the above results, it is evident that the effect of different crosslinkers on MgHA/Coll composite showed substantial changes in total porosity and pore size distribution, thus affecting the overall compositional and scaffold dimensional properties. Nevertheless, the obtained pore size in these composites was highly adequate for a favourable cellular response with capability to facilitate cellular penetration and exchange of metabolic products, which is also later confirmed from the cell-material interaction study.

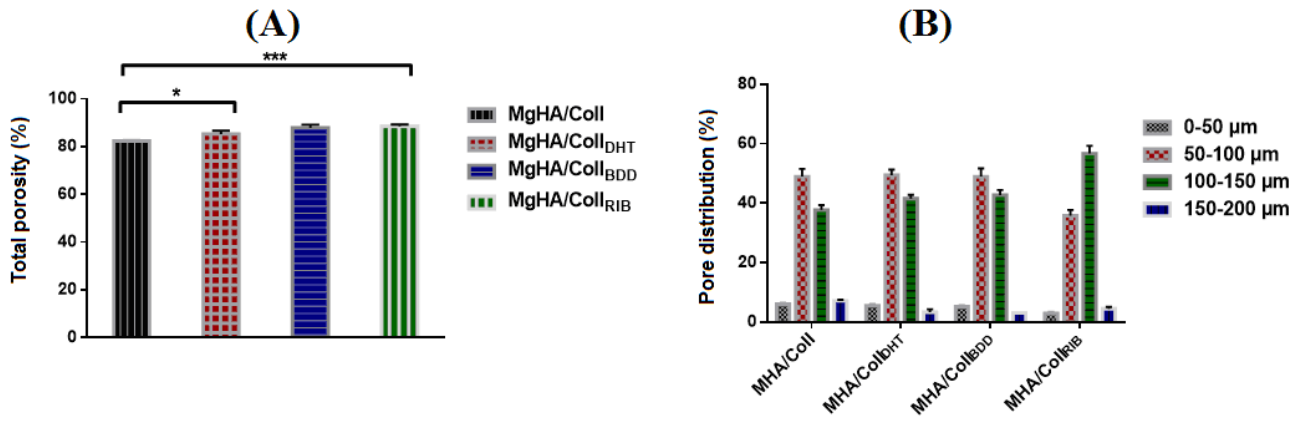

Figure. 4: *Dimensional properties of the compsoites (A) Total porosity, (B) Pore size distribution at wet conditions. Data are mean ± SEM from 3 samples each type of scaffold. Statistically significant differences between MgHA/Coll respect to MgHA/Coll$_{BDD}$ and MgHA/Coll$_{RIB}$ (***$p \leq 0.001$) and between MgHA/Coll and MgHA/Coll$_{DHT}$ (*$p \leq 0.05$).*

3.4. Physical-Chemical characterization

3.4.1 ICP Analysis

The quantitative determination of Mg^{2+}, Ca^{2+} and PO_3^{-4} ions present in the scaffolds that constitutes the inorganic mineral component was measured by Inductively coupled plasma-optical emission spectrometry (ICP-OES, Agilent Technologies 5100 ICP-OES, Santa Clara, USA) Briefly, 40 mg of composite was subjected to 2 ml nitric acid (65 wt %) digestion followed by subsequent sonication and dilution with 100 ml of milli-Q water. The following analytical emission wavelengths were used for Ca (422 nm), Mg (279 nm) and P (214 nm) ions.

The chemical mimesis of the natural bone was achieved by the addition of Mg^{2+} ions in the apatite lattice. The result ICP demonstrates that value of (Ca+Mg)/P ratio was 1.54 ± 0.013, 1.52± 0.002, 1.58± 0.014, 1.57 ± 0.040 for MgHA/Coll, MgHA/Coll$_{DHT}$, MgHA/Coll$_{BDD}$ and MgHA/Coll$_{RIB}$ composites respectively as illustrated in Table.1. These values construe that the developed composites are calcium deficient, ion-substituted apatite nanophases and typical of low crystalline (1.45 – 1.60) range which is mainly due to the presence of HPO_2^{-4} ions [32]. This result confirms that the mineral phase was preserved during the various crosslinking reactions with evident

magnesium substitution of calcium ions. Moreover, the presence of Mg^{2+} ions can prevent the excessive crystallization of apatite particles thus guaranteeing the formation of a high biomimetic mineral phase [33]. Therefore, the different crosslinking treatments, do not affect the ion-substitution and allows the partial substitution of Mg within the HA lattice as similar to non-crosslinked MgHA/Coll composite.

	Ca/P (mol)	**Mg/Ca (mol%)**	**(Ca+Mg)/P (mol)**
MgHA/Coll	1.49 ± 0.013	3.19 ± 0.031	1.54 ± 0.013
MgHA/Coll$_{DHT}$	1.46± 0.001	3.59± 0.035	1.52± 0.002
MgHA/Coll$_{BDD}$	1.52± 0.011	3.40± 0.034	1.58± 0.014
MgHA/Coll$_{RIB}$	1.53 ± 0.028	3.20 ± 0.027	1.57 ± 0.040

Table.1: *Chemical composition of MgHA/Coll, MgHA/Coll$_{DHT}$ and MgHA/Coll$_{BDD}$ and MgHA/Coll$_{RIB}$ composites obtained from ICP analysis.*

3.4.2 FTIR Analysis

The functional group alteration due to crosslinking was evaluated by infrared spectrum using Nicolet 380 FT-IR spectrometer (Thermo Fisher Scientific Inc, Waltham, USA). Briefly, 2 mg of the composite was mixed with 100 mg of anhydrous potassium bromide and then pressed at 8000 psi into 7 mm diameter pellets. All spectra's were recorded in the wavelength ranging from 400 to 4000 cm^{-1} with 2 cm^{-1} of resolution.

The functional alteration due to chemical interaction of mineral phase MgHA and collagen fibres are evident in FTIR spectral peaks as seen in Fig.5. The shift from 1340 to 1337 cm^{-1} indicates the stretching of carboxyl groups mainly due to the chemical bond between Ca^{2+} ions on the apatite surface with COO^- groups of collagen which emphasizes the active interaction of collagen functional groups with the positively charged apatite crystals. The characteristic spectra at 873 cm^{-1} implies the carbonation of the MgHA nucleation on the collagen fibrils. The carbonation was noticeable in all the composites which clearly manifests that the various crosslinking reactions did not hinder the carbonation of the inorganic phase Fig.5.(A). Apparently, the distinct three carbonation peaks in the B position of the HA was evident at 1540, 1455 and 1413 cm^{-1} and the

typical peak corresponding to acid phosphate (HPO_2^{-4}) in the mineral lattice was also evident between 550 to 560 cm^{-1} [34].

The effect of individual crosslinker on the conformational changes of MgHA/Coll composite was also noticeable, for DHT crosslinking, a definitive peak increase was observed around 1700 cm^{-1} due to ester bond formation [35]. For BDDGE crosslinking, slight changes between 2932-2890 cm^{-1} indicates the presence of aliphatic moieties contributed by the BDDGE [36]. Whereas in case of ribose crosslinking mild vibrational changes between 1035 and 1081 cm^{-1} indicates the C-O, C-C stretching as well as C-O-H and C-C-O bending due to the interaction between the carbonyl group of ribose and the amine group of collagen [37] as seen in Fig.5.(B).

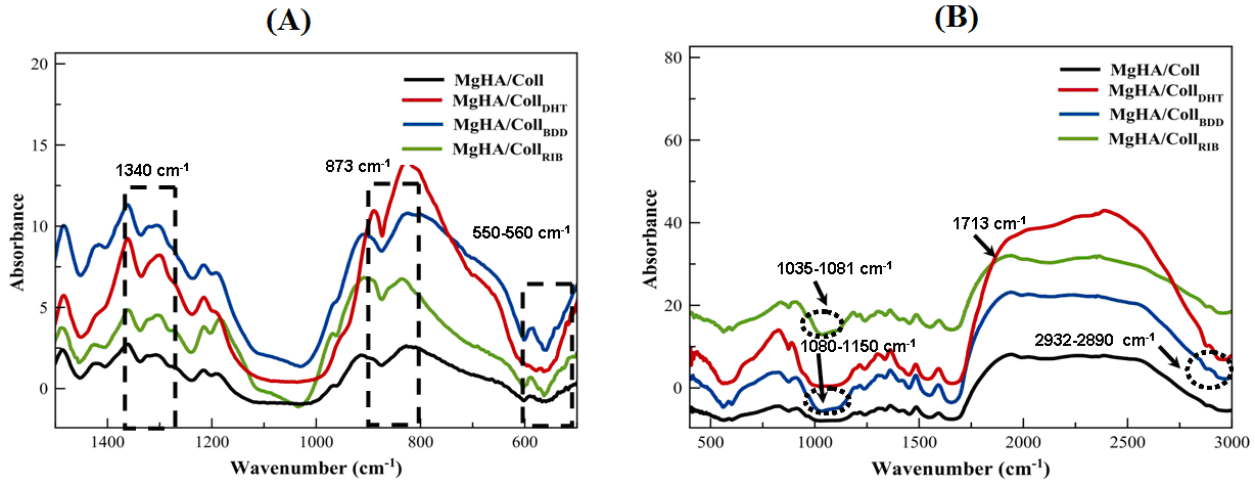

Figure. 5: *FTIR spectral peaks, (A) Functional interaction of collagen and HA crystals with evidence of collagen and apatite interaction and MgHA carbonation, (B) The peaks contributing to DHT, BDDGE and ribose interaction on MgHA/Coll.*

3.4.3 XRD Analysis

X-ray diffraction (XRD) measurement was carried out using Cu Kα radiation (λ = 1.5418 Å) on a diffractometer (Panalytical X'Pert PRO, Bruker, Germany) coupled with Pixcel detector operating at 40 mA and 45 kV. The XRD patterns were recorded in the 2θ range from 20 to 80° with a step size of 0.02° and scan time of 0.5 s.

The XRD patterns of all composites displayed a low crystalline pattern with band patterning of broad peaks as seen in Fig.6.(A). The composite synthesis at 25 ± 2 °C highly influenced in obtaining an amorphous phase without any long-range periodic regularities. The large broadening of reflections in the XRD pattern shows that during the nucleation process, the nano-sized dimensions of crystallites were growing along the collagen fibrils with preferential *c*-axis orientation [38]. The presence of intensive diffraction peaks between (2θ: 30 to 35°) showed slight shift changes in the peak position due to the effect of different crosslinking treatments. Moreover, the crystallinity of the mineral phase is largely determined during the nucleation and crystallization processes where the competition between magnesium and calcium ions occurs in occupying the crystal lattice [11]. Moreover, the low crystallinity can also be contributed by the foreign ions (Mg^{2+}, CO_2^{-3} and HPO_2^{-4}) in the apatite lattice as similar to the natural bone niche. These multiple ions affect the biological activity of cells thus directly influencing bone metabolic activities [39]. This demonstrates that, the various crosslinking interactions did not significantly modify the structure and crystallinity of the inorganic phase.

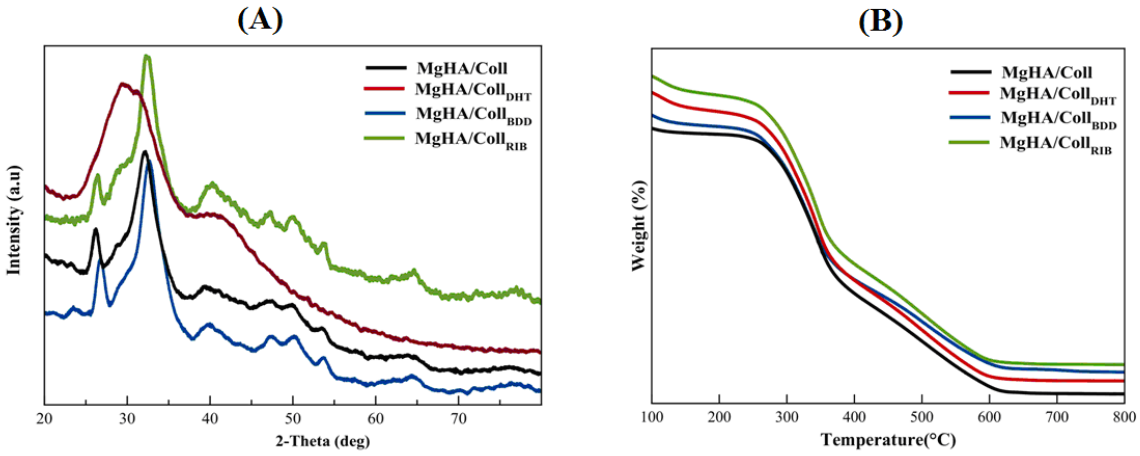

Figure. 6: *(A) XRD pattern, (B) TGA curves of MgHA/Coll, MgHA/Coll$_{DHT}$, MgHA/Coll$_{BDD}$, and MgHA/Coll$_{RIB}$ composites.*

3.4.4 TGA Analysis

The pyrolytic curves were determined using Thermo Gravimetric Analyser (TGA) (STA 449/C Jupiter, Netzsch, Germany). Briefly, 20 mg of the composite was placed in aluminium crucible and then crushed and press sealed for complete contact with the crucible. The experiment was carried in the temperature range of 30-800° C at a heating rate of 10° C/min in nitrogen atmosphere.

The nucleation of the mineral phase on the collagen was quantified by TGA. Initially, all scaffolds had a nominal composition of HA/Coll of 70/30 wt %, the amount of inorganic phase was calculated as residual mass of the sample at 800 °C from the TGA curves. The pyrolysis of the all the composites experienced a similar trend with three steps decomposition pattern [40]. Initially, below 100 °C there is the first loss attributed due to the loss of physically absorbed water, around 250 °C the second decomposition occurs due to the destabilization of chains and fragments of the macromolecule. Finally, at 600 °C, there is the residual inorganic phase. The residual inorganic mass was greater than 50 wt % for MgHA/$Coll_{BDD}$ and MgHA/$Coll_{RIB}$ whereas in MgHA/Coll and MgHA/$Coll_{DHT}$ the residual inorganic mass was below 45 % as seen in Fig.6.(B). The results confirm that during the various crosslinking reactions, the nucleation of mineral phase wasn't hampered and the reaction yield was significantly better than the non-crosslinked MgHA/Coll composites. The residual mass of (> 50 wt%) for MgHA/$Coll_{BDD}$ and MgHA/$Coll_{RIB}$ composites corresponds to mineral phase which is comparable to the mineral phase of natural bone [12].

3.5. Mechanical Analysis

For the dynamic mechanical analysis (DMA), cylindrical scaffolds with dimensions of 10 mm in diameter and 10 mm in thickness was prepared and hydrated for 24 h prior to testing in PBS solution. Both static compression test and dynamic mechanical test were performed in compression clamp using Q800 DMTA analyser (USA). To mimic the physiological conditions, every test was performed at 37 °C and initial small preload force of (0.01 N) was applied to each sample to ensure a complete contact between the composites surface and the compression plates. The static

compression test was performed uniaxially with control force ramp of 0.5 to 5 N and a speed of 0.5 N/min. The obtained stress-strain curve was used to measure the compressive modulus from the linear elastic region up to 10 % strain. The visco-elastic properties of the scaffolds under oscillating frequencies were measured using multi-frequency DMA test with frequency scan from 0.1 until 10 Hz measurements. A constant strain amplitude of 75 μm was applied and the storage modulus (E') and loss factor (tan δ) were obtained from the graph. The final presented values were averaged from six parallel measurements.

The catastrophic failure plateau and the densification regions of the scaffolds can be observed from the typical stress-strain curve as seen in (Fig.7.A). The stress-strain curve represents a typical trend of porous materials, the composite compression did not show either composite failure or rupture but densification was noticeable after force withdrawal. From the stress-strain curve, identifying and determining the initial linear region (elastic zone) was truly difficult due to the micro-fractures of the collagen fibrils at initial stress which is likely due to strut buckling and collapsing of the fibrils. In order to standardise the results, the compressive modulus was calculated between 1-10 % strain values. The compressive modulus of the MgHA/Coll scaffolds was improved greatly due to various crosslinking reactions as a consequence of material reinforcement. The MgHA/$Coll_{DHT}$ represented to the strongest material with highest compressive modulus of (30.93±6.14 KPa) followed by MgHA/$Coll_{BDD}$ (22.30±0.710 KPa), MgHA/$Coll_{RIB}$ (20.60±1.75 KPa) and MgHA/Coll (13.9±2.75 KPa) as seen in (Fig. 7.B). The enhanced mechanical characteristics of MgHA/$Coll_{DHT}$ is probably due to swelling kinetics, where this composite imbibed minimum water content when compared to other composites. The high swelling capacity can directly weaken the mechanical features, because under full hydration the composite is less stiff and more elastic, which apparently causes reduction in compressive modulus [31].

On observing the visco-elastic behaviour of the composites, the storage modulus (E') of all the composites increased with increase in frequency. In response to oscillating frequencies, each

composite represented significant variation in their E' value. MgHA/$Coll_{DHT}$ composite showed the highest E' value which increased from 60.19±33.66 Kpa at 0.1 Hz to 112.60±33.87 Kpa at 10 Hz. Similar trend was followed by MgHA/$Coll_{BDD}$ and MgHA/$Coll_{RIB}$ composites where the E' value increased from 43.46±7.29 Kpa at 0.1 Hz to 98.01±28.95 Kpa at 10 Hz and 36.83±3.93Kpa at 0.1 Hz to 69.05±10.91Kpa at 10 Hz respectively as seen in (Fig. 8.A). The increasing E' value in crosslinked (MgHA/$Coll_{DHT}$, MgHA/$Coll_{BDD}$ and MgHA/$Coll_{RIB}$) composites in response to vacillating frequency signifies the ability of the composites to store energy during deformation thus enhancing the stiffness of the composite. On the other hand, the loss factor (tan δ) represents the ratio of the amount of energy dissipated by the viscous portion to the energy stored in the elastic portion [41]. Accordingly, the tan δ value varied in each composite with increasing frequency, in case of MgHA/Coll, MgHA/$Coll_{BDD}$ and MgHA/$Coll_{RIB}$ the tan δ value increased mildly at lower frequencies and remained constant until 10 Hz thus indicating their damping ability due to mechanical vibrations. Whereas, in MgHA/$Coll_{DHT}$, the tan δ value increased rapidly initially, however at later frequencies, the tan δ value dropped significantly and remained constant until 10 Hz thus demonstrating the elastic response. The increased tan δ value for MgHA/$Coll_{BDD}$ and MgHA/$Coll_{RIB}$ suggests the composite is more viscous and less elastic. This aspect can be ascribed to the sufficient pore size and porosity of these composites which greatly helped in achieving sufficient water retention upon hydration within the pore wall due to hydrostatic effect [42]. Overall, on observing the mechanical results, crosslinking reaction significantly improved the resistance to compression in all the composites, but the extend of rise in mechanical resistivity is largely dependent on the material compositional properties and their respective crosslinking method employed. Therefore, the enhanced mechanical performances of the crosslinked composites represents a good level of crosslinking status with favourable mechanical resistivity and structural recovery.

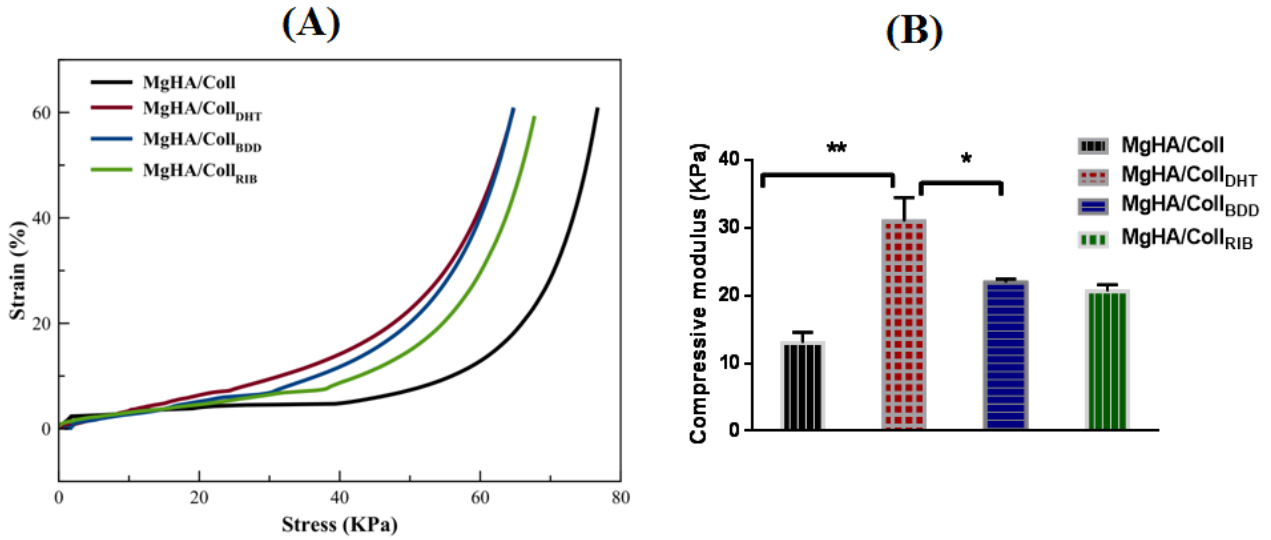

Figure.7: *Mechanical analysis, (A) The typical stress-strain curve (B) Compressive modulus of MgHA/Coll, MgHA/Coll$_{DHT}$, MgHA/Coll$_{BDD}$ and MgHA/Coll$_{RIB}$ scaffolds. Data are mean ± SEM from 6 samples each type of scaffold. Statistically significant differences between MgHA/Coll and MgHA/Coll$_{DHT}$ (**$p \leq 0.01$) and between MgHA/Coll$_{BDD}$ and MgHA/Coll$_{RIB}$ (*$p \leq 0.05$).*

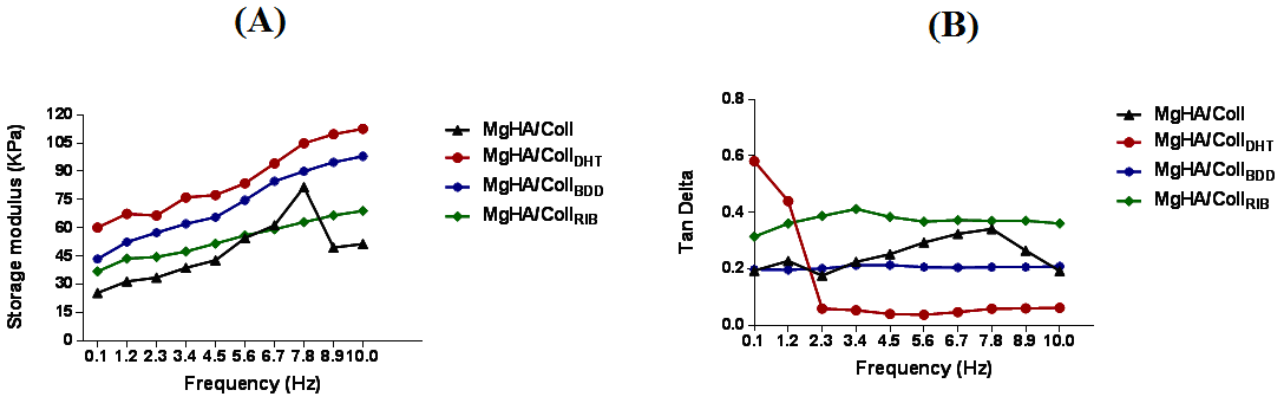

Figure. 8:*Viscoelastic properties, (A) Storage modulus (B) Tan delta of MgHA/Coll, MgHA/Coll$_{DHT}$, MgHA/Coll$_{BDD}$ and MgHA/Coll$_{RIB}$ scaffolds. Data are mean ± SEM from 6 samples each type of scaffold.*

3.6. Cell Culture

For cell-material interaction evaluation, mouse pre-osteoblast cell line (MC3T3-E1) was supplied by ATCC® (USA) and was used to investigate the cytotoxicty of the composites. MC3T3-E1 cells were cultured in α-MEM containing ribonucleosides, deoxyribonucleosides, L-glutamine,

supplemented with 10% FBS and 1% penicillin/streptomycin (100 U ml^{-1}/100 µg ml^{-1}) and incubated at 37 °C with 5% CO_2 atmosphere. At 85% of confluence the cells were detached by trypsinization and centrifugation, later the cell number and viability were assessed by trypan blue dye exclusion test. The experimental composites were prepared in dimensions of 5.0 mm in diameter and 6.0 mm in thickness and were gamma-ray sterilized (25 kGy). All composites were pre-incubated with 1 ml of culture media for 48 h at 37 °C. One per well, pre-incubated composites were placed in a 24-well plate and a drop of 20 µl containing 7.5 x 10^4 cells suspension in culture media was added on upper-surface of the composites for initial cell attachment for 30 min. Later, 1.5 ml of cell culture media supplemented with 50 µg/mL ascorbic acid and 10 mM β-glycerophosphate was added for cell proliferation and differentiation and incubated at 37 °C, 5% CO_2 for 7 days. Due to lack of crosslinking, the non-crosslinked (MgHA/Coll) composite is prone to rapid degradation under physiological conditions therefore, only MgHA/$Coll_{DHT}$, MgHA/$Coll_{BDD}$ and MgHA/$Coll_{Pre}$ scaffolds were studied and compared in cell culture experiments. All cell handling procedures were performed in a sterile laminar flow hood. Live/Dead assay (Molecular probes) was used to evaluate cell viability which is based on the simultaneous detection of live and dead cells with two probes, Calcein and Ethidium homodimer-1, that measures the recognized parameters of cell viability: intracellular esterase activity and plasma membrane integrity respectively. At regular time points of 1, 3 and 7 days of cell culture the composites were withdrawn and washed in PBS (1X) for 5 min and stained with Calcein acetoxymethyl (2 µM) and Ethidium homodimer-1 (4 µM) for 15 min at 37 °C. Then, the composites were again washed in PBS (1X) for 5 min and examined under inverted Ti-E fluorescence microscopy (Nikon).

The preliminary *in-vitro* test on different composites evaluated by MC3T3-E1 cells represented a favourable cell-material interaction. The cell viability of the pre-osteoblasts cultured on different composites was observed using the Live/Dead assay, which demonstrated greater cellular attachment with stronger composite colonization at each time point. In general, all the composites were cytocompatible and cells proliferated after 24 h in all composites with good survival rate. As

expected, the cell density increased in a time-dependent manner with greater cell distribution on day 7 as shown in Fig.9. As the effect of different crosslinkers no obvious changes in cellular viability was observed, therefore all crosslinkers demonstrated to be a safe reticulating agent without exhibiting any toxic cellular response. This apart, the beneficial cellular response is likely attributed to the surface properties of the composites, especially the presence of HA and Mg^{2+} ions which directly influences the osteoconductivty and osteogenesis of the composites. As a consequence of this, the surface roughness is greatly improved which strongly enhances the cellular activities [43,44,45].

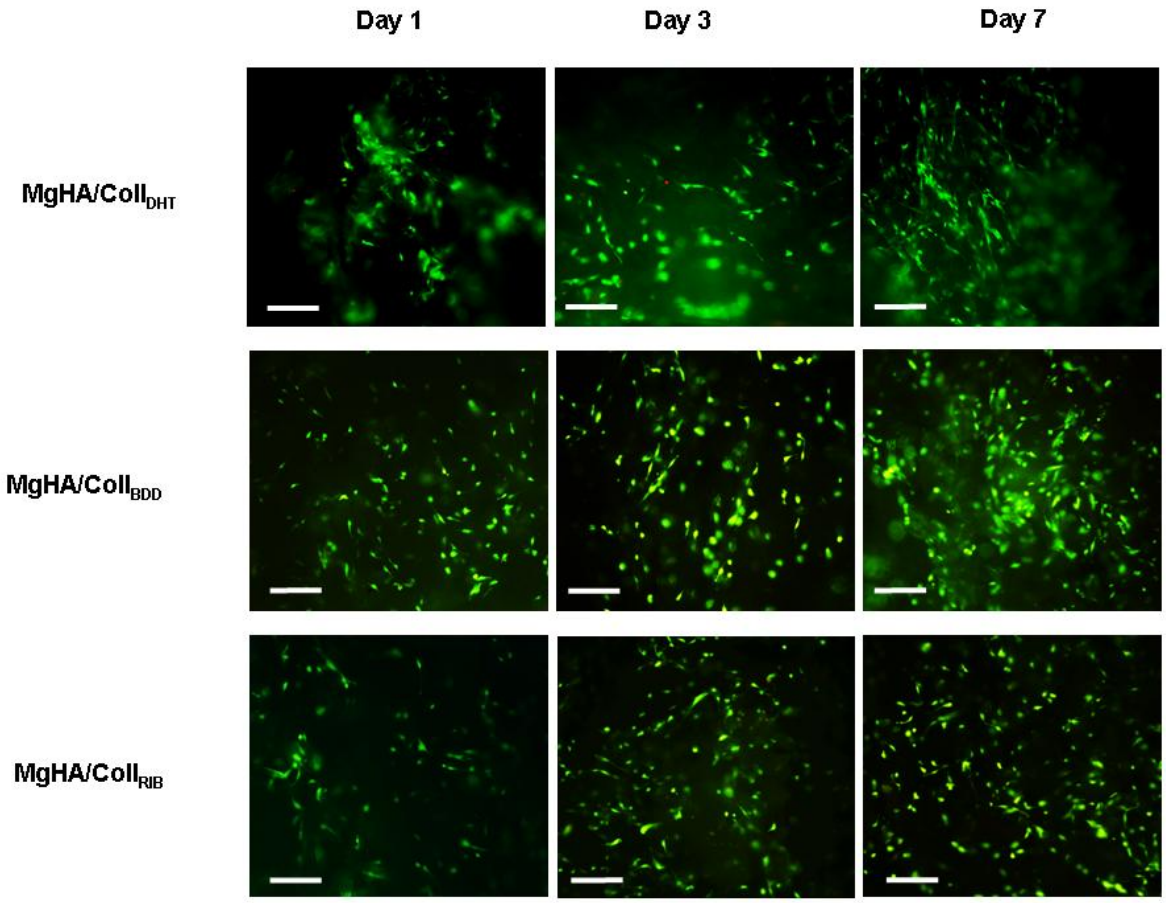

Figure. 9: *Cell viability analyzed by the live/dead assay (Calcein stains live cells in green, Ethidium homodimer-1 stains dead cells in red) of MgHA/Coll$_{DHT}$, MgHA/Coll$_{BDD}$ and MgHA/Coll$_{Post}$ scaffolds on 1 day, 3 days and 7 days . Scale bar: 200 µm.*

4. Conclusion

This study demonstrates that different crosslinking reactions can greatly modify the physical-chemical and mechanical features of MgHA/Coll composite. Earlier studies have suggested that these crosslinkers are potentially safe, however the final compositional properties of the biomaterial can be varied largely by controlling the crosslinking degree [18]. This apart, each of the above mentioned crosslinkers have their own limitations and disadvantages. For examples, high concentration of ribose can significantly cause toxic response [46], whereas, the DHT crosslinking treatment can often result in less surface energy availability due to complete remove of bound water from the material [47]. Similarly, the reactivity of BDDGE is pH and temperature dependent which can potentially affect the crosslinking efficiency [48]. Therefore, this study collectively analyzed the effect of different crosslinkers in modifying MgHA/Coll composite, generally all the crosslinkers greatly improved the physical-chemical and mechanical properties when compared to non-crosslinked composites. Furthermore, the biological performance was favourable with stronger cell-material interaction in all the composites.

Taken together, the results obtained demonstrates that the analyzed crosslinking mechanisms and their respective composites are promising candidates in hard tissue engineering to develop to tissue specific biomimetic biomaterials. In case of bone tissue engineering all the above studied composites ($MgHA/Coll_{DHT,}$ $MgHA/Coll_{BDD}$ and $MgHA/Coll_{RIB}$) would be beneficial, because these composites possess enhanced enzymatic resistivity, sufficient swelling ability, good mechanical resistivity, adequate structural and dimensional (porosity and pore size) properties and satisfactory biological performance. However, the preliminary *in-vitro* experiment is the limitation of this study, therefore, large *in-vitro* testing with longer incubation time can provide a more information on how the effect of different crosslinkers can possibly impact the bone matrix production and expression of selective markers of osteogenic phenotype.

Finally, the present results demonstrate that functionalization of MgHA/Coll composites with suitable crosslinkers can potentially help in reinforcing the 3D composite differently which is

strongly dependent on the crosslinking procedures. Because, the degree of crosslinking can greatly influence the scaffold chemistry, mechanics and biological characteristics. Therefore, the final choice of crosslinkers largely depends upon the applicability of the developed material in order to tune/tailor the final properties of the material differently towards a tissue specific application. For example, if a study aims to preserve the native status of collagen but requires adequate crosslinking reaction, then DHT method can be a good option as this treatment does not alter the functional composition of collagen. Similarly, if a study requires extensive crosslinking bridges between adjacent collagen molecules, then BDDGE treatment would be a viable choice as this chemical reactant increases the crosslinking density greatly. For instance, if a study needs to evaluate the effect of sugar-induced changes in bone due to chronic diseases, then ribose treatment can be better option. Because, ribose crosslinking is a simple, natural process occurring in the biological tissue and this can also serve as potent *in-vitro* model to study extra cellular matrix changes due to sugar-induced bone pathologies. To conclude, this study illustrates the possibility and versatility to design and tailor new biomimetic bone substitutes through various crosslinking reactions, thus providing a platform for scaffold development addressed to hard tissue engineering applications, with potential of personalization on the basis of specific clinical needs.

5. References

1). N. M. Alves, I. B. Leonor, H. S. Azevedo, R. L. Reis J. F. Mano. J. Mater. Chem., 2010,20, 2911-292.

2). Zhengwen Yang, Yinshan Jiang, Li xin Yu, Bo Wen, Fangfei Li, Shemmei Sun, Tianyi Hou. J. Mater. Chem. 15 (2005) 1807-1811.

3). Filardo G, Kon E, Tampieri A, Cabezas-Rodríguez R, Di Martino A, Fini M, Giavaresi G, Lelli M, Martínez-Fernández J, Martini L, Ramírez-Rico J, Salamanna F, Sandri M, Sprio S, Marcacci M. Tissue Eng Part A. 2014;20(3-4):763-73.

4). Islam MM, Khan MA, Rahman MM. Mater Sci Eng C Mater Biol Appl. 2015;49:648-55.

5). Sionkowska A, Kozłowska J. Int J Biol Macromol. 2010 Nov 1;47(4):483-7.

6). Suchanek W, Yashima M, Kakihana M, Yoshimura M. Biomaterials. 1996;17(17):1715-23.

7). Sionkowska A, Kozłowska J. Int J Biol Macromol. 2013;52:250-9.

8). Wahl DA, Czernuszka JT. Eur Cell Mater. 2006 28;11:43-56.

9). Basu J, Ludlow JW. Trends Biotechnol. 2010;28(10):526-33.

10). Tampieri A, Sprio S, Sandri M, Valentini F. Trends Biotechnol. 2011 Oct;29(10):526-35.

11). Tampieri A, Sandri M, Landi E, Pressato D, Francioli S, Quarto R, Martin I. Biomaterials. 29(26) (2008) 3539-46.

12). Minardi S, Corradetti B, Taraballi F, Sandri M, Van Eps J, Cabrera FJ, Weiner BK, Tampieri A, Tasciotti E. Biomaterials. 62 (2015) 128-37.

13). Tampieri A, Iafisco M, Sandri M, Panseri S, Cunha C, Sprio S, Savini E, Uhlarz M, Herrmannsdörfer T. ACS Appl Mater Interfaces. 6(18) (2014) 15697-707.

14). Panseri S, Montesi M, Dozio SM, Savini E, Tampieri A, Sandri M. Front Bioeng Biotechnol. 4(48) (2016) doi: 10.3389/fbioe.2016.00048.

15). Poursamar SA, Lehner AN, Azami M, Ebrahimi-Barough S, Samadikuchaksaraei A, Antunes AP. Mater Sci Eng C Mater Biol Appl. 2016;63:1-9.

16). Shankar KG, Gostynska N, Montesi M, Panseri S, Sprio S, Kon E, Marcacci M, Tampieri A, Sandri M. Int J Biol Macromol. 2017;95:1199-1209.

17). Lin WH, Tsai WB. Biofabrication. 2013;5(3):035008.

18). Davidenko N, Schuster CF, Bax DV, Raynal N, Farndale RW, Best SM, Cameron RE. Acta Biomater. 25 (2015) 131-42.

19). Palmer LC, Newcomb CJ, Kaltz SR, Spoerke ED, Stupp SI. Chem Rev. 2008;108(11):4754-83.

20). Deshpande AS, Beniash E. Cryst Growth Des. 2008;8(8):3084-3090.

21). Tampieri A, Celotti G, Landi E, Sandri M, Roveri N, Falini G. J Biomed Mater Res A. 67(2) (2003) 618-25.

22). Veronesi F, Giavaresi G, Guarino V, Raucci MG, Sandri M, Tampieri A, Ambrosio L, Fini M. J Biomed Mater Res A. 103(9) (2015) 2932-41.

23). Ozeki M, Tabata Y. J Biomater Sci Polym Ed. 2005;16(5):549-61.

24). Koh LB, Islam MM, Mitra D, Noel CW, Merrett K, Odorcic S, Fagerholm P, Jackson WB, Liedberg B, Phopase J, Griffith M. J Funct Biomater. 2013;4(3):162-77.

25). Avery NC, Bailey AJ. Pathol Biol (Paris). 2006;54(7):387-95.

26). Nagahama H, Rani VV, Shalumon KT, Jayakumar R, Nair SV, Koiwa S, Furuike T, Tamura H. Int J Biol Macromol. 2009 May 1;44(4):333-7.

27). Pulieri E, Chiono V, Ciardelli G, Vozzi G, Ahluwalia A, Domenici C, Vozzi F, Giusti P. J Biomed Mater Res A. 2008;86(2):311-22.

28). Z. She, B. Zhang, C. Jin, Q. Feng, Y. Xu. Polymer Degradation and Stability 93(2008) 1316–1322.

29). N. Inoue, Y. Omata, K. Yonemasu, F.G. Claveria, I. Igarashi, A. Saito, N. Suzuki, Veterinary Parasitology 63 (1996) 17–23.

30). Charulatha V, Rajaram A. Biomaterials. 24(5) (2003) 759-67.

31). Kozłowska J, Sionkowska A. Int J Biol Macromol. 2015;74:397-403.

32) Ramírez-Rodríguez GB, Delgado-López JM, Iafisco M, Montesi M, Sandri M, Sprio S, Tampieri A. J Struct Biol. (2016) doi: 10.1016/j.jsb.2016.06.025.

33). Bertinetti L., Tampieri A., Landi E., Martra G., Coluccia S. (2006). J. Eur. Ceram. Soc. 26, 987–991.

34). E. Landi, G. Celotti, G. Logroscino, A. Tampieri. Carbonated hydroxyapatite as bone substitute, J. Eur. Ceram. Soc. 23 (2003) 2931-2937.

35). Madaghiele M, Calò E, Salvatore L, Bonfrate V, Pedone D, Frigione M, Sannino A. J Biomed Mater Res A. 2016;104(1):186-94.

36). Nicoletti A, Fiorini M, Paolillo J, Dolcini L, Sandri M, Pressato D. J Mater Sci Mater Med. 2013;24(1):17-35.

37). Roy R, Boskey A, Bonassar LJ. J Biomed Mater Res A. 93(3) (2010) 843-51.

38). Roveri N, Falini G, Sidoti MC, Tampieri A, Landi E, Sandri M, Parma B. Mat Sci Eng. 23(3) (2003) 441–446.

39). Landi E, Logroscino G, Proietti L, Tampieri A, Sandri M, Sprio S. J Mater Sci Mater Med. 19(1) (2008) 239-47.

40). Salima Ziani, Samira Meski, HAfit Khireddine. Int. J. Appl. Ceram. Technol. 11 (1) (2014) 83-91.

41). Rodrigues SC, Salgado CL, Sahu A, Garcia MP, Fernandes MH, Monteiro FJ. J Biomed Mater Res A. 101(4) (2013) 1080-94.

42). Yan LP, Wang YJ, Ren L, Wu G, Caridade SG, Fan JB, Wang LY, Ji PH, Oliveira JM, Oliveira JT, Mano JF, Reis RL. J Biomed Mater Res A. 95(2) (2010) 465-75.

43). Wang T, Yang X, Qi X, Jiang C. J Transl Med. 2015 8;13:152.

44). Zan X, Sitasuwan P, Feng S, Wang Q. Langmuir. 2016; 32(7):1808-17.

45). Deligianni DD, Katsala ND, Koutsoukos PG, Missirlis YF. Biomaterials. 200;22(1):87-96.

46). Vicens-Zygmunt V, Estany S, Colom A, Montes-Worboys A, Machahua C, Sanabria AJ, Llatjos R, Escobar I, Manresa F, Dorca J, Navajas D, Alcaraz J, Molina-Molina M. Respir Res. 16(82) (2015) 1-15.

47). I. Prasertsung, R. Mongkolnavin, S. Damrongsakkul, C.S. Wong, Surf. Coat. Technol. 205(1) (2010) 133-138.

48). Zeeman R, Dijkstra PJ, van Wachem PB, van Luyn MJ, Hendriks M, Cahalan PT, Feijen J. J Biomed Mater Res. 1999 Se5;46(3):424-33.

Conclusion and Future perspectives

The major objective of this work was to study how the effect of different crosslinking strategies can functionally modify various characteristics of biological macromolecules relevant for scaffold development in bone tissue engineering. The research study was classified into three different phases: (i) different crosslinking strategies in gelatin functionalization, (ii) ribose mediated crosslinking in collagen-hydroxyapatite scaffold (iii) different crosslinking mechanisms in functional modification of bone-like scaffold. The obtained results were highly positive in all the three investigated phases. Though the core aim of this research was to explore the available crosslinking strategies in different biological macromolecules, the present study generated significant findings, largely contributing to provide optimum solutions in understanding how the crosslinking density can fine-tune the overall performance of a scaffold, relevant for its functioning in vivo. In particular, this study demonstrated that different crosslinkers at different conditions (pH and temperature) can modify the functional properties of the scaffolds differently, therefore this optimization strategies on these crosslinkers as obtained from this study results will help material scientists in the design and development of bioactive hybrid biomaterials for hard tissue regeneration.

The final choice of crosslinkers largely depends upon the applicability of the developed material, because the different crosslinkers can tune/tailor the final properties of the material differently, therefore potent crosslinker must chosen for tissue-specific application to largely address the structure-function relationship. With this information, future studies must be devoted towards recognizing how the effect of different crosslinkers can regulate cellular and host response to understand the balance between stability and functional remodelling.

Firstly, the above mentioned crosslinkers must be studied at molecular and protein level to examine how the individual crosslinker molecule can modulate the gene specific expression. A comparative study is necessary to assess the differences in chondrogenic and osteogenic specific gene expression, which can reveal if any crosslinker can disrupt the lineage specific proliferation and differentiation.

In this way, any specific inept crosslinker can be avoided in case of bone or cartilage tissue engineering so avoid any deleterious aftermath effects. Secondly, more pre-clinical studies are needed to see if the inflammatory host response varies due to different crosslinking densities. A detailed study on pro-inflammatory response (macrophage activation and population) and mediator's distribution (cytokine and chemokine status) at the site of implantation can provide detailed information about host immune and inflammatory response and susceptibility to disease progression/destruction can be determined.

Furthermore, pre-clinical and clinical studies must be combined to identify the characteristic variations in tissue healing with more comprehensive techniques to better understand and compare the host response and the reparative process in two different populations. Finally, the recent advances in material technology will greatly assist in refining experiments to develop more alternative crosslinking strategies considering the current limitations and to provide a better strategy with sufficient balance of stability, inflammation and remodelling. Additionally, what is more important, when comes to bone tissue engineering is the resilience to mechanical loading, therefore more research must be devoted towards developing scaffolds with bone-like mechanical features. To conclude, this study offers insightful discussions on how different crosslinkers and their physical-chemical properties can help in deriving new avenues for developing a new class of functional, bioinspired bone-like scaffolds.